# The Effect of Stromal cell Derived Factor-1 (SDF-1) and Collagen-GAG (Glycosaminoglycan) Scaffold on Skin Wound Healing

by

**Aparajita Sarkar**

Submitted to the Department of Mechanical Engineering
in partial fulfillment of the requirements for the degree of

Master of Science in Mechanical Engineering

at the

MASSACHUSETTS INSTITUTE OF TECHNOLOGY

June 2008



Author .....
Department of Mechanical Engineering
May 27, 2008

Certified by .....
**Robert S. Langer**
Institute Professor, Thesis Supervisor

Certified by .....
**Ioannis V. Yannas**
Professor of Mechanical Engineering, Thesis Supervisor

Certified by .....
**François Berthiaume**
Assistant Professor, Harvard Medical School, Thesis Supervisor

Accepted by .....
**Rohan Abeyaratne**
Department Head of Mechanical Engineering

Accepted by .....
**Lallit Anand**
Graduate Officer

**Dedicated to Rohan Abeyaratne and Michael Maier:**

*To my caro Sir, for the gift of wings.*

*To my beloved Mike, for always encouraging me to fly.*

# The Effect of Stromal cell Derived Factor-1 (SDF-1) and Collagen-GAG (Glycosaminoglycan) Scaffold on Skin Wound Healing

by

**Aparajita Sarkar**

Submitted to the Department of Mechanical Engineering
on May 27, 2008, in partial fulfillment of the
requirements for the degree of
Master of Science in Mechanical Engineering

## Abstract

Wound healing is an intricate biological process requiring the appropriate balance of matrix and growth factors. Apart from causing physical deformity, adult wound healing results in the formation of scar tissue, which can hinder functionality and mobility due to excessive wound contraction. Wound care is a significant clinical problem for chronic wounds (eg. diabetic ulcers), acute injuries (eg. burns) and in elective surgeries (eg. scar revision). With an overall annual cost of $\$16 - 22$ billion, wounds severely burden the U.S. healthcare system, and are the fastest growing area in the medical sector. Thus, the goal of promoting faster healing with "scar-less" wound resolution remains unchanged.

Skin substitutes, such as Integra$^{TM}$ and Alloderm$^{TM}$, have been developed to treat chronic wounds and extensive burns. However, they are susceptible to infection, prone to shearing and exhibit poor biodegradation. These limitations could potentially be overcome by expediting blood vessel growth which would promote a more rapid integration of the skin substitute with the surrounding tissue. Experimental evidence also suggests that down-regulating inflammatory cells and up-regulating stem cells and progenitors cells would yield less scar formation. But, these therapies require an expensive isolation and culturing process from the patient's bone marrow. Additional risks include immune rejection concerns, limited shelf-life and stringent storage requirements.

To meet this need, a stem cell-attractant and inflammatory cell-repellant chemokine, Stromal cell Derived Factor-1 (SDF-1) was incorporated into a highly porous collagen-glycosamino-glycan (GAG) matrix (skin substitute). The hypothesis is that this enhanced skin substitute would expedite wound healing and decrease abnormal scarring by a mechanism where stem cells from the patient's circulation would be attracted to the wound site while inflammatory cells would be repelled. The purpose of this study is, thus, to elucidate the potential of SDF-1 to improve skin wound healing.

Experimental results demonstrated that topical application of SDF-1 induced changes in wound-healing kinetics (contraction and re-epithelialization) compared to spontaneous healing in un-treated wounds (Control group). A reproducible dorsal full-thickness excision wound model in wild-type mice was used and wound repair was assessed both macroscopically and microscopically. The SDF-1 treated group demonstrated the fastest rates of wound closure and cell proliferation as compared to the Control group, with re-epithelialization occurring more rapidly by 36%. Qualitatively, the amount of early cell infiltrate in the SDF-1 group was also significantly less when compared to the Control group, which is indicative of a decreased inflammatory response. In addition, wounds treated with SDF-1 exhibited reduced wound contraction initially during the healing process.

These experimental results demonstrated a synergy between SDF-1 and the scaffold that promoted faster wound closure and reduced contraction. Thus, the SDF-1 treated-dermal matrix may

be a new tool to stimulate wound closure and quality tissue formation in acute and chronic wounds. Other potential applications include tissues that exhibit poor regeneration after injury, such as cornea, spinal cord and heart. The development of such solutions would, therefore, be of significant benefit to human health.

Thesis Supervisor: **Robert S. Langer**
Title: Institute Professor, Thesis Supervisor

Thesis Supervisor: **Ioannis V. Yannas**
Title: Professor of Mechanical Engineering, Thesis Supervisor

Thesis Supervisor: **François Berthiaume**
Title: Assistant Professor, Harvard Medical School, Thesis Supervisor

# Acknowledgments

This thesis would not have been possible without the synergistic assistance of various individuals.

First, I would like to thank Dr. François Berthiaume, my research advisor at the Shriners Burns Hospital for Children-Boston. Without his support, this research would not have been possible. I sincerely value the freedom of thought and flexibility that I enjoyed which enabled me immensely to develop as a researcher.

I would also like to thank my MIT advisors Prof. Ioannis V. Yannas and Prof. Robert S. Langer. Being passionate about skin and tissue regeneration, I am very appreciative of the opportunity to learn under their tutelage and for their expert feedback. In addition, Prof. Myron Spector's and Dr. Roderick Bronson's assistance with analysis of the histology and interpretation of wound contraction were invaluable.

I am also grateful to Dr. Dennis P. Orgill, at the Brigham and Women's Hospital-Boston, and Dr. Robert Sheridan, at the Shriners Burns Hospital for Children-Boston, for sharing their clinical experience about skin substitutes and surgery. Members of Dr. Orgill's group, especially Dr. Sandra Saja Scherer, generously shared their knowledge without which this project would not have progressed as rapidly as it did.

I would also like to acknowledge the Shriners Burns Hospital-Boston and the Deshpande Center at MIT for supporting this work, the latter via the Ignition grant award in Fall 2007. I also appreciate Dr. Berthiaume's, Prof. Langer's and Prof. Yannas' critical review of this manuscript, and am indebted to Sankha Banerjee and Michael Maier for their aid with its final structuralization and the figures respectively.

Finally, I would like to thank Michael Maier and Prof. Rohan Abeyaratne for their unwavering support and encouragement, without which my years and experience at MIT would not have been possible, and as wonderful and enjoyable as it has been. Thank you!

# GLOSSARY

| Acronym | Definition |
|---|---|
| **CTL** | Cytotoxic T Lymphocyte |
| **CXCR4** | Chemokine (C-X-C motif) Receptor 4 |
| **GCSF** | Granulocyte Colony-Stimulating Factor |
| **H&E** | Hematoxylin and Eosin |
| **IL-8** | interleukin-8 |
| **PBS** | Phosphate Buffered Saline |
| **PECAM** | Platelet/Endothelial Cell Adhesion Molecule |
| **SDF-1** | Stromal cell Derived Factor-1 |
| **SMC** | Smooth Muscle Cell |
| **$\alpha$-SMA** | Alpha-Smooth Muscle Actin |
| **VEGF** | Vascular Endothelial Growth Factor |
| **bFGF** | Basic Fibroblast Growth Factor |
| **Stellate scar** | Scar with radial protrusions (of curved arrow form) |
| **4X** | 4X Magnification |
| **10X** | 10X Magnification |
| **40X** | 40X Magnification |
| **s.c** | Subcutaneous |

# Contents

# List of Figures

# List of Tables

# Chapter 1

# Introduction

## 1.1 Background and Significance

Even with the evolution of wound care, the goal of promoting faster and better wound healing remains unchanged. Apart from causing deformity and death, wounds are a severe burden on the U.S. healthcare system with an annual overall cost of $\$16-22$ billion.[1] With an annual growth rate of 10%, it is the fastest growing area in the medical sector per Espicom Business Intelligence.[2] The Centers for Disease Control and Prevention (CDC) estimated that 27 million surgical procedures are performed annually.[3] This includes emergency procedures, like burns, and elective procedures, such as scar revision.

As the U.S. population ages, the incidence of chronic wounds is projected to increase to 5 million a year, costing $4 billion in 2004 per Taglich Brothers Inc.[4] Diabetes mellitus contributes to 50% of all lower extremity amputations in the United States with approximately 15% of all patients developing foot ulceration with infection.[5],[6] Thus, foot ulcers are the leading cause for hospitalization in diabetic patients with an annual health care cost greater than $1 billion.[7] Wound care and management of pressure sores and venous stasis ulcers are also very expensive. Even though most pressure and venous ulcers do not require amputation, they result in reduced quality of life for the patient (Figure 1-1, (a)).

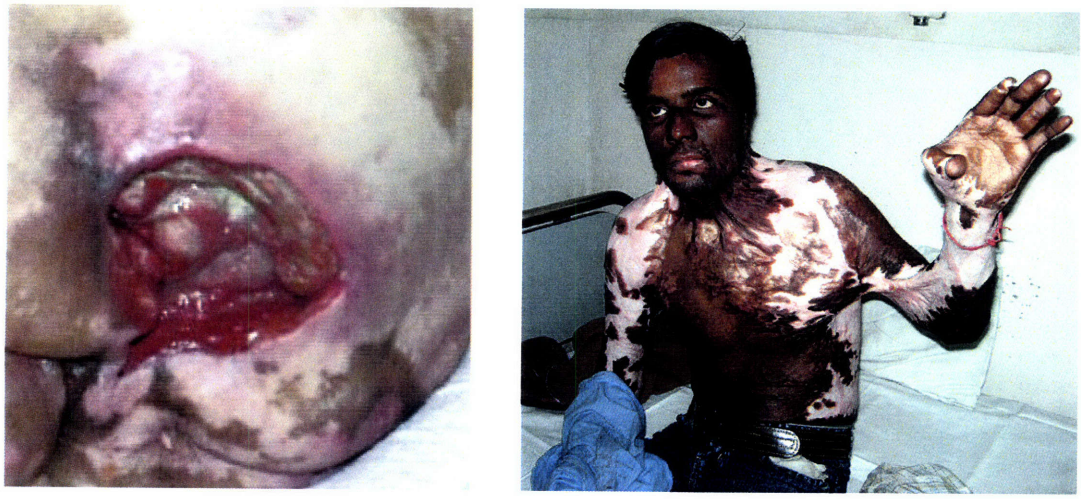

(a) Pressure sore on Buttock

(b) Scarring in Burn Patient

Figure 1-1: **Clinical Problems**

With an annual rate of approximately 600,000 wounds in the United States, the average cost of treating venous leg ulcers is estimated at $2400 per month.[8] Pressure ulcers have a prevalence ranging from 8.8% in institutionalized patients to 14.8% in patients in acute care facilities, with an average cost of treatment of up to $70,000.[8] The number of burn victims stands at 2.4 million per year and is expected to grow by 5% every year (Figure 1-1, (b)).

Around 30% of these injuries are treated by medical professionals and of those hospitalized, 20,000 have major burns involving at least 25% of their total body surface area, and 12,000 of these patients die.[9] Burns are one of the most expensive catastrophic injuries to treat and require a multi-disciplinary team of medical professionals. For example, a burn involving 30% of the total body surface area costs as much as $200,000 in initial hospitalization and physician fees. Furthermore, undesirable scars result in as many as 50% of cases with deep burns (*www.burnsurgery.org*), which results in a reduced quality of life due to a loss of mobility and functionality. Burn patients often undergo repeated reconstructive surgeries to ameliorate the scars, as well as extensive rehabilitation. Severe burns also frequently lead to post-traumatic stress syndrome and long-term psychological damage due to physical disfigurement.

## 1.2 Skin and the Physiology of Wound Healing

### 1.2.1 Anatomy of Skin

At $12-15\%$ of the total body weight and with a surface area of 25 square feet, the skin is the largest organ in the body. It maintains homeostasis by providing a protective barrier against the outside elements and microorganisms, by regulating the internal body temperature through sweat-producing glands and dilation of blood vessels, and by preventing excessive water and extracellular fluid loss. Other functions of the skin include synthesis of vitamins and hormones, such as Vitamin D, and sensory reception via specialized nerve receptors for touch, temperature, pain and pressure.

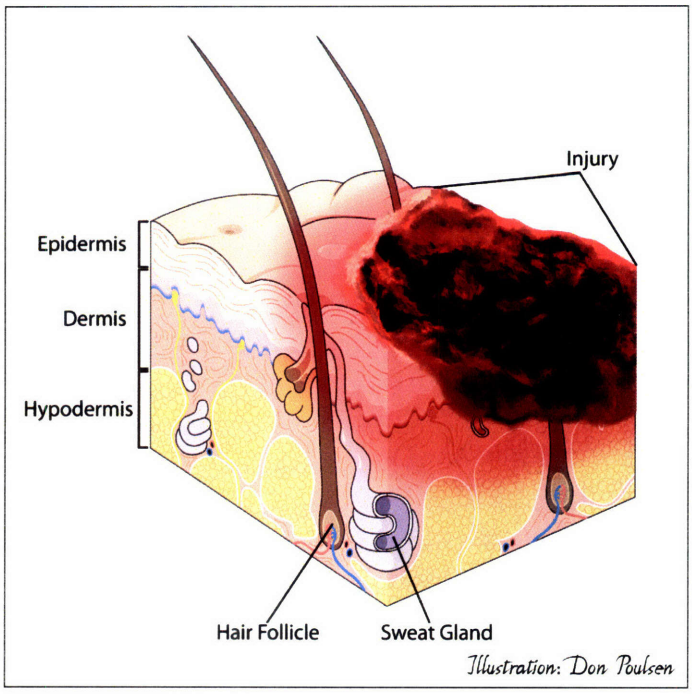


Figure 1-2: **Anatomy of Skin and Wound**

*Normal skin consists of the following distinct primary layers* (Figure 1-2):

1. **Epidermis** - The epidermis is the outermost layer of the skin and is a transparent membrane contiguous with the mucous membranes. Its primary function is to form a barrier to the external environment against dehydration and the entry of microbes, such as viruses and bacteria, into the body. Acidic secretions from the skin also help retard fungal growth. The

epidermis receives its nutrients from the dermis as it does not have any blood vessels. The basic cell type of the epidermis is the keratinocyte, which contains an insoluble fibrous protein called keratin. Keratin water-proofs the surface of the epidermis while giving it properties of strength and flexibility. Keratin is also the major component of hair and nails. Thick skin epidermis typically has 5 strata. The innermost layer of the epidermis (stratum basale) comprises of basal cells and melanocytes. The melanocytes produce the pigment melanin and store carotenoids, both of which are responsible for imparting color to the skin.[10] The melanin also helps protect the skin from harmful ultraviolet radiation. Langerhans cells are also present in the epidermis. These cells are dendritic cells that are responsible for alerting the immune system of the presence of pathogens and foreign materials.[11] The outer epithelial layer of dead keratinocytes (stratum corneum) is replaced every 3 to 4 weeks by new epithelial cells that are pushed up to the surface from the dermis.[12]

2. **Dermis** - The dermis is the layer beneath the epidermis and comprises the largest segment of skin. Its primary function is to provide structural integrity to the skin and supply blood and nutrients to the epidermis. The dermis has two layers that are closely associated. The innermost layer (reticular layer) is made of a dense, criss-crossing, connective network of collagen fibers. The basic material properties of skin are due to the collagen protein providing it strength and structure, and elastin protein giving it flexibility.[13] Sensory receptors for deep pressure (Pacinian corpuscles), sweat and oil producing glands, lymph vessels and hair follicles are also present in the reticular layer. The outermost layer (papillary layer) has loose connective tissue and connects to the epidermis via papillae (finger-like projections). These papillae contain sensory touch receptors (Meissner's corpuscles), thermoreceptors and vessels that nourish the epidermis. Collagen producing fibroblast cells are also present in the papillary layer.[12]

3. **Hypodermis** - The hypodermis layer or the subcutaneous tissue layer, lies beneath the dermis. It primarily consists of adipose (fat) tissue and blood and lymph vessels. Adipose tissue aids in conserving heat within the body, cushions the body against physical forces and gives the

body its shape and form.[14]

### 1.2.2 Classification of Skin Wounds: Acute versus Chronic

A wound is defined as a "disruption of the normal anatomic structure and function", per the Wound Healing Society.[15] Wounds are typically categorized as being either acute or chronic.

In acute wounds, reparative healing progresses normally in an orderly and timely process. Whereas, in chronic wounds the repair process has failed to ensue and result in closure of the wound area. This is typical in non-healing wounds such as venous stasis ulcers, pressure sores and diabetic ulcers. Large trauma areas with extensive tissue loss, such as third-degree burns, are also at risk of developing in to chronic wounds.[15]

### 1.2.3 Types of Healing: Regeneration versus Repair

In superficial injuries and burns, the dermis is largely intact and enough epidermal cells remain that can proliferate, stimulated by factors released by the dermis underneath. Therefore, complete regeneration can occur spontaneously in four weeks or less.[13] Regeneration involves the gross replacement and restoration of tissue mass with normal architecture and function.

In deep acute wounds, the epidermis is completely destroyed and the dermis is significantly damaged (Figure 1-2). Thus, the healing process is reparative and not regenerative. Wound repair involves the synthesis of scar tissue without restoration of the normal structure and function of the tissue or organ.[13]

*The process occurs by either primary, secondary or tertiary intention which is described in further detail below*[16]:

1. **Healing by primary intention** - This process typically occurs in most surgical wounds whose skin edges have been adequately brought together (apposed). These wounds types heal rapidly and the resultant scar will depend on the skin type of the patient and the direction of the scar in relation to Langer's lines (alignment of the collagen fibers within the dermis).[15]

2. **Healing by secondary intention** - Wounds that are left open and heal by the natural wound

reparative process, by and large, heal by secondary intention. Wound types that undergo healing by secondary intention include large wounds with extensive tissue loss following massive trauma, such as third-degree burns. The wound phases of the wound reparative process are more pronounced than in healing by primary intention resulting in severe wound contraction and scar formation.[15]

3. **Healing by tertiary (delayed primary) intention** - Wounds that are infected or have foreign material, cannot be closed surgically until the complications have been resolved. Healing by tertiary intention can also be induced by surgical skin graft reconstruction in large open wounds caused as a result of severe trauma. This is extremely important as failure to heal within one month could result in a sub-acute state that may evolve into a chronic state if healing by secondary intention is not achieved within three months.[15]

Primary or tertiary wound healing is preferred to secondary healing. This is because healing by secondary intention involves a more severe wound reparative process of wound contraction and scar formation, which may result in physical impairments of decreased functionality and abnormal appearance.[13] Furthermore, deep injuries involving large surface areas do not heal spontaneously and must be covered with full-thickness skin grafts, which are obtained from other healthy donor areas of the body. In addition, life-threatening complications, associated with large open wounds of greater than 20% area, can arise from systemic shock caused by excessive fluid loss[17] or due to the onset of sepsis.[18]

### 1.2.4 Physiology of Wound Repair Process

*The process of skin wound healing by repair can be divided in to the following phases*:

1. **Inflammatory Phase** (from time of injury to Day 4 post-injury) - The inflammatory phase sets in within minutes of injury. First, blood supply to the wound site increases which leads to aggregation of platelet cells and fibrin clot formation (hemostasis).[19] The purpose of hemostasis is to cease the bleeding and provide a temporary barrier to protect the underlying tissue

from the external environment and microbial invasion. In addition, blood-borne leukocytes (neutrophils and monocytes) and macrophages enter the wound site to clear away any cellular debris or foreign material. Gross macroscopic characteristics of the inflammatory phase include reddening of the wound area and edema.[12],[20] (Figure 1-3 and Figure 1-4)

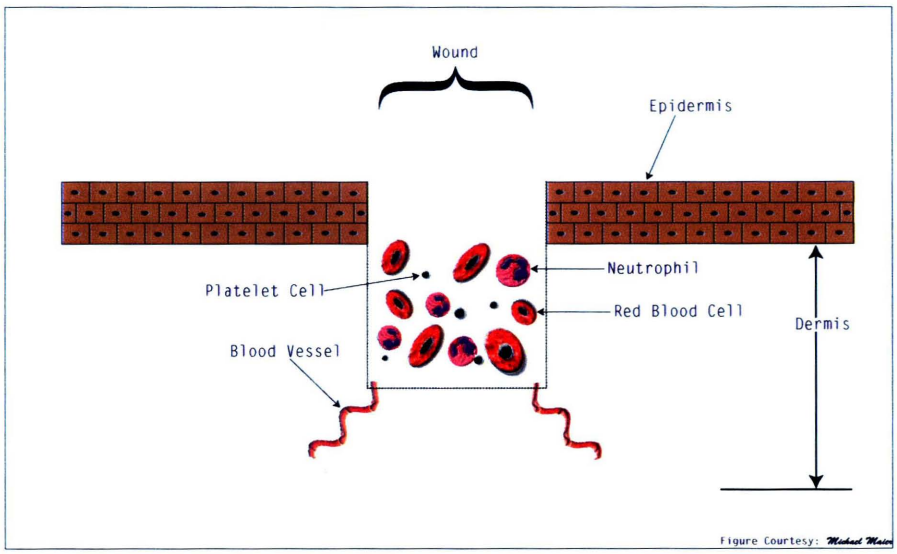


Figure 1-3: **Cell Migration in Inflammatory Phase**

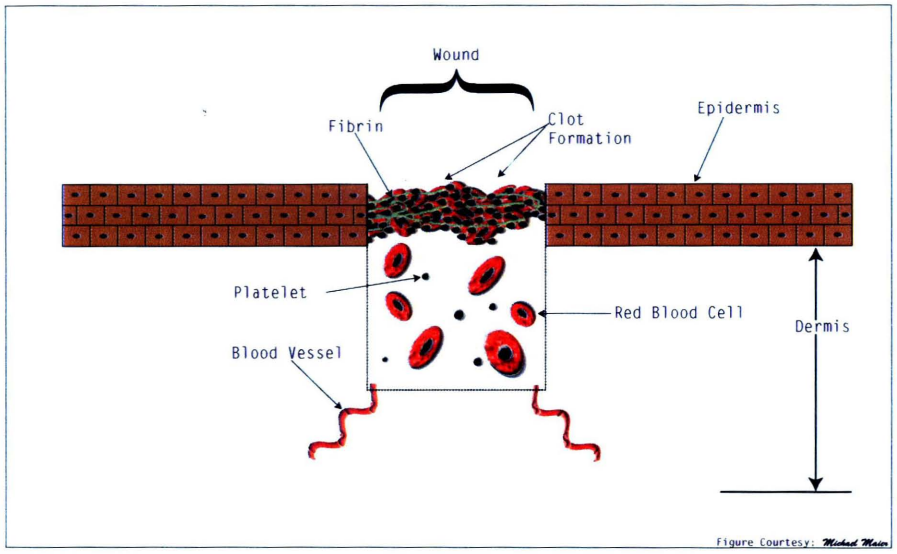


Figure 1-4: **Clot Formation in Inflammatory Phase**

2. **Proliferative Phase** (from Day 5 to Day 14 post-injury) - The proliferative phase involves the initiation of repair of the epidermis and the dermis. Fibroblast cells and endothelial (vascular)

cells migrate in to the wound site and work in concert to fill in the wound area from the base of the wound with a richly vascularized collagen and connective tissue dermal composite called granulation tissue.[12] The granulation tissue is deposited in to the wound area in a disorganized manner by the increased synthesis of fibrillar collagen and fibronectin. Simultaneously, the wound contraction process is induced by growth factors such as TGF-$\beta$1 wherein contractile myofibroblast cells decrease the dermal gap by binding to the surrounding collagen network using proteins such as integrins.[21],[22],[23],[24] As the actin filaments in the myofibroblast cell contract, the dermal edges of the wound are pulled together, while fibroblasts synthesize more collagen to reinforce the wound area. A prolonged contraction process, which is common after large and deep burns, can inhibit joint movement depending on the wound location.[25],[26] In addition, keratinocytes from the wound edges begin to migrate over the granulation tissue to re-epithelialize the wound surface by forming a new epidermis. In the absence of a clean and moist wound environment with healthy blood flow, the re-epithelialization process will not progress normally and necrotic tissue (eschar) will develop, which would need to be debrided before the normal healing process can resume.[12] The formation of eschar is very common in burn injuries (Figure 1-5)

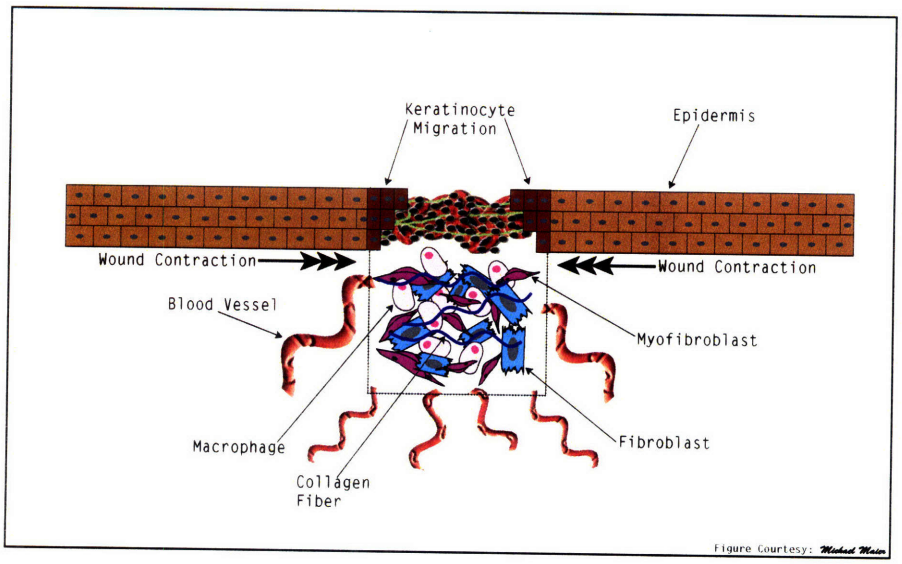


Figure 1-5: **Proliferative Phase**

3. **Maturation Phase** (from Day 15 to months or years post-injury) - Once the myofibroblasts commit apoptosis and the fibroblasts stop proliferating, the healed wound enters the maturation phase. The granulation tissue continues to be remodeled and the epidermis matures. The neo-epidermis may be distinguished from the epidermis of normal unwounded skin by a "smoothened" appearance, which is caused due to lower densities of undulations (rete pegs).[27] The granulation tissue is eventually converted in to an avascular cutaneous scar composed primarily of fibrous connective tissue produced by fibroblasts. The immature scar is typically denser and thicker with a higher concentration of immature Type III collagen than in the surrounding normal dermis.[28] Over time as the scar matures, the collagen type is mainly replaced by a mature Type I collagen.[29] Rarely do skin appendages such as hair follicles and sweat glands return and the normal architecture and functionality of the tissue is not fully restored.[13] The tensile strength of the scar formed is, at best, 70% of the tensile strength of normal unwounded skin.[30] Since the scar tissue is less elastic, it is vulnerable to further breakdown. In addition, fibrotic scar formation can result in complications such as an abnormal appearance due to skin discoloration and excessive granulation tissue deposition (hypertrophic scars and keloids), and impaired mobility and functionality.[20],[13] (Figure 1-6)

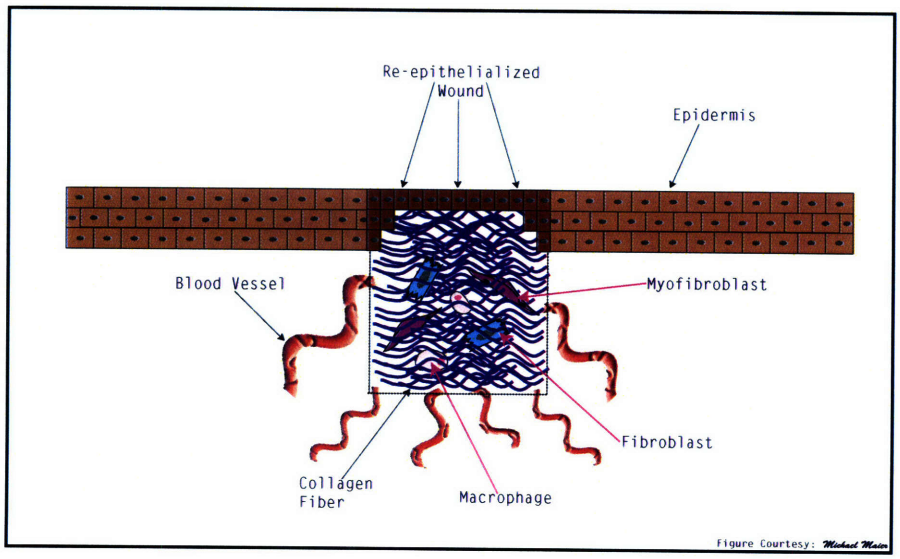


Figure 1-6: **Maturation Phase**

# Chapter 2

# Current Treatment Methods For Skin Wounds

## 2.1 Tissue-Engineered Skin: Role of Skin Substitutes

Tissue-engineered skin, also known as skin substitutes, refers to skin products consisting only of cells or only of extracellular matrix materials, or to a combination of both. Their function is to aid the healing process by providing the needed matrix, growth factors or cells.[31] The extent of damage to the dermis has been directly correlated with an increased propensity to develop scarring. Skin substitutes have been developed to promote regeneration of the dermis, such as Integra$^{TM}$ (Integra Life Sciences, Plainsboro, NJ) and Alloderm$^{TM}$(LifeCell Co., Branchburg, NJ). These dermal skin substitutes are applied onto the cleaned wound bed and provide a support structure for blood vessels and other cells to migrate and grow into. After 2 weeks, they are sufficiently vascularized to support an epidermal skin graft, which is required to regenerate the epidermis. (Figure 2-1)

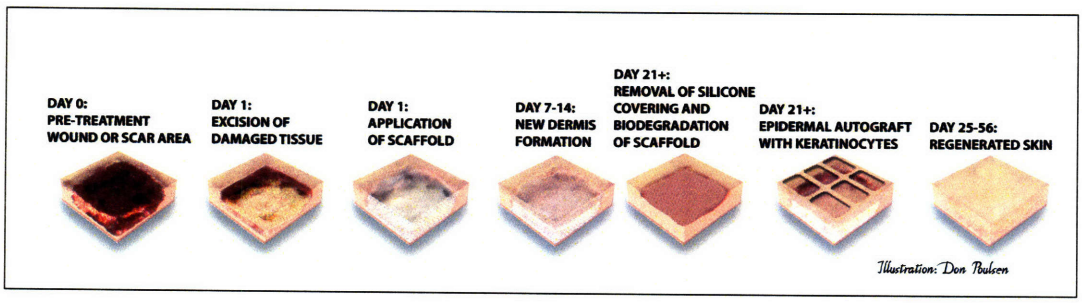


Figure 2-1: **Use of Skin Substitutes for Deep Wounds**

## 2.2 Role of Circulating Stem Cells

Data from literature suggest that during injury, bone marrow-derived stem cells and vascular progenitor cells which are released into the circulation, can spontaneously migrate into the site of injury and participate in the wound healing process.[32],[33] Experiments where isolated stem cells, such as mesenchymal and hematopoietic stem cells, were directly injected into injuries have demonstrated enhanced regeneration characterized by better functionality and decreased scar tissue.[34],[35],[36],[37]

## 2.3 Role of Inflammatory Cells

The recruitment of blood-borne immunocompetent cells, such as T cells and B cells, into the wound site is a major component of the local inflammatory response, which plays a key role in the formation of granulation tissue and the initiation of the wound healing response. Increased levels of T cells have also been associated with post-burn hypertrophic scar formation.[38]

Over 10 years ago, a new population of leukocytes called "fibrocytes", that entered the wound at the same time as inflammatory leukocytes, was identified, which appear to emanate from the stromal compartment of the bone marrow .[39] More recently, a significant increase in circulating levels of fibrocytes was documented in burn patients.[40] Although these cells may contribute to the wound healing process, there is evidence that these cells are also involved in fibrotic responses including hypertrophic scars and keloids.[41] On the other hand, in established scars and keloids, their presence (based on CD34 antigen expression) seems to correlate with locally decreased collagen

synthesis activity.[42]

An intriguing fact is that the lack of an inflammatory response is not always detrimental, as is the case in fetal wound healing. A hallmark of fetal wound healing is the lack of a significant inflammatory response. The switch from scar-less fetal wound healing to wound healing leading to scar formation, which is characteristic of adults, is thought to correlate with the development of the immune system and the appearance of immunocompetent cells.[43] Depending on the wound size and depth, fetal skin wounds heal scarlessly during periods of early skin differentiation; but this ability is progressively lost in late periods of gestation.[44] Thus, the inability to fully regenerate damaged tissues as the fetus progresses to later stages may also be due to other factors, such as the lack of cues that were originally present during skin development which guide morphogenesis of the tissue. The lack of progenitor cells with sufficient proliferative capacity to restore the tissue could be yet another contributing factor.

## 2.4 Limitations of Current Treatment Methods

Although the existing dermal skin substitutes are tremendous advances in the treatment of severe skin injuries, they lack intrinsic antimicrobial activity and are susceptible to infection due to slow vascularization.[45] Infection increases the incidence of scarring.[46] Other complications, such as shearing of the skin substitute from the wound bed due to inadequate angiogenesis and deposition of non-degraded fibers in the wound bed due to poor biodegradation, have also been observed.[47] Furthermore, skin substitutes do not inhibit long-term wound contraction.[45] These limitations could potentially be overcome by expediting blood vessel growth into the skin substitute as active blood vessels enable infection-fighting immune cells to enter and "monitor" the wound site. Blood vessel growth is a rate-limiting process for the migration and proliferation of cells from the wound bed. Therefore, faster blood vessel growth would promote a more rapid integration of the skin substitute with the surrounding tissue, thus, reducing the risk of its shearing and avulsion from the wound site. Faster vascularization of the skin substitute would decrease the time needed before epidermal skin grafts can be applied onto the wound. This would result in faster wound healing

overall. Finally, faster wound healing is correlated with better appearance and less scarring of the healed wound, based on VEGF antigen expression.[31] Thus, a strategy that speeds up blood vessel growth may also reduce scar formation.

Stem cell-based therapies require an expensive process of isolating and culturing large numbers of cells from the patient's bone marrow. Also, cell-based therapies are not easily amenable to becoming off-the-shelf products due to immune rejection concerns, limited shelf life and stringent storage requirements.

# Chapter 3

# Proposed Approach

## 3.1 Stromal cell Derived Factor-1 (SDF-1)

The proposed approach is to enhance commercially available skin substitutes by incorporating a stem cell attractant peptide that promotes the homing-in and recruitment of circulating stem cells and progenitor cells into the wound site while repelling inflammatory cells. A well characterized full-thickness skin wound experimental model will be used in this study.

The selected peptide is Stromal cell Derived Factor-1 (SDF-1), which is also known as CXCL12. SDF-1 is an 8 kD CXC chemokine known to bind receptor CXCR4. Binding of the receptor triggers downstream signaling events inside the cell that eventually lead to cell migration towards the source of SDF-1. SDF-1 is structurally grouped into two subfamilies, SDF-1$\alpha$ and SDF-1$\beta$, with similar activity. It is expressed during homeostasis in many organs, including adult bone marrow endothelium and the stem cell rich endosteum region. Multiple stromal cell types such as bone forming osteoblasts, adipocytes, fibroblasts and endothelial cells produce this chemokine. The human and mouse chemokines are very similar.

Although its half-life in vivo is unknown, SDF-1 can be cleaved at the N-terminus and can be degraded by a wide array of proteolytic enzymes.[48] Because cell migration is a process that occurs over several days, SDF-1 must be delivered over an extended time course. Thus, the timing and

dosage of administration of exogenous SDF-1 may significantly affect the concentration of active SDF-1, which may in turn lead to complex dynamics of attractant and repellent effects of the chemokine on CXCR4 cells in the wound site.

SDF-1 is a stable peptide and can be incorporated during or after the manufacture of existing FDA-approved (U.S. Food and Drug Administration) skin substitutes. Therefore, it would not require any changes to their existing storage or handling requirements. With this approach, the benefits of stem cell-induced regeneration can be leveraged in vivo without the need for a costly cell-based product.

## 3.2 Role of SDF-1 in the Local Response to Injury

There is evidence in literature that increasing SDF-1 levels can be beneficial to wound healing. Synthesis and expression of SDF-1 is regulated by hypoxia-inducible factor 1, and has been shown to occur in skin and liver as a result of oxygen deprivation induced by injury or infection.[49],[50],[51] SDF-1 is part of an endogenous mechanism that recruits stem cells into damaged tissues.[52],[53],[54] This was also seen in a study where injection of genetically modified cells that over express SDF-1 into a model of myocardial infarction in mice showed increased stem cell recruitment into the damaged heart area, greater left-ventricular mass and better cardiac function.[53] Another study involving the administration of SDF-1 into diabetic wounds demonstrated enhanced endothelial progenitor cell mobilization, homing, and wound closure.[55] In addition, transgenic mice that express higher levels of SDF-1 exhibited accelerated closure rate of skin wounds.[56] An interesting and alternative theory with regards to the role of SDF-1 in burn injury has been proposed recently where a study found that blocking endogenous levels of SDF-1 resulted in increased re-epithelialization and decreased eosinophil infiltration in second-degree dermal burn wounds 5 days post-wounding.[57] However, since the healing process was not followed until complete wound closure occurred, it is unclear as to what the long-term effects of blocking SDF-1 would be on burn injuries.

## 3.3 Role of SDF-1 in the Attraction of Stem Cells

Based on literature data, it has been observed that SDF-1 is chemotactic (attractant) for several different types of cells, namely, Hematopoietic stem cells[58],[59],[60],[61], Endothelial progenitor cells[62],[63],[64],[65],[66],[67], and Mesenchymal stem cells[68],[69]. Endogenous SDF-1 also plays a key role in the induction of blood vessel growth triggered by well-known angiogenic factors, such as VEGF and bFGF.[67],[70],[71] (Figure 3-1)

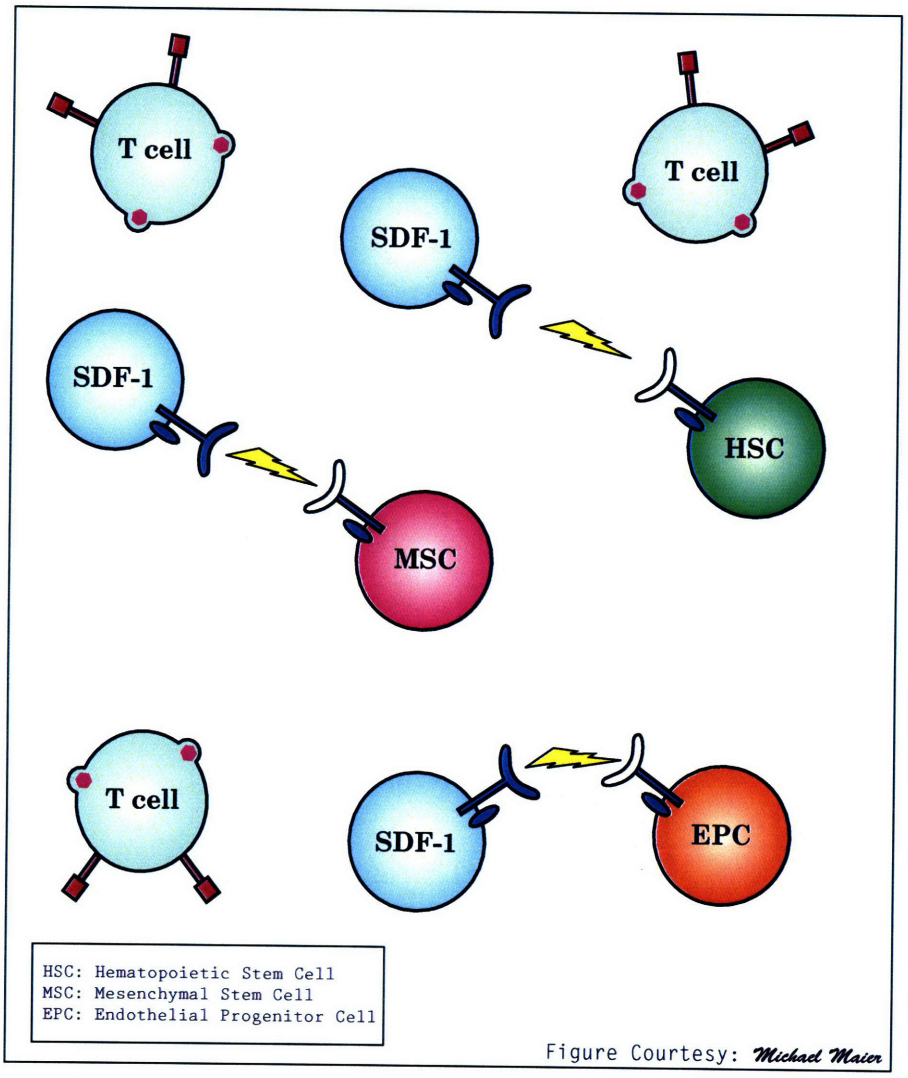


Figure 3-1: **Role of SDF-1 in Attraction and Repulsion of Cells**

## 3.4 Role of SDF-1 in the Repulsion of Inflammatory Cells

Until recently, chemokines such as SDF-1 were thought only to have chemoattractant activity for specific subpopulations of leukocytes. However, it was recently demonstrated that the effect of SDF-1 is dose dependent. Specifically, while it is chemotactic for T cells at concentrations up to 100 nM, it repels CD4 and CD8 T cells at concentrations above 100 nM. This mechanistic property is termed "fugetaxis" or "chemorepulsion". T cell fugetaxis was shown to be CXCR4-dependent but to have a signal transduction pathway that was distinct from that for chemoattraction. T cell fugetaxis was also shown to play a physiological role in the exit of mature T cells from the thymus and may contribute to a novel mechanism by which HIV-1 and certain forms of cancer evade the immune system.[72],[73],[74],[75] More recently, other chemokines, such as eotaxin-3, CXCR3 ligands, and IL-8 were shown to act as chemorepellents for human monocytes, dendritic cells and neutrophils, respectively.[76],[77],[78] Furthermore, recent studies have shown that high levels of SDF-1 production by transplanted cells resulted in the survival of the allograft in diabetic mice, significant reductions in their blood glucose levels and T cell infiltration into the transplanted tissue in contrast to control group where the transplanted cells were rejected and the mice remained diabetic.[79] (Figure 3-1)

## 3.5 Hypothesis

The basis for this research topic is that exogenous SDF-1 can improve skin wound healing by altering the dynamics of recruitment of CXCR4-expressing cells, including inflammatory cells (such as lymphocytes), endothelial progenitor cells, and several other types of stem cells. Standardized quantification of the main characteristics of wound healing, such as re-epithelialization, wound contraction, angiogenesis, cell proliferation and collagen deposition, is necessary to evaluate the effect of SDF-1. The dosage and delivery time period of SDF-1 to the wound site is critical to ensure attraction of stem cells and repulsion of inflammatory cells.

# Chapter 4

# Materials and Methods

## 4.1 Rationale for Design of Experiment

The basis for this study is to investigate the effect of exogenously applied SDF-1 on dermal wound healing. This model uses a full-thickness excision wound in mice grafted with a Collagen-GAG dermal scaffold. Wild-type C57BL/6 mice were used as they have been shown to have limited regeneration and poor healing with scar formation.[80] Although there are significant anatomical and physiological differences between rodent skin and human skin, the mouse model is a convenient and commonly used animal model for studying dermal wound healing kinetics.[81]

The scaffold has two purposes: (a) it is a convenient delivery vehicle for SDF-1 in to the wound, and (b) it has been shown to significantly reduce contraction when grafted in to skin defects in rodents.[82] Since contraction accounts for more than 95% of the healing process in rodents as compared to humans[13], the use of the scaffold may facilitate observation of important biological events that could be relevant to human dermal wound healing. In contrast, humans heal less through contraction and more through re-epithelialization except in areas around joints.[81]

A group of animals were pre-treated with GCSF subcutaneous injections prior to surgery in order to increase circulating levels of stem cells through mobilization from the bone marrow.[52] Exogenous GCSF has not been widely tested in burns, but appears to have positive effects on the immune system

in animal studies and without adverse effects in burn patients.[83] GCSF may also contribute locally to the wound healing process, as it has been shown to enhance bone marrow cell differentiation into vascular endothelium and speed up angiogenesis in a hindlimb-ischemic model.[84] Though the use of GCSF in order to release cells from the bone marrow is not a clinically relevant protocol, this study was designed at the onset to maximize potential therapeutic effects.

Thus, to test the hypotheses related to the goals of this research study, four groups of animals were selected. Untreated animals grafted with a scaffold serve as the baseline Control group. In addition, three treated groups grafted with a scaffold of GCSF only (GCSF), a combination of GCSF and SDF-1 (GCSF+SDF-1) and SDF-1 only (SDF-1) will help elucidate the effect of GCSF and SDF-1 on wound healing.

## 4.2 Materials

Male homozygous $29 - 35$ day old wild-type mice (C57BL/6) were purchased from Charles River Laboratories (Wilmington, MA) and maintained in accordance with National Research Council guidelines. Animal were housed in an AAALAC (Association for Assessment and Accreditation of Laboratory Animal Care) accredited facility at the Shriners Burns Hospital for Children-Boston.

Recombinant mouse CXCL12/SDF-1$\alpha$ was purchased from R&D Systems (Minneapolis, MN). The 50 $\mu$g of SDF-1$\alpha$ was diluted in 5 mL of 1X PBS and 100 $\mu$L of this solution was administered per treatment for a dosage of 1 $\mu$g/mouse.[67] GCSF was purchased as commercially available Neupogen (Filgrastim) in 300 MCG/mL concentration from Amgen (Thousand Oaks, CA). The 1 mL of Filgrastim was diluted in 9 mL of 0.9% saline (Baxter Healthcare, Deerfield, IL) solution. For 300 $\mu$g/kg GCSF dosage per animal, 200 $\mu$L of the solution was administered per animal.[52]

The 1 mm thick Collagen-GAG (matrix of bovine collagen and chondroitin-6-sulfate, a shark-derived glycosaminoglycan) dermal scaffold was manufactured in-house to match the thickness of murine skin using collagen obtained from Integra Life Sciences (Appendix B). Apart from differences in the pore structure (pores are of uniform size), porosity (top surface of scaffold has less porosity) and cross-linking method (dehydrothermal instead of glutaraldehyde treatment), it is similar to the

commercially available Integra$^{TM}$ product used in humans.

## 4.3 Methods

### 4.3.1 Experimental Design and Wound Model

All procedures on animals were approved by the Subcommittee on Research Animal Care at the Massachusetts General Hospital. Mice were housed five animals per cage before surgery or any treatment and individually caged post wounding in standard microisolator polycarbonate caging. Animal rooms were maintained at $64-79°$F with $30-70\%$ humidity on a 12-hour light/dark cycle. Commercial rodent ration (LabDiet 5P00 Prolab RMH3000) was provided ad libitum as was acidified (pH 2.5) water to protect against opportunistic infections.

Wound healing in the animals was examined at an early time-point three days post wounding (Day 3) and on the day of closure by macroscopic gross appearance (closure day was Day 18).

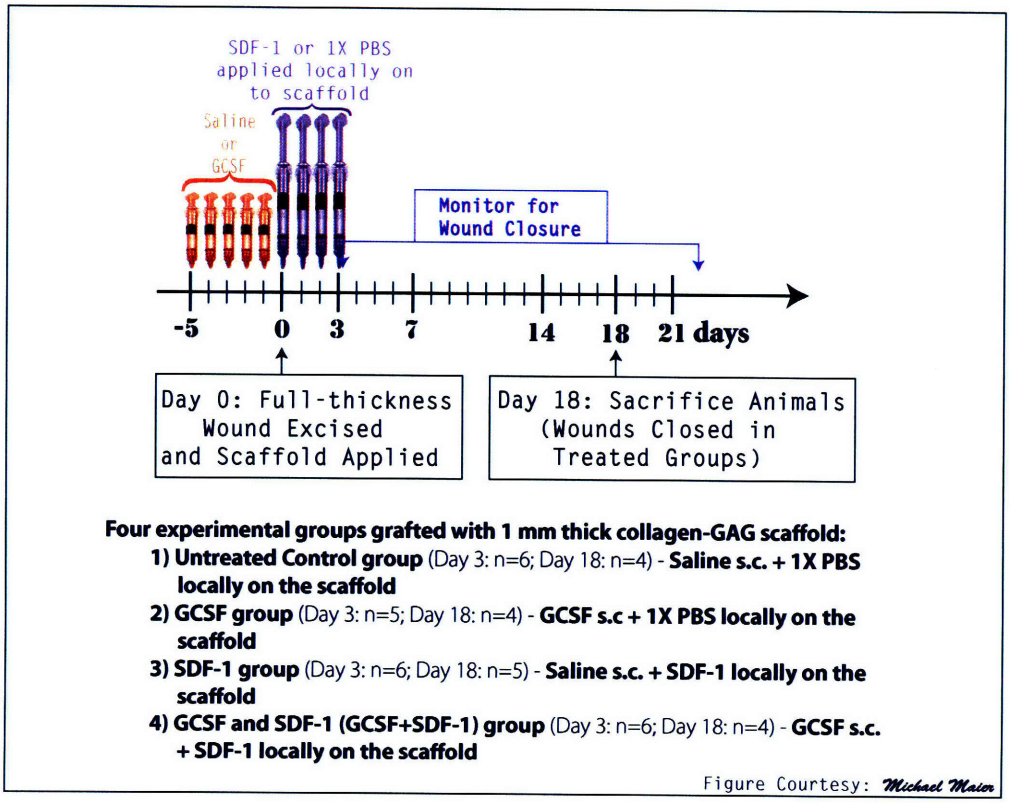


Figure 4-1: **Timeline of Experiment**

*The animals were divided in to the following four experimental groups* (Figure 4-1):

1. **Control group** (Day 3: n=6; Day 18: n=4) - The animals were pre-treated with 300 $\mu$g/kg daily subcutaneous saline injections for 5 days prior to surgery. 100 $\mu$L of 1X PBS solution was administered locally on to the wound once a day for 4 days.

2. **GCSF group** (Day 3: n=5; Day 18: n=4) - The animals were pre-treated with 300 $\mu$g/kg GCSF daily subcutaneous injections for 5 days prior to surgery. 100 $\mu$L of 1X PBS solution was administered locally on to the wound once a day for 4 days.

3. **GCSF and SDF-1 (GCSF+SDF-1) group** (Day 3: n=6; Day 18: n=4) - The animals were pre-treated with 300 $\mu$g/kg GCSF daily subcutaneous injections for 5 days prior to surgery. 100 $\mu$L of SDF-1$\alpha$ solution was administered locally on to the wound once a day for 4 days.

4. **SDF-1 group** (Day 3: n=6; Day 18: n=5) - The animals were pre-treated with 300 $\mu$g/kg daily subcutaneous saline injections for 5 days prior to surgery. 100 $\mu$L of SDF-1$\alpha$ solution was administered locally on to the wound once a day for 4 days.

### 4.3.2 Surgical Procedure and Wound Model

One day prior to surgery, the animals were shaved and depilated (Nair®, Church & Dwight Co., Princeton, NJ). On the day of the surgery (Day 0), the mice were weighed and anesthetized with 60 mg/kg Nembutal (Pentobarbital). The dorsal skin was marked with a standardized 1.0 $cm^2$ template. A full-thickness wound was created on the dorsal area of the mouse by excising a 1 cm X 1 cm square of skin (epidermis, dermis and panniculus carnosus). An equivalent piece of Collagen-GAG dermal scaffold (skin substitute) was grafted on to the wound ensuring that its porous bottom surface was in contact with the wound bed. After grafting the wound, 100 $\mu$L SDF-1 was administered on top of the scaffold for the SDF-1 and GCSF+SDF-1 groups. The Control and GCSF groups received an equivalent amount of 1X PBS solution. Benzoin Tincture Compound (Paddock Laboratories, Minneapolis, MN) was applied around the wound margins. Once dry, the wound area was covered with a semi-occlusive polyurethane dressing (Tegaderm$^{TM}$, 3M, St. Paul, MN). This

thin, transparent dressing transmits oxygen but prevents excessive evaporation. The subsequent 100 $\mu$L SDF-1 or 1X PBS solution treatments were given once a day for 3 additional days by injecting the solution on top of the scaffold without disturbing the Tegaderm dressing. (Figure 4-2)

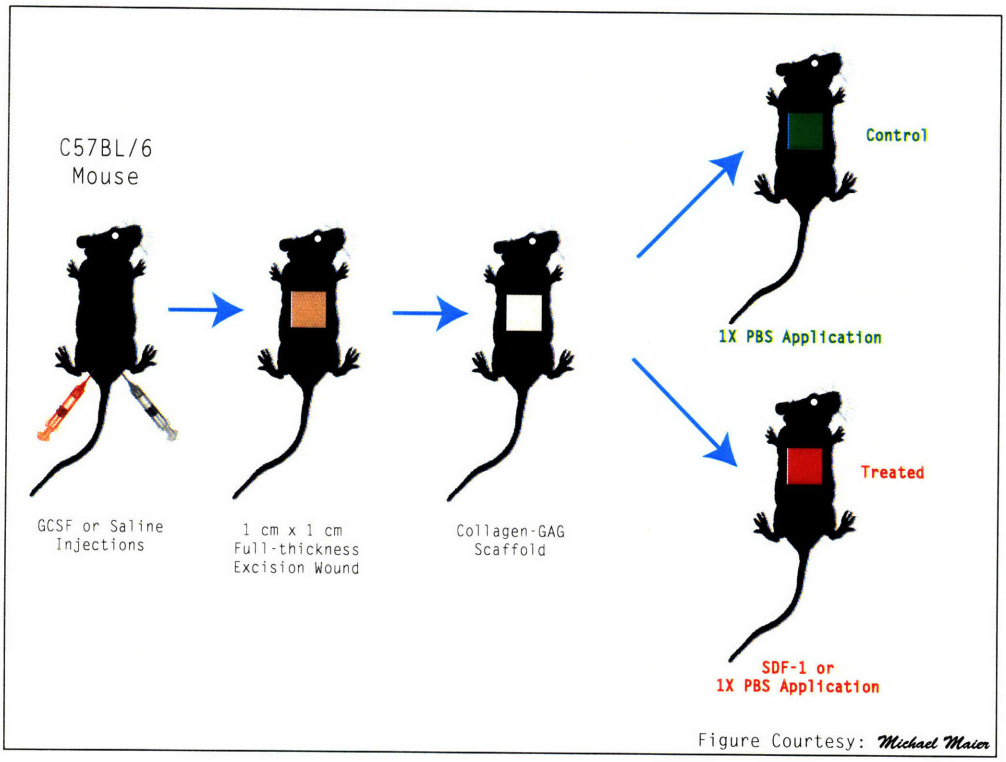


Figure 4-2: **Wound Model and Surgical Procedure**

Three days post surgery, animals from the Day 3 group were euthanized via Isoflurane inhalation (Isoflurane, USP, NOVAPLUS, Lake Forest, IL, USA) and the wounds were prepared for histological examination. The rest of the animals were monitored daily till re-epithelialization was observed macroscopically in the SDF-1, GCSF and GCSF+SDF-1 groups on Day 18 $\pm$ 5 hours and then sacrificed. The wounds were harvested en block including the surrounding skin and underlying tissue areas. Wound tissues were fixed in 10% neutral-buffered formalin solution for 24 hours and then stored in 70% alcohol at 4°C.

Wounds were digitally photographed with a Canon PowerShot Pro1 8.0 megapixels camera from a standard height using an Aurich tripod on the day of surgery (Day 0) prior to application of the Tegaderm dressing and the day the animals were sacrificed (Day 3 and Day 18).

## 4.4 Histological and Morphometrical Analysis

Central wound cross-sections were embedded in paraffin, sectioned in to 5 $\mu$m sections and stained according to standard Hematoxylin and Eosin (H&E), Masson's Trichrome and immunohistochemistry (PECAM-1, Ki67, $\alpha$-SMA) protocols. The histological images were photographed using a Nikon Labophot (Japan) microscope equipped with a Polaroid DMC2 color camera (Concord, MA) with analysis software version v2.1. In order to ensure consistency in the comparison of the histological sections, all images were taken from the same area of the histological slide and compared to their respective H&E images of 10X magnification.

Lateral wound margins in the histological sections were determined by the presence of appendages (hair follicles, sweat glands) and an organized epidermis and dermis. The healed wound area on Day 18 in comparison had fewer or no appendages and an altered epidermal and dermal structure.[85] In the early time-point Day 3 histological sections, the grafted scaffold was clearly evident in the wound bed.[47]

### 4.4.1 Macroscopic Wound Closure Analysis

The initial wound size on Day 0 and the final wound size of the re-epithelialized wound (Day 18) were measured from the digital macroscopic wound photographs. For quantification of the wound area, the raw digital files were imported into NIH ImageJ software v1.40g (Image J, NIH, Bethesda, MD) for processing. Planimetry was used to calculate the scar area by comparing wound contraction as a percentage of the initial wound area.[85] Macroscopically, the borders of the wound area was defined by the dermal edges enclosing a region without hair growth. (Figure 4-3 and Figure 4-4).

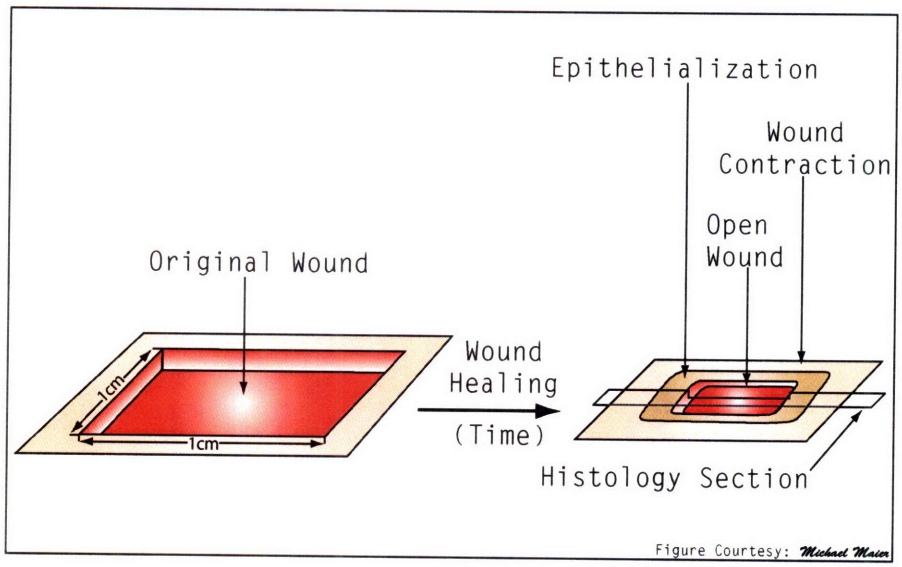


Figure 4-3: **Stylized Illustration of Parameters of Wound Analysis**

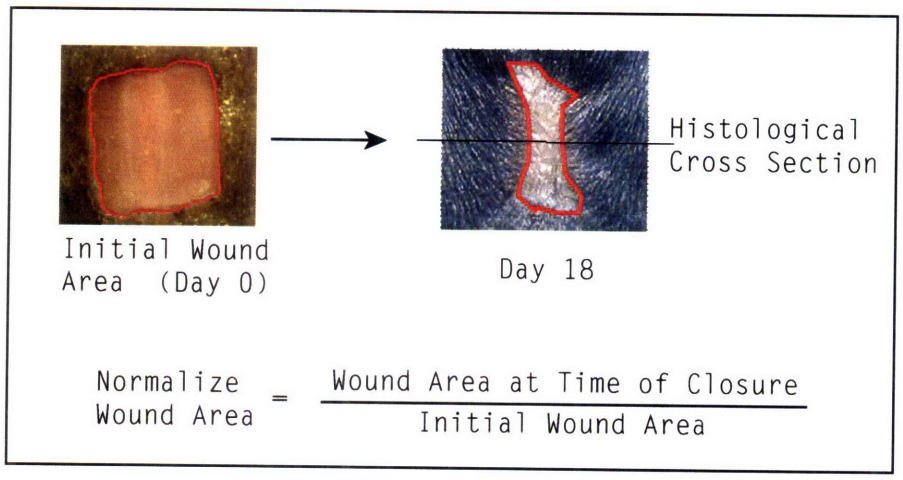


Figure 4-4: **Macroscopic Quantification of Wound Area**

### 4.4.2 Tissue Morphology

H&E stain was performed to visualize and compare the wound morphology of the early time point (Day 3) and re-epithelialized wound (Day 18) among animal groups.[86] Images were taken in the center of each histological section at 4X, 10X and 40X magnifications for both Day 3 and Day 18 animal groups. The digital images at 40X magnification were taken in the center of the wound scaffold area. The 4X magnification helped maximize the wound closure area being photographed.

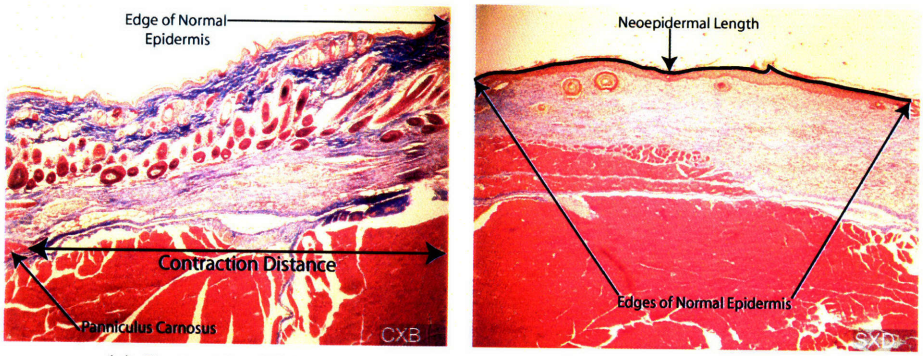


(a) Contraction Distance

(b) Neoepidermal Length

Figure 4-5: **Microscopic Quantification of Wound Area**

### 4.4.3 Collagen Analysis

After deparaffinization and rehydration, central wound sections from the Day 18 animal group were stained with Masson's Trichrome to visualize collagen fibers in the wound bed and surrounding tissue area of the various animal groups. Digital images of the Masson's Trichrome stained histological sections were taken at 4X, 10X and 40X magnifications for each slide. The Neoepidermal Length (NL) and Contraction Distance (CD) were measured using planimetry after processing the digital images via NIH ImageJ v1.40g software. The Neoepidermal Length defines the distance of re-epithelialization between the edges of a distinct multi-layer neoepidermis. Contraction Distance was defined as the distance between the panniculus carnosus in the uninjured normal dermis to the junction between the normal epidermis and the neoepidermis (Figure 4-5). CD was measured on both lateral aspects of the wound and averaged.

The maturation of collagen fibers was investigated using polarized light in Masson's Trichrome stained wound sections, where the tissue specimens were viewed through polarizing filters oriented at 90°.[47] Polarized light microscopy images were taken in the center of the wound area of each histological section at 10X magnification. In addition, 10X magnification images of the normal dermis in each histological section were also taken for comparison.

### 4.4.4 Immunohistochemistry Procedure: Cell Proliferation and Endothelial Cell Markers

The paraffin-embedded central wound sections from the Day 3 animal group were rehydrated using a decreasing alcohol chain and stained for cell proliferation (Ki67) and endothelial cell (PECAM-1) markers according to standard protocols (Appendix A).[86] The tissue sections stained with the primary antibodies, PECAM-1 (Pharmingen, San Jose, CA) and Ki67 (LabVision, Freemont, Ca), were incubated at 4°C overnight. The tissue sections for endothelial cell markers were treated with 40 $\mu$g/mL Proteinase K (Roche Diagnostics Corp., Indianapolis, IN)) for 20 minutes at 37°C. Antigen retrieval for the Ki67 cell proliferation marker was accomplished by microwaving in 10 mM sodium citrate (pH 6.0) for 10 minutes. Signals were then intensified using a tyramide amplification system (PerkinElmer, Boston, MA).

### 4.4.5 Quantification of Cell Proliferation Rate

The cell proliferation rate in Day 3 wound tissue of the various animal groups was analyzed using the Ki67 stain.[86] High-power 40X magnification digital images of Ki67 stained wound sections were used to measure the number of Ki67 positive cells (brown nuclei) relative to the total number of nuclei present in the center of the wound scaffold area of each histological section. The cell proliferation rate was quantified over the entire wound section using 3 fields per histological section (one in the middle of the granulation tissue and two on either lateral aspect) and expressed as a percentage of proliferating nuclei (Ki67 positive) to total nuclei. The cell proliferation results of the various animal groups were then plotted together and statistical analysis was performed.

### 4.4.6 Quantification of Blood Vessels

The capillary and blood vessel densities in Day 3 wound tissue from the various animal groups were analyzed using the PECAM-1 (CD31) stain.[86] The endothelial cell density was evaluated by assessing 3 fields per histological stained slide (one in the middle of the wound scaffold area and two on either lateral aspect) at 40X magnification. Blood vessels (CD31 positive brown nuclei) in

each high-powered field image were counted using Adobe Photoshop CS software (Adobe Systems Incorporated, San Jose, CA). Only those histological slides that did not exhibit excessive background staining were considered. The mean values of the results were graphed and statistical analysis was performed.

### 4.4.7 Immunohistochemistry Procedure: Myofibroblast Cell marker

Histological slides from the Day 18 animal group were analyzed for the presence of $\alpha$-smooth muscle actin ($\alpha$-SMA) expressing myofibroblast cells using a standard staining protocol.[87] Briefly, the deparaffinized histological slides were treated with 0.1% trypsin (Sigma Chemical Co., St. Louis, MO) to facilitate antibody penetration for 1 hour at room temperature. Endogenous peroxidase was quenched with 3% hydrogen peroxide (Sigma). Nonspecific sites were blocked with 1% goat serum (Sigma) for 30 minutes. The slides were then incubated at room temperature with anti-$\alpha$-SMA (Clone 1A4, Monoclonal, Sigma Chemical Co., St. Louis, MO) at 1:400 dilution for 1 hour. Next, the slides were incubated with biotinylated goat anti-mouse IgG secondary antibody (Sigma) for 30 minutes followed by 15 minutes of incubation with affinity-purified avidin (Sigma). The labeling was done with the use of the aminoethyl carbazole (AEC) chromogen kit (Zymed Laboratories Inc., South San Francisco, CA) for 10 minutes. Counterstaining with Mayer's hematoxylin for 5 minutes was followed by a tap water wash and the application of coverslips with glycerol gelatin. Negative controls of each histological section were also performed, which were stained with Myeloma $IgG_{2\sigma}$ instead of the primary antibody.

### 4.4.8 Quantification of Myofibroblast Cells

The myofibroblast cell densities in Day 18 wound tissue of the various animal groups were analyzed using the $\alpha$-SMA stain.[87] Cells were identified as SMA-positive if they displayed the reddish-brown color for the chromogen used in the $\alpha$-SMA staining and the intensity of their color was comparable to that of the smooth muscle cells present in the walls of blood vessels. Digital images of the histological wound sections at 4X magnification were used to measure the relative percentage of $\alpha$ SMA-positive

cell area in the total wound tissue area via the NIH ImageJ software v1.40g and planimetry. Due to the high $\alpha$ SMA-positive cell density and the overlap of the cells in the histological sections, the area of $\alpha$ SMA-positive cells was calculated as there was difficulty in accurately determining the number of individual cells present. The results were graphed and statistical analysis was performed.

### 4.4.9 Statistical Analysis

Results are expressed as mean $\pm$ standard deviation. Independent Student's t-test (two-tailed) analysis was used to evaluate significant differences between two treatment groups. A p-value $<0.05$ was considered significant.

# Chapter 5

# Results

## 5.1 Modulation of Wound Healing Kinetics

In this study, changes in wound-healing kinetics (contraction and re-epithelialization) were compared between the SDF-1 treated group, GCSF treated group, GCSF+SDF-1 treated group and the Control group (un-treated wounds).

### 5.1.1 Macroscopic Wound Closure Analysis

The wounds were followed macroscopically post-surgery (Day 0) until wound closure (re-epithelialization) was observed.[85] By macroscopic observation, when the gross surface of the wound area exhibited a similar appearance as that of the surrounding un-wounded normal skin region with no redness being evident, it was determined that wound closure (re-epithelialization) had occurred. By Day 18 all the groups except the Control group had closed and a marked decrease in the wound surface area was observed ($p < 0.005$) (Figure 5-1, Appendix K).

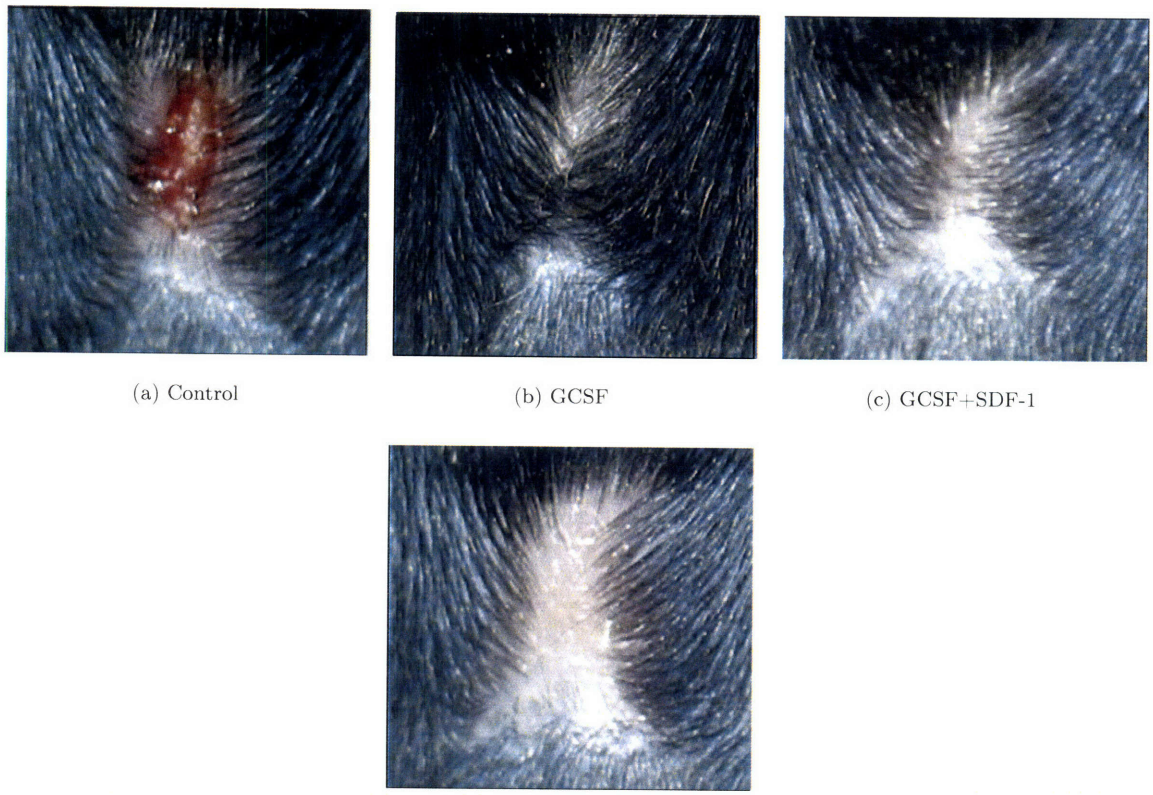

(a) Control (b) GCSF (c) GCSF+SDF-1

(d) SDF-1

Figure 5-1: **Macroscopic Photos of Study Groups (Day 18 post-surgery)**

which is mainly attributable to differences in contraction rate. Macroscopic wound closure was quantified using digital photographs of the wound area taken on Day 0 and Day 18 of the study. The scar tissue area was quantified as a percentage of the initial wound area.

### Wound Closure (Re-epithelialization) Rate

The SDF-1 treated group exhibited the fastest wound closure of all groups and re-epithelialization was observed by Day $16 \pm 5$ hours post-surgery. The GCSF+SDF-1 treated group demonstrated faster wound closure as compared to the GCSF and Control groups and re-epithelialization was observed by Day $17 \pm 5$ hours post-surgery. The GCSF group exhibited the slowest wound closure among all the treated groups and re-epithelialization was observed by Day $18 \pm 5$ hours post-surgery. The wounds in the Control group were not re-epithelialized by gross macroscopic observation on

Day 18 and closed only by Day $25 \pm 5$ hours.

### Wound Contraction Rate

By Day 18, the SDF-1 closed wounds were $8.86 \pm 0.85\%$ of their initial wound area (Day 0) and showed a significant inhibition of wound contraction when compared to all other study groups ($p < 0.002$). The GCSF+SDF-1 closed wounds were $3.34 \pm 0.48\%$ of their initial wound area (Day 0) and showed a significantly greater contraction as compared to the SDF-1 and Control groups ($p < 0.0001$), but less contraction as compared to the GCSF group ($p < 0.0004$). The GCSF wounds closed by stellate scar formation and were $0.98 \pm 0.27\%$ of their initial wound area (Day 0), demonstrating the most contraction amongst all the study groups ($p < 0.0004$). The wounds in the Control group had not closed by gross macroscopic observation on Day 18 and they were $6.53 \pm 0.59\%$ of their initial wound area (Day 0). The Control wounds showed a significant inhibition of contraction only when compared to the GCSF and GCSF+SDF-1 treated groups ($p < 0.0004$) (Figure 5-2).

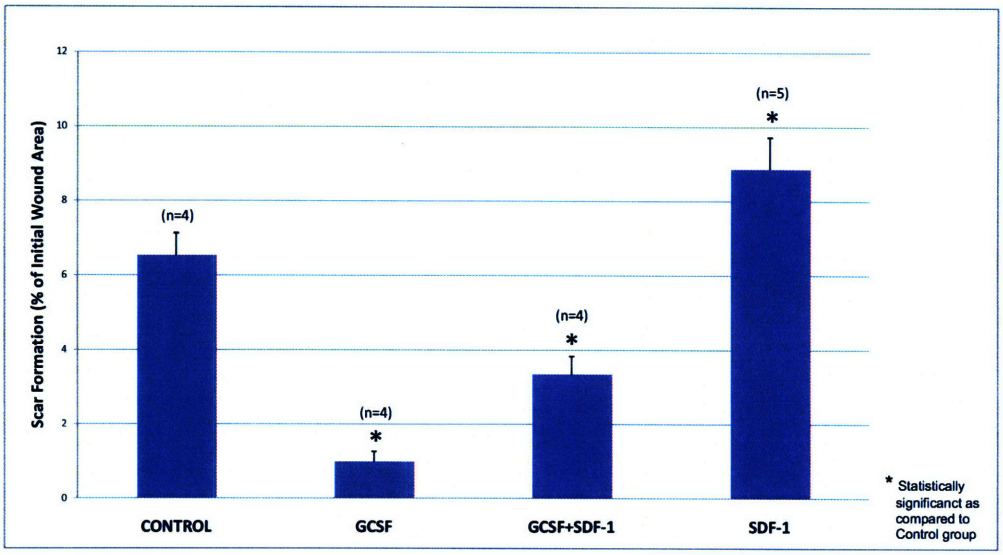


Figure 5-2: **Macroscopic Analysis of Scar Area (%) (Day 18 post-surgery)**

| Statistics | Control | GCSF | GCSF+SDF-1 | SDF-1 |
|---|---|---|---|---|
| **Average** | 6.532 | 0.989 | 3.342 | 8.862 |
| **Standard Deviation** | 0.591 | 0.277 | 0.486 | 0.859 |

Table 5.1: **Scar Area** (%)

| p-value | Group comparison types | ttest value |
|---|---|---|
| $p < 0.05$ is significant | Control versus SDF-1 | 0.00202 |
| | Control versus GCSF+SDF-1 | 0.000195 |
| | Control versus GCSF | 0.0000450 |
| | GCSF versus GCSF+SDF-1 | 0.000497 |
| | GCSF versus SDF-1 | $0.699E-5$ |
| | SDF-1 versus GCSF+SDF-1 | $1.089E-5$ |

Table 5.2: **Scar Area Analysis**

### 5.1.2 Results of Macroscopic Wound Closure Analysis

The SDF-1 treated group exhibited the fastest rate of wound closure (re-epithelialization) and the most significant inhibition of wound contraction. When compared to the Control group, the SDF-1 group exhibited faster wound closure by 36%.

### 5.1.3 Microscopic (Histological) Wound Closure Analysis

Wound tissue for histological assessment by Masson's Trichrome stain was collected on Day 18 when all the animals in the treated groups had achieved wound closure by re-epithelialization and digital images of the Masson's Trichrome stained histological sections were taken at 4X magnification for each slide (Appendix G). The lateral margins of the neoepidermis were distinguishable from the surrounding normal uninjured epidermis by its "smoothened" appearance and by its lack of appendages (hair follicles, sweat glands).[85],[27] The Neoepidermal Length (NL) microscopically

measures the distance of re-epithelialization between the edges of a distinct multi-layer neoepidermis. Contraction Distance (CD) microscopically measures the distance between the panniculus carnosus in the uninjured normal dermis to the junction between the normal epidermis and the neoepidermis (Figure 4-5). The wound contraction rate, which is a reduction in the wound size by a centripetal movement of skin from the margins of the defect, correlates with the Neoepidermal Length and the Contraction Distance. Thus, the greater the Neoepidermal Length and the lesser the Contraction Distance, the more wound contraction is inhibited.

### Neoepidermal Length

By Day 18, the Neoepidermal Lengths of the SDF-1, GCSF+SDF-1 and GCSF closed wounds were $3.36 \pm 1.2$ mm, $3.04 \pm 0.9$ mm and $2.1 \pm 0.74$ mm respectively. Of all the wounds in the Control group, only one had re-epithelialized by Day 18 and the Neoepidermal Length of the wounds was $1 \pm 0.8$ mm. There was a significant difference in Neoepidermal Lengths between the un-treated Control group and the treated SDF-1 and GCSF+SDF-1 groups ($p < 0.01$). However, there was no statistically significant difference observed between the Control and GCSF groups ($p < 0.09$), or amongst the treated groups ($p < 0.6$) (Figure 5-3).

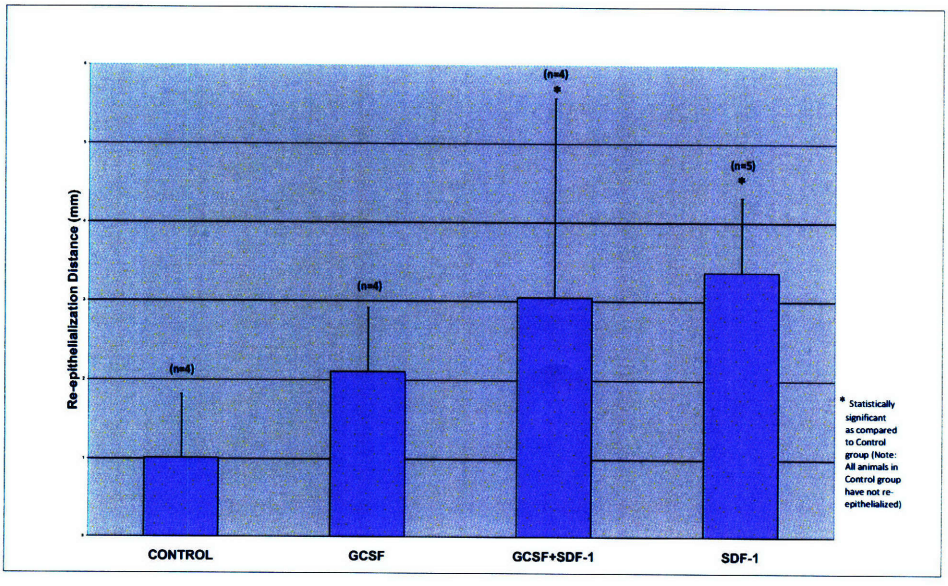


Figure 5-3: **Microscopic Analysis of Neoepidermal Length (mm) (Day 18 post-surgery)**

| Statistics | Control | GCSF | GCSF+SDF-1 | SDF-1 |
|---|---|---|---|---|
| **Average** | 1.009 | 2.104 | 3.048 | 3.369 |
| **Standard Deviation** | 0.829 | 0.740 | 0.900 | 1.232 |

Table 5.3: **Neoepidermal (Re-epithelialization) Length (mm)**

| p-value | Group comparison types | ttest value |
|---|---|---|
| $p < 0.05$ is significant | Control versus SDF-1 | 0.011 |
| | Control versus GCSF+SDF-1 | 0.015 |
| | Control versus GCSF | 0.096 |
| | GCSF versus GCSF+SDF-1 | 0.158 |
| | GCSF versus SDF-1 | 0.100 |
| | SDF-1 versus GCSF+SDF-1 | 0.665 |

Table 5.4: **Neoepidermal Length Analysis**

### Wound Contraction Distance

By Day 18, the SDF-1 closed wounds had contracted the least ($3.17 \pm 0.94$ mm) and exhibited a significant inhibition of wound contraction when compared to the Control and GCSF groups ($p < 0.001$). However, there was no statistically significant difference in Contraction Distance between the SDF-1 and GCSF+SDF-1 groups ($p < 0.16$). The GCSF+SDF-1 closed wounds had contracted by $5.47 \pm 2.53$ mm, which was not significantly different from the other study groups ($p < 0.7$). The GCSF closed wounds had contracted by $6.24 \pm 0.8$ mm, and showed a significantly higher Contraction Distance than the SDF-1 group ($p < 0.001$) but not the Control or GCSF+SDF-1 groups ($p < 0.59$). The wounds in the Control group had contracted by $5.99 \pm 0.8$ mm, which was significantly more than the SDF-1 group ($p < 0.001$) but not the GCSF or GCSF+SDF-1 groups ($p < 0.6$) (Figure 5-4).

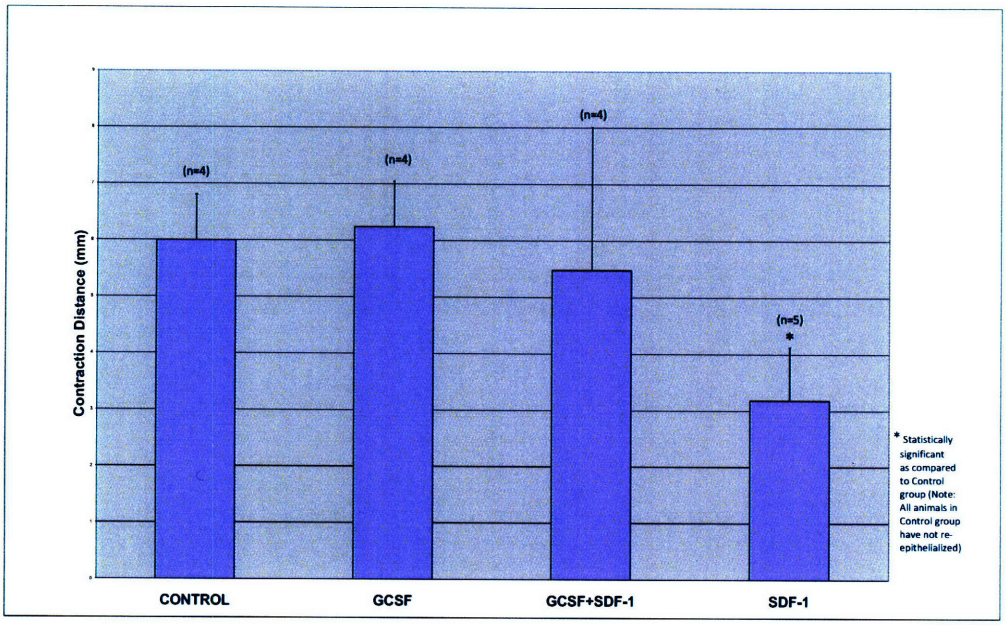


Figure 5-4: **Microscopic Analysis of Contraction Distance (mm) (Day 18 post-surgery)**

| Statistics | Control | GCSF | GCSF+SDF-1 | SDF-1 |
|---|---|---|---|---|
| **Average** | 5.993 | 6.241 | 5.475 | 3.178 |
| **Standard Deviation** | 0.807 | 0.808 | 2.531 | 0.945 |

Table 5.5: **Contraction Distance (mm)**

| p-value | Group comparison types | ttest value |
|---|---|---|
| $p < 0.05$ is significant | Control versus SDF-1 | 0.001 |
| | Control versus GCSF+SDF-1 | 0.718 |
| | Control versus GCSF | 0.679 |
| | GCSF versus GCSF+SDF-1 | 0.598 |
| | GCSF versus SDF-1 | 0.001 |
| | SDF-1 versus GCSF+SDF-1 | 0.166 |

Table 5.6: **Contraction Distance Analysis**

### 5.1.4 Results of Microscopic Wound Closure Analysis

The SDF-1 treated group exhibited the most significant inhibition of wound contraction.

## 5.2 Analysis of Tissue Morphology

In order to compare the wound morphology of both the early time point (Day 3) and closed (re-epithelialized) wounds (Day 18), H&E stain was performed on the histological sections and digital images were taken of each slide at 4X, 10X and 40X magnifications.[86] In the Day 3 wounds, the Control group showed the maximum cell infiltrate (blue nuclei) qualitatively when compared to the treated (SDF-1, GCSF+SDF-1 and GCSF) groups. There was no significant difference observed qualitatively between the treated groups in the amount of cell infiltrate in the wound area. (Figure 5-5, Appendix C).

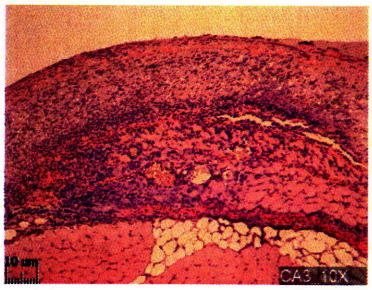


(a) Control

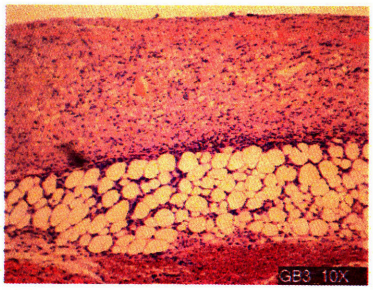


(b) GCSF

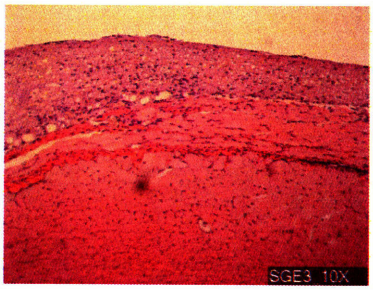


(c) GCSF+SDF-1

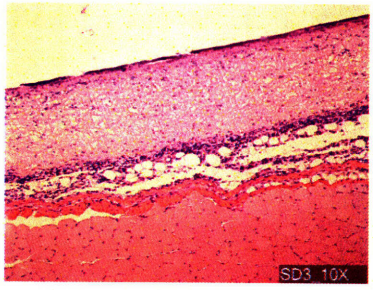


(d) SDF-1

Figure 5-5: **Cell Infiltration in Study Groups (Day 3 post-surgery)**

In the Day 18 wounds, the wound areas were completely epithelialized in all the treated (SDF-1,

GCSF+SDF-1 and GCSF) groups. There was no significant difference observed qualitatively in the granulation tissue area or re-epithelialized region amongst the treated groups. In the Control group, only one wound had completely re-epithelialized by Day 18. (Figure 5-6, Appendix D).

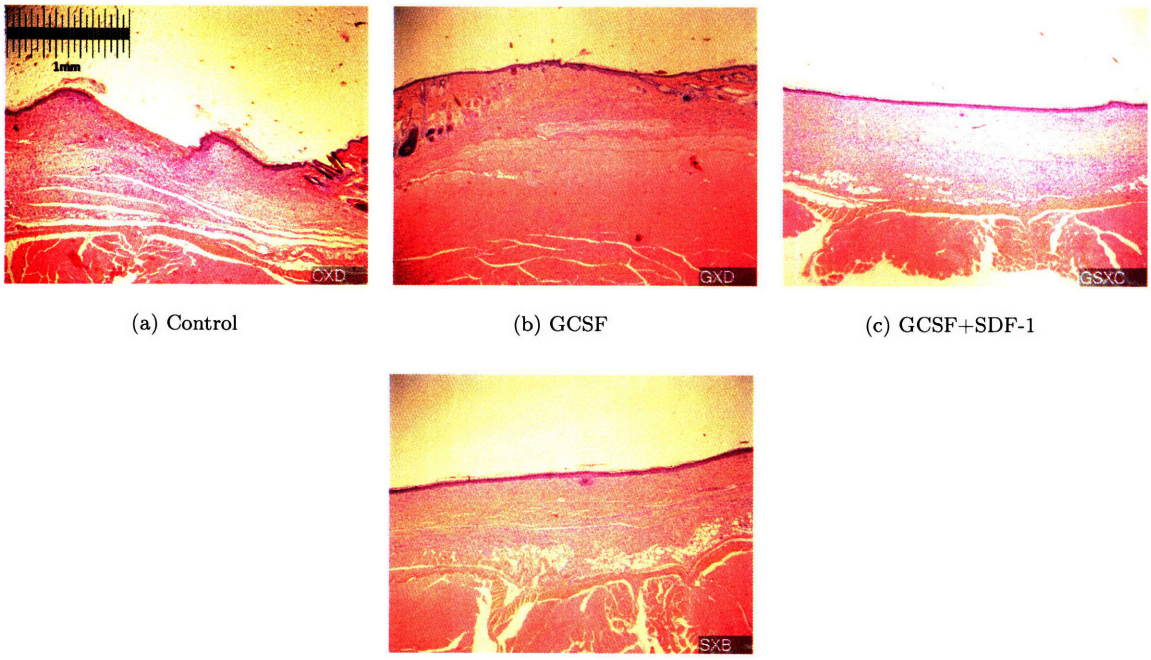


(a) Control (b) GCSF (c) GCSF+SDF-1

(d) SDF-1

Figure 5-6: **Tissue Morphology of Study Groups (Day 18 post-surgery)**

### 5.2.1 Results of the Tissue Morphology Analysis

The treated (SDF-1, GCSF+SDF-1 and GCSF) groups demonstrated less cell infiltrate qualitatively in the wound area when compared to the Control group in the early time-point (Day 3). Also, all the wounds in the treated groups had re-epithelialized by Day 18 but not in the Control group.

## 5.3 Analysis of Quality of Scar Tissue: Wound Collagen Deposition and Orientation

Another objective of this study was to assess the quality of the scar tissue. Digital images of the Masson's Trichrome stained histological sections taken at 4X, 10X and 40X magnifications of the

wound area were qualitatively analyzed (Figure 5-7, Appendix E).[47]

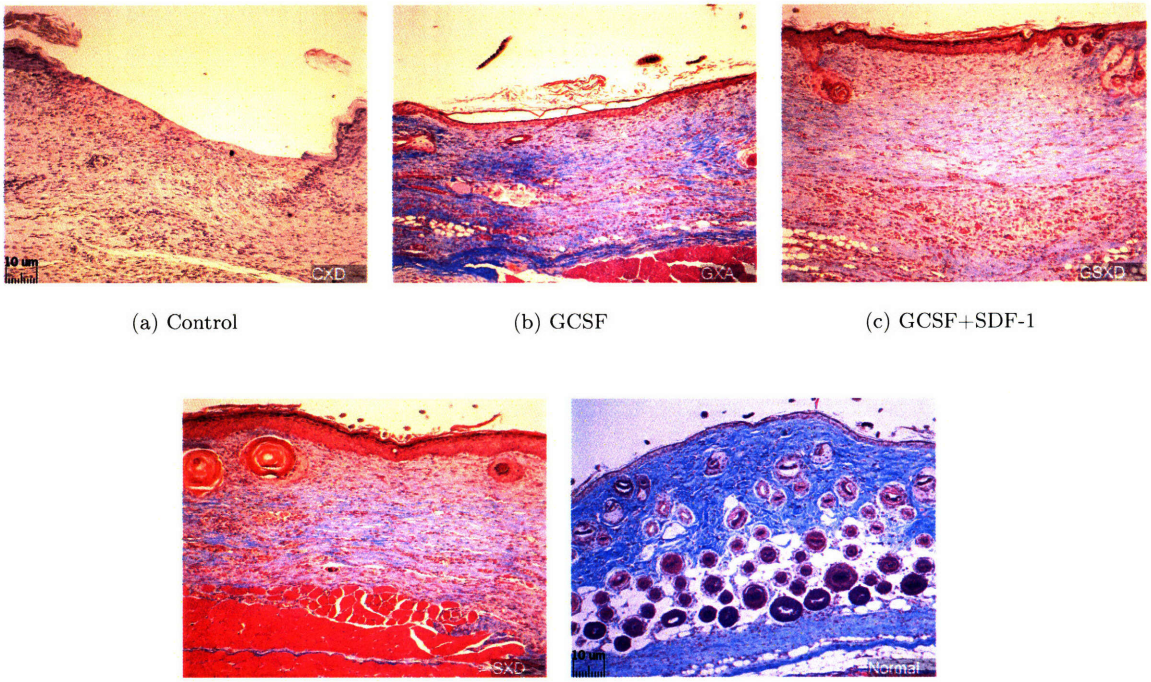


(a) Control (b) GCSF (c) GCSF+SDF-1

(d) SDF-1 (e) Normal Dermis

Figure 5-7: **Collagen Morphology in Study Groups and Normal Dermis (Day 18 post-surgery)**

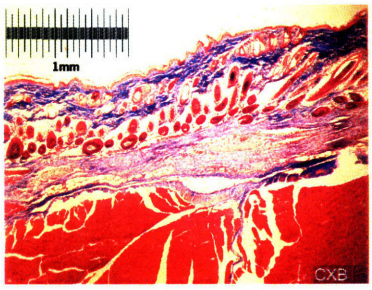


Figure 5-8: **Scar Extending in to Normal Dermis**

It was apparent that 18 days post-surgery (Day 18), the collagen bundle organization and cell density in the scar area of all wound groups (treated and un-treated) were not comparable to the surrounding un-wounded normal skin. The collagen fibers in the normal dermis were mature (darker blue), more wavy, thicker and inter-woven. In contrast, the collagen fibers in the scar area were

immature (light blue), thinner and aligned in an orderly manner parallel to the epidermis, which is typical for immature scar tissue.[47] Another indication of the collagen bundles being organized in a parallel fashion was that most of the fibroblast cells in the scar area were oriented parallel to the epidermis. There was no significant difference observed qualitatively in the collagen deposition and orientation in the scar area amongst the treated groups (SDF-1, GCSF+SDF-1 and GCSF) (Figure 5-7). The wound area in the Control group showed significantly less collagen deposition as compared to the treated groups since the wounds had not completely re-epithelialized. An interesting observation was noted with regards to the spread and distribution of the scar tissue. In all the study groups, the underlying scar tissue (light blue immature collagen) extended beyond the wound region and well in to the normal dermis region, stretching either above or below the panniculus carnosus in some tissue sections (Figure 5-8).

The histological sections were also examined under polarized light microscopy and digital images were taken at 10X magnification of the scar area and the surrounding un-wounded normal dermis for each slide. By qualitative observation, it was evident that the scar collagen of the treated (SDF-1, GCSF+SDF-1 and GCSF) groups exhibited weak birefringence as compared to the normal dermal collagen (Figure 5-9, Appendix F). This is indicative of immature scar tissue.[88] Examination of the scar areas in the treated groups showed that the collagen fibers were slightly more mature in the middle and lower part of the scar tissue. There was no significant difference observed qualitatively in the birefringence of the scar collagen amongst the treated groups. The scar collagen in the Control group exhibited almost no birefringence since the wounds had not completely re-epithelialized.

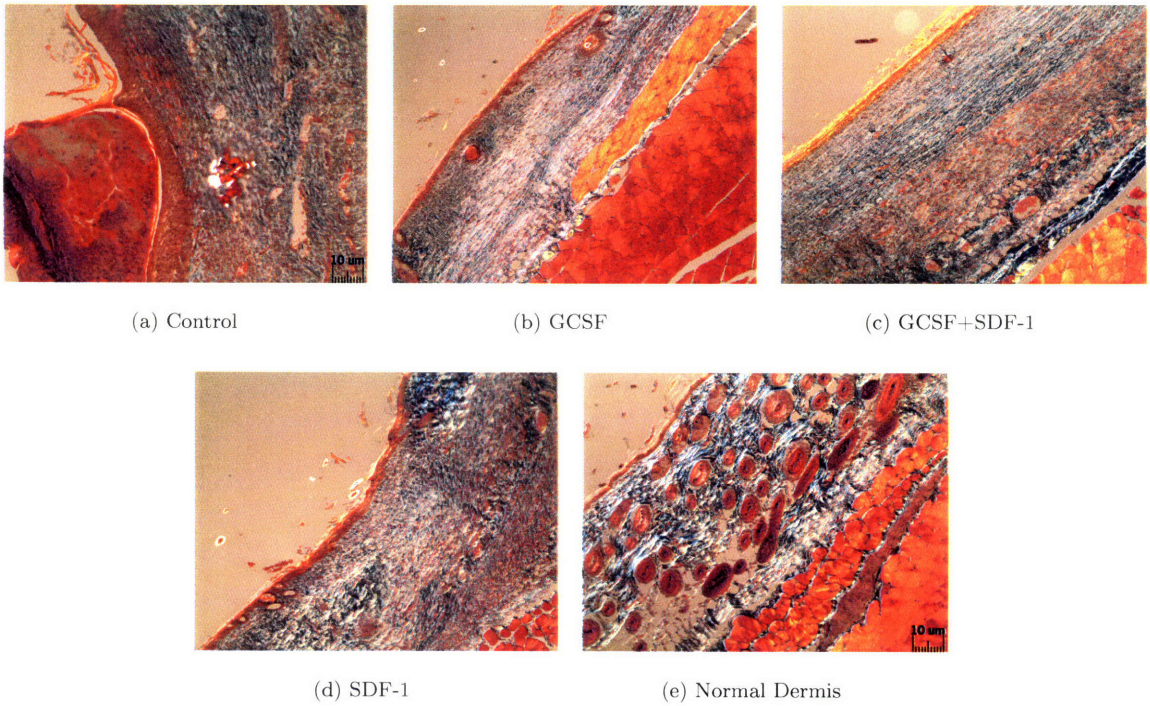


(a) Control (b) GCSF (c) GCSF+SDF-1

(d) SDF-1 (e) Normal Dermis

Figure 5-9: **Birefringence of Collagen in Study Groups and Normal Dermis (Day 18 post-surgery)**

### 5.3.1 Results of the Quality of Scar Tissue Analysis

The treated (SDF-1, GCSF+SDF-1 and GCSF) groups demonstrated the typical orderly collagen deposition and orientation as well as weak birefringence that is indicative of immature scar tissue when qualitatively compared to the un-wounded normal dermis. Since all the wounds in the Control group had not re-epithelialized by Day 18, the wound areas exhibited significantly less collagen deposition and almost no birefringence when compared to the treated groups.

## 5.4 Analysis of Cell Proliferation in Wound

The number of proliferating cells in the center of the wound scaffold area of each histological section was quantified per high-power field (40X magnification) at the early time-point (Day 3 post-surgery)[86] (Figure 5-10, Appendix H).

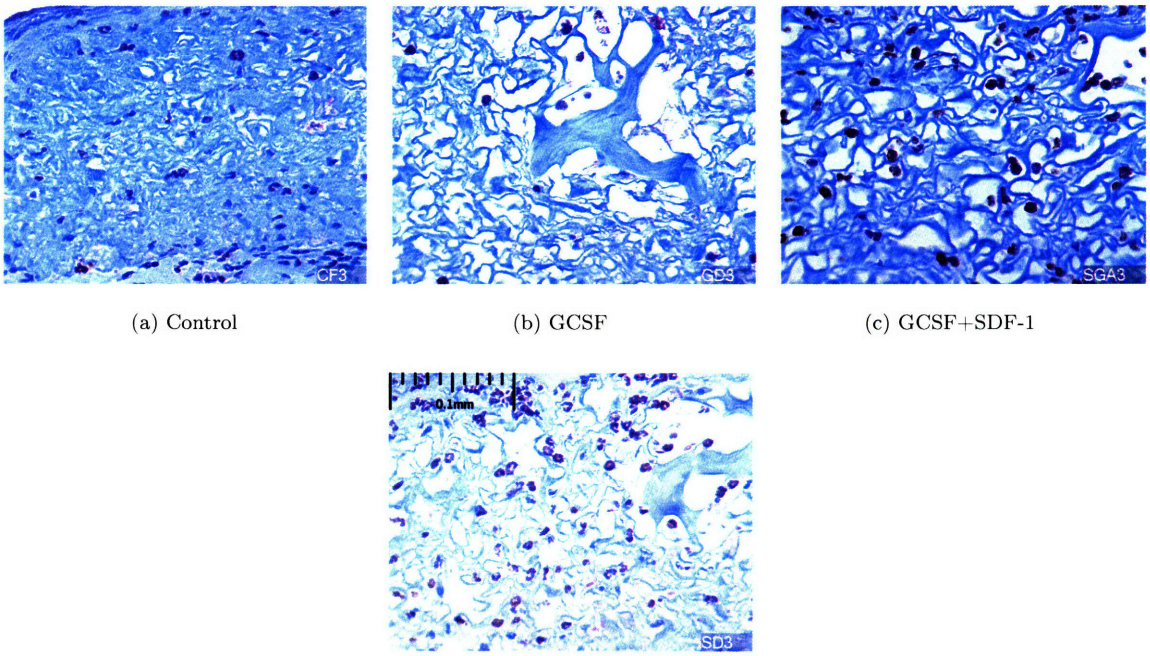


(a) Control (b) GCSF (c) GCSF+SDF-1

(d) SDF-1

Figure 5-10: **Cell Proliferation (Ki67+) in Study Groups (Day 3 post-surgery)**

There was a statistically significant difference observed in the cell proliferation rate between the SDF-1 and Control groups ($p < 0.04$) (Figure 5-11).

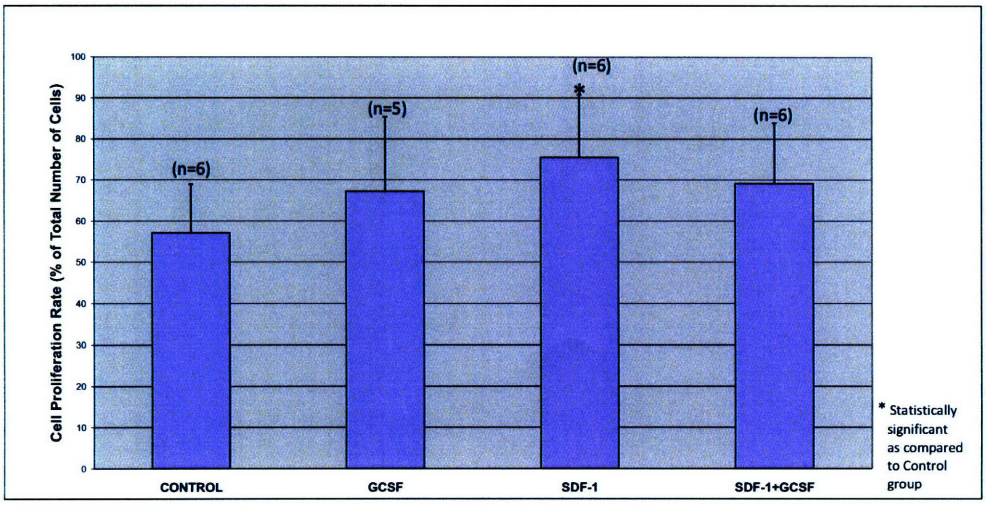


Figure 5-11: **Cell Proliferation Rate (%) (Day 3 post-surgery)**

| Statistics | Control | GCSF | GCSF+SDF-1 | SDF-1 |
|---|---|---|---|---|
| **Average** | 57.076 | 67.257 | 75.509 | 69.177 |
| **Standard Deviation** | 11.926 | 18.207 | 15.282 | 14.810 |

Table 5.7: **Cell Proliferation Rate (Ki67+)** (%)

| p-value | Group comparison types | ttest value |
|---|---|---|
| $p < 0.05$ is significant | Control versus SDF-1 | 0.043 |
| | Control versus GCSF+SDF-1 | 0.151 |
| | Control versus GCSF | 0.320 |
| | GCSF versus GCSF+SDF-1 | 0.854 |
| | GCSF versus SDF-1 | 0.444 |
| | SDF-1 versus GCSF+SDF-1 | 0.482 |

Table 5.8: **Cell Proliferation Rate Analysis**

However, there was no statistical difference observed between any of the other treated (GCSF+SDF-1 and GCSF) groups and the Control group, or amongst the treated (SDF-1, GCSF+SDF-1 and GCSF) groups.

### 5.4.1 Results of the Cell Proliferation in Wound Analysis

A statistical difference in the cell proliferation rate was observed only between the SDF-1 treated and Control groups in the center of the wound scaffold region 3 days post-surgery.

## 5.5 Analysis of Wound Vascularity

Wound vascularization was quantified as the number of endothelial cells and blood vessels present in the center of the wound scaffold region per high-power field (40X magnification) at the early time-point (Day 3 post-surgery)[86] (Figure 5-12, Appendix I).

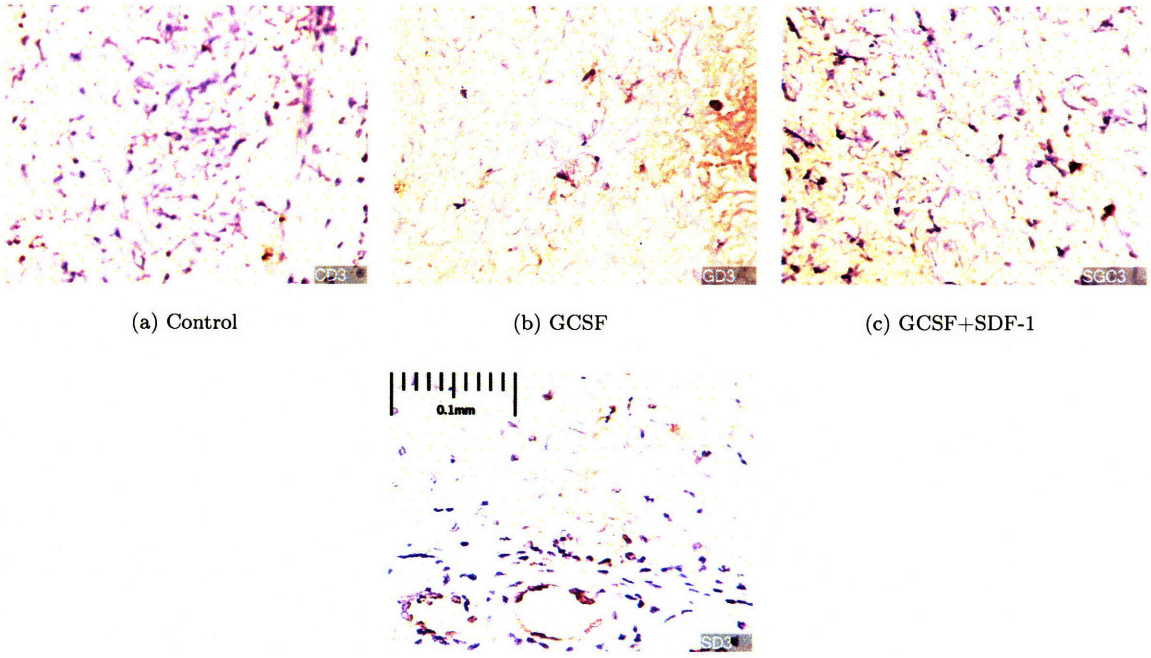


(a) Control (b) GCSF (c) GCSF+SDF-1

(d) SDF-1

Figure 5-12: **Endothelial Cell Count (CD31+) in Study Groups (Day 3 post-surgery)**

There was no statistically significant difference observed in the endothelial cell density between all the study groups (Figure 5-13).

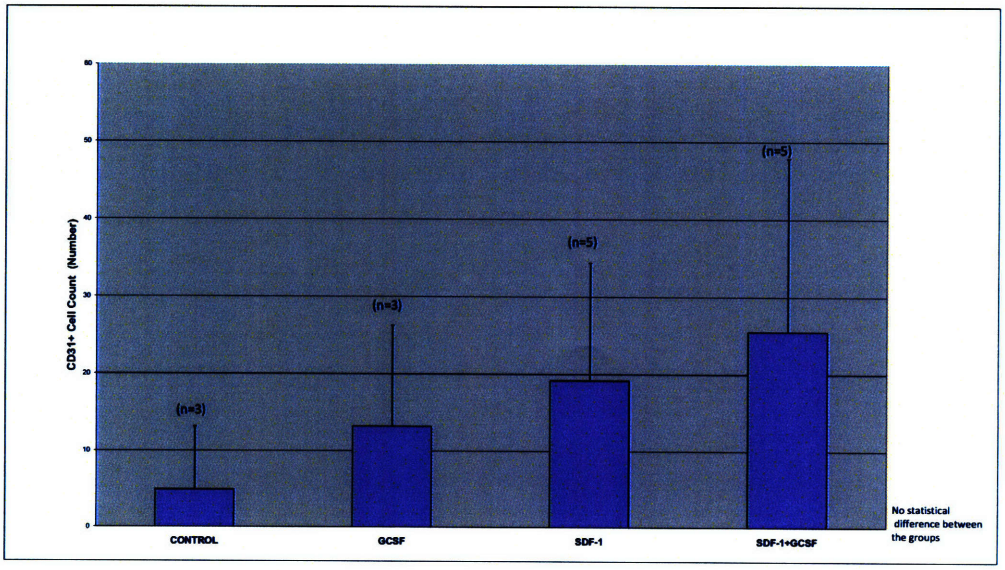


Figure 5-13: **Wound Vascularity (Day 3 post-surgery)**

| Statistics | Control | GCSF | GCSF+SDF-1 | SDF-1 |
|---|---|---|---|---|
| **Average** | 5 | 13.2 | 25.5 | 19.166 |
| **Standard Deviation** | 8.148 | 13.084 | 22.367 | 15.237 |

Table 5.9: **Endothelial Cell (CD31+) (Number)**

| p-value | Group comparison types | ttest value |
|---|---|---|
| $p < 0.05$ is significant | Control versus SDF-1 | 0.081 |
| | Control versus GCSF+SDF-1 | 0.077 |
| | Control versus GCSF | 0.265 |
| | GCSF versus GCSF+SDF-1 | 0.288 |
| | GCSF versus SDF-1 | 0.502 |
| | SDF-1 versus GCSF+SDF-1 | 0.580 |

Table 5.10: **Endothelial Cell Analysis**

### 5.5.1 Results of the Wound Vascularity Analysis

No statistically significant difference was observed amongst all the study groups (treated and untreated) in the endothelial cell density in the center of the wound scaffold region 3 days post-surgery.

## 5.6 Analysis of Myofibroblast Activity in Wound

The final objective of this study was to measure the relative percentage of $\alpha$ SMA-positive cells in the total wound tissue in closed (re-epithelialized) wounds (Day 18 post-surgery) using digital images of the histological wound sections at 4X magnification[87] (Figure 5-14, Appendix J).

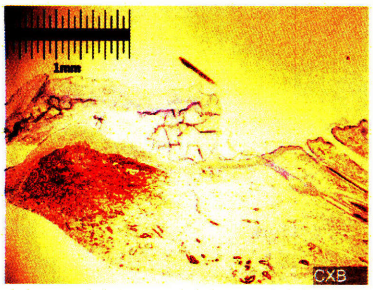


(a) Control

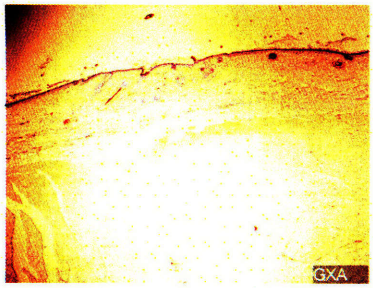


(b) GCSF

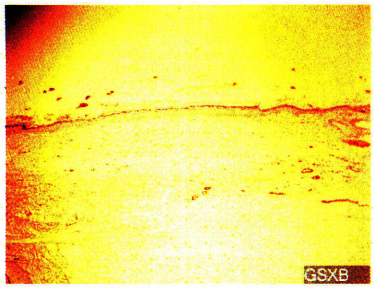


(c) GCSF+SDF-1


(d) SDF-1

Figure 5-14: **Myofibroblast ($\alpha$ SMA+) Cells in Study Groups (Day 18 post-surgery)**

However, the wounds in the Control group were not completely closed (re-epithelialized) on Day 18. The relative percentage of $\alpha$ SMA-positive cells in the SDF-1, GCSF+SDF-1, GCSF and Control groups were 14.34±5.5%, 13.18±8.38%, 5.15±1.12% and 12.41±13.02% respectively. In the Control and GCSF+SDF-1 groups, a large variation was observed within the individual group itself which accounts for the large standard deviation. There was a statistically significant difference between the GCSF and SDF-1 treated groups only ($p < 0.02$) in the relative percentage of $\alpha$ SMA-positive cells. Conversely, no statistical difference was observed amongst the other treated groups (SDF-1 and GCSF+SDF-1), or between the Control and treated (SDF-1, GCSF+SDF-1, GCSF) groups (Figure 5-15).

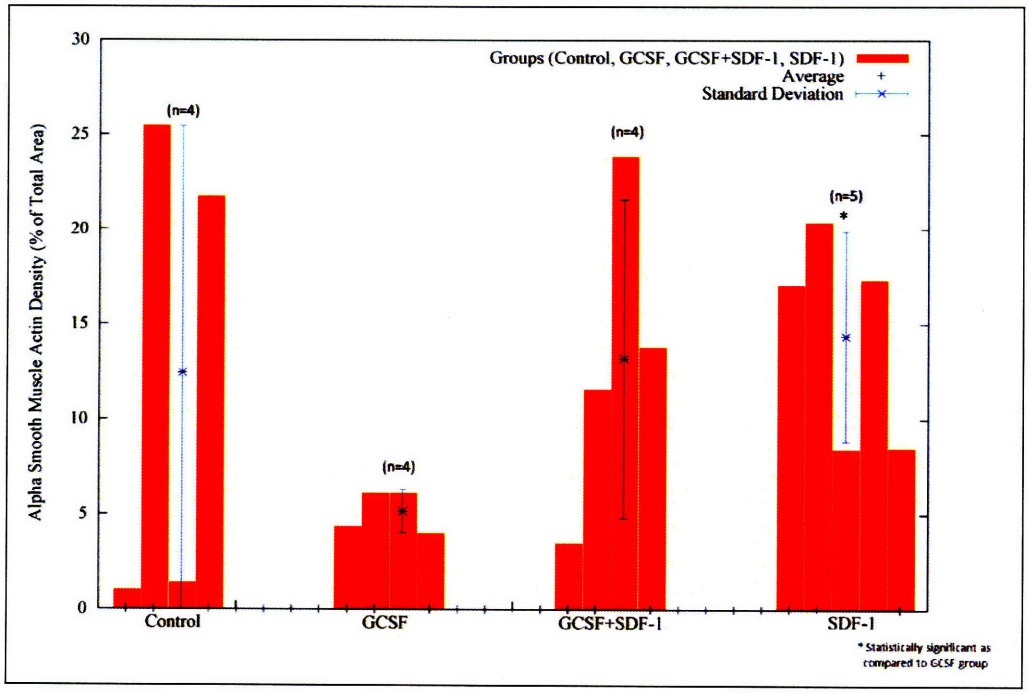


Figure 5-15: **Myofibroblast Cell Density (%) (Day 18 post-surgery)**

| Statistics | Control | GCSF | GCSF+SDF-1 | SDF-1 |
|---|---|---|---|---|
| **Average** | 12.416 | 5.159 | 13.185 | 14.347 |
| **Standard Deviation** | 13.025 | 1.125 | 8.380 | 5.514 |

Table 5.11: **Relative $\alpha$-SMA Area** (%)

| p-value | Comparison of Groups | ttest value |
|---|---|---|
| $p < 0.05$ is significant | Control versus SDF-1 | 0.654 |
| | Control versus GCSF+SDF-1 | 0.924 |
| | Control versus GCSF | 0.346 |
| | GCSF versus GCSF+SDF-1 | 0.150 |
| | GCSF versus SDF-1 | 0.022 |
| | SDF-1 versus GCSF+SDF-1 | 0.820 |

Table 5.12: **Relative $\alpha$-SMA Area Analysis**

Based on the data, it can be determined that the SDF-1 group exhibited the most relative percentage of $\alpha$ SMA-positive cells in the wound region while the GCSF group exhibited the least amongst all the treated groups. This interesting observation is also evident in $\alpha$ SMA-stained tissue sections of the wound area located approximately 2 mm superior to the central wound region. In addition, it was qualitatively observed that $\alpha$ SMA-positive cells were also present around the hair follicles in the surrounding un-wounded normal dermis region, with the SDF-1 group showing the most number of $\alpha$ SMA-positive cells and the GCSF group showing the least amongst the treated groups. (Figure 5-16) Thus, the data clearly indicates that the SDF-1 and GCSF+SDF-1 treated groups were undergoing further wound contraction 18 days post-surgery, whereas, the process of wound contraction in the GCSF treated group was nearly complete.

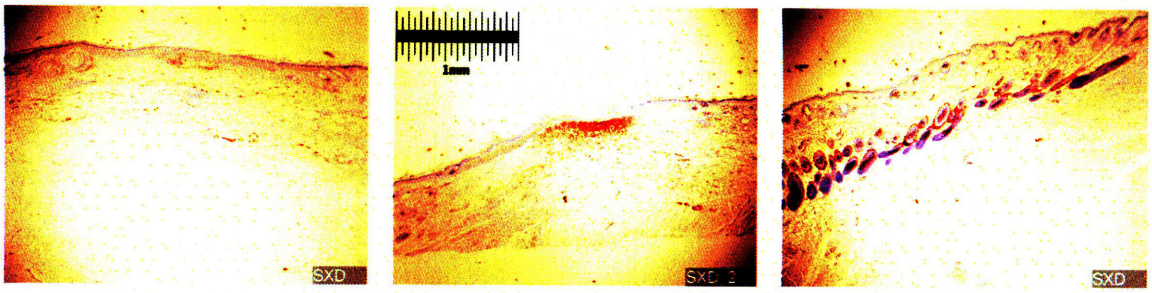


(a) SDF-1 (b) SDF-1 (c) Normal

Figure 5-16: **Myofibroblast ($\alpha$ SMA+) Cells in Wound and Normal Tissue Regions Superior to Central Wound Region (Day 18 post-surgery)**

### 5.6.1 Results of the Myofibroblast Activity in Wound Analysis

Wounds treated with SDF-1 experienced a comparable delay in wound contraction as the Control group. In contrast, the GCSF treatment appeared to promote wound contraction.

# Chapter 6

# Discussion

## 6.1 Discussion of Results

Topical application of Stromal cell Derived Factor-1 (SDF-1) in this study induced changes in wound-healing kinetics (contraction and re-epithelialization) compared to GCSF treated group, GCSF+SDF-1 treated group and spontaneous healing in un-treated wounds (Control group). A reproducible 1.0 $cm^2$ dorsal full-thickness excision wound model in wild-type mice was used to investigate the wound healing kinetics which was monitored macroscopically and microscopically. The SDF-1 treated group demonstrated the fastest rates of wound closure and cell proliferation as compared to the un-treated Control group, with re-epithelialization occurring more rapidly by 36%. The amount of early cell infiltrate in the SDF-1 group was also significantly less when compared to the Control group, which is indicative of a decreased inflammatory response in the SDF-1 group. Although they experienced the same overall delay in wound contraction as the Control group, wounds treated with SDF-1 exhibited a significant reduction in wound contraction during the initial healing process. However, there was no significant difference observed amongst the treated (SDF-1, GCSF+SDF-1 and GCSF) groups in early wound vascularization or in the quality of the scar tissue based on collagen deposition and orientation.

On the whole, the observed results were consistent with that reported in literature, demonstrating

a decrease in early inflammatory cell infiltration[79],[73] and increased wound re-epithelialization.[67],[56],[55] Prior experimental results have demonstrated that a small population of bone marrow-derived stem cells are present in circulation and that some of these bone marrow-derived endothelial cells contribute to the healing of cutaneous wounds by promoting epithelialization.[89] In addition, topically applied bone marrow-derived mesenchymal stem cells also enhanced dermal wound healing by accelerating angiogenesis and re-epithelialization.[90] Thus, the observed results of this study support the hypothesis that SDF-1 can improve skin wound healing by altering the dynamics of recruitment of CXCR4-expressing cells such as bone marrow-derived mesenchymal stem cells and endothelial cells. However, additional studies will be needed to determine the number of stem cells and endothelial cells that have been recruited into the wound site.

An alternative theory has been recently proposed where a study found that blocking endogenous levels of SDF-1 resulted in increased re-epithelialization and decreased eosinophil infiltration in second-degree dermal burn wounds 5 days post-wounding.[57] Discrepancies between the re-epithelialization results may be due to variations in the wound model, handling techniques, methodology and experimental model. A key difference is that the dermal burn wound study did not incorporate the use of scaffolds. Also, a second-degree burn injury model is not comparable to a full-thickness excision wound model and could yield different results. Furthermore, it is unclear as to what the long-term effects of blocking SDF-1 would be as complete re-epithelialization of the burn wounds had not occurred. In order to compare results across different studies, consistency in experimental methodologies and definitions is required.

## 6.2 Advantages of the Proposed Approach

The proposed approach for skin wound healing, using the well characterized full-thickness skin wound experimental model, could be applied to chronic wounds (eg. diabetic or venous ulcers), acute injuries (eg. burns) and elective surgeries, such as cosmetic procedures, with an estimated 2005 market of $1.6 billion per The Freedonia group.[91] Other potential applications include tissues that exhibit poor or incomplete regeneration after injury. Enhancing the healing of other injured

tissues, such as corneal scarring from corneal ulcers, spinal cord injuries, scarification of hand tendons and myocardial infarction, would provide enormous clinical benefit. In addition, the reduction of graft rejection and fibrosis around medical implants, such as stents and orthopedic implants, is another area which might prove helpful to clinicians.

## 6.3 Limitations of this Study

It is important to note the limitations of this study. There are known problems associated with the use of wild-type mice, such as their rapid dorsal hair re-growth rate which posed difficulties with wound dressing maintenance. It has been reported that maintaining the dressing through the follow up is crucial to prevent wound contamination.[92] The diabetic mouse (db/db) model is commonly used in dermal wound healing studies as db/db mice exhibit less contraction and a greater degree of epithelialization, which facilitates observation of the wound healing mechanisms, whereas wild-type mice heal approximately 90% by contraction.[92] However, it was opted to not use mouse models that exhibit underlying diseases in this study.

Additional difficulties in this study arose from the usage of the Collagen-GAG scaffold. The 1 mm thick scaffold was extremely fragile and susceptible to tearing which posed a significant challenge during the surgical procedure. Microscopic evaluation also showed non-degraded collagen scaffold fibers in some of the wounds with giant cells and other inflammatory cells in the scar tissue area.[47] In addition, the scaffold was also prone to infection.[45] Few studies have used Collagen-GAG scaffolds similar to Integra$^{TM}$ in mice. Alternatives such as the Alloderm$^{TM}$ acellular dermis, which have been extensively used in mice studies, could be considered instead.[93],[94]

Another drawback of this study is that the progression of wound healing was not observed over an extended time-course. Only the early time-point (Day 3) and closure time-point (Day 18) were evaluated. In order to investigate and further explore the healing mechanisms of the inflammatory phase, angiogenesis, wound contraction and re-epithelialization (keratinocyte migration), experiments at additional time-points (for example, defect contraction half-life at Day 9) would need to be conducted.[95] Additional studies at later time-points (for example, Day 30) are also required to

analyze the final scar tissue formed along with functional tests to test the tensile strength of the healed wounds.

## 6.4 Future Work

Additional studies are necessary to determine the optimal dosage and administration schedule of SDF-1 to maximize the wound healing benefits. Detailed characterization of the morphological and histological aspects of the wound healing dynamics (inflammation, angiogenesis, fibroblast migration, wound contraction, scar formation and re-epithelialization) would provide additional insight in to the underlying mechanism of action of SDF-1. Stem cell, endothelial progenitor cell and inflammatory cell activity can also be investigated, using cell culture, flow cytometry, quantitative (Q) PCR, Western blotting and immunohistochemistry or immunofluorescence techniques, to study the chemotactic and fugetactic (repellant) role of SDF-1 during wound healing. The dynamics of this process in the wound environment is important since the timing of cell recruitment and their subsequent differentiation likely determine the specific roles played by the stem cells and endothelial cells in the wound healing response. To characterize this phenomenon, the recruitment of stem cells and endothelial cells in a standardized full-thickness excision skin wound would need to be monitored. It remains to be seen whether the dosage and administration of SDF-1 can support a reduction in wound contraction recurrence long-term.

Although its half-life in vivo is unknown, SDF-1 can be cleaved and degraded by a wide array of proteolytic enzymes,[48] which may limit the effectiveness of SDF-1 in therapeutic settings. Thus, the use of new forms of SDF-1 that are resistant to proteolysis should be investigated, as they may help overcome this potential problem. These experiments would help determine the bioactivity of SDF-1 in this wound healing model. Although no murine model precisely emulates human wound healing, the db/db animal model could be considered as an alternative to the wild-type mouse model as it demonstrates reduced wound contraction and hair growth.[92]

It would be advantageous to incorporate the best SDF-1 dosage and administration strategy determined from above into a skin substitute using a controlled drug delivery method (Figure 6-1).

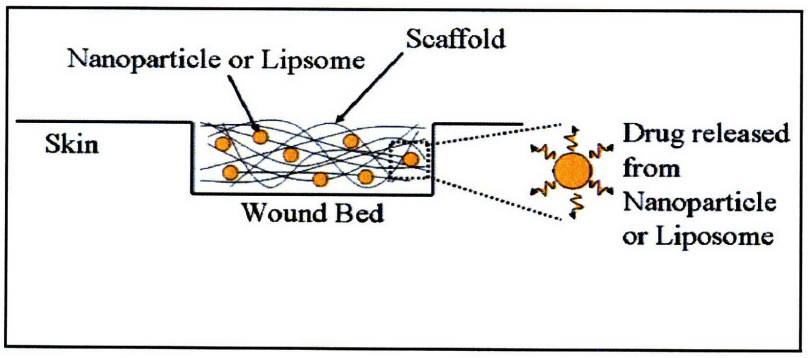


Figure 6-1: **Proposed Drug Delivery Approach of SDF-1 via a Scaffold**

This approach would eliminate the need for repeated manual administration of SDF-1 in to the wound site, thus resulting in less perturbation of the wound bed. Additional benefits include the meticulous maintenance of the scaffold and wound dressing along with more stringent control of infection, which are also important aspects necessary for the standardization of this experimental protocol. Multiple drug delivery schemes would need to be explored, such as nanoparticles made of polylactic-co-glycolic acid (PLGA), alternating polyelectrolyte layers and liposomes.[96],[97] In order to determine the optimal parameters of the delivery vehicle (such as, particle size, concentration of SDF-1 in the particle and concentration of particles in the scaffold), in vitro experiments testing the various drug delivery schemes would need to be performed to assess the release kinetics of SDF-1.

For clinically relevant studies, further experiments could extend this work to a porcine model of wound healing, which is more analogous and to human skin than rodents. The wound healing process should be characterized macroscopically and microscopically by multiple parameters, each one reflecting a major stage in the typical wound healing process: homing in of inflammatory cells, angiogenesis, fibroblast migration, wound contraction, re-epithelialization and scar tissue formation. Immunohistochemical studies to test for the presence of stem cells (hematopoietic and mesenchymal) and progenitor cells (endothelial) should also be considered. Functional tests to analyze the tensile strength and mechanical properties of the newly formed tissue in the healed wounds are also necessary. In addition, the solutions developed may be translated to in vivo therapeutic schemes for human patients.

## 6.5 Conclusion

In spite of advances made in the care and management of wounds, the goal of promoting faster healing with "scar-less" wound resolution remains unchanged. As Dr. Anthony Atala aptly remarked, "In tissue engineering, everything goes back to scar formation."[98] Wound healing is a complicated biological process requiring the appropriate balance of matrix and growth factors. Apart from causing physical deformity, adult wound healing in humans unfortunately results in the formation of fibrotic scar tissue which can hinder function and mobility of the organ.

As with dermal substitutes, the proposed approach of treating the scaffold with SDF-1 has demonstrated the ability to reduce wound contraction at early time points, which would be useful in the treatment of wounds in functional areas, such as joints. In addition, this approach also exhibited a faster rate of wound re-epithelialization as compared to un-treated wounds with the dermal scaffold alone. These results suggest that the SDF-1 treated-dermal matrix may be a new tool to stimulate wound closure and quality tissue formation in acute and chronic wounds. This approach would therefore be applicable to the regeneration of poorly healing tissues, and the development of such solutions would be of significant benefit to human health.

# Appendix A

# Immunohistochemistry Protocols for Cell Proliferation (Ki67) Stain and Endothelial Cell (CD31) Stain

IMMUNOHISTOCHEMISTRY STAINING – *PARAFFIN EMBEDDED SECTIONS*

**General explanation:**

1. To stain paraffin embedded sections, the paraffin material must first be removed and then the sample must be re-hydrated. Re-hydration also reactivates enzymes that must be blocked with H202.

2. Prior fixation with formalin has caused many proteins to cross-link preventing accessibility to surface antigens. These antigens are retrieved using a protease. When trying to detect an internal antigen, the cell membrane is broken by microwaving samples in a basic citrate releasing the internal antigen.

3. In order for the primary antibody to bind only to the antigen of interest, the samples are treated with an unspecific protein-based blocker *TNB* (that acts like a blanket). Now, the

antigen of interest is marked with its specific *primary antibody.* This antibody is a highly specific "rat anti-mouse antibody" made by injecting the mouse antigen into a rat.

4. A biotinlated anti-rat (mouse adsorbed) *secondary antibody* is then added (super-specific). The biotin unspecifically binds to negatively-charged molecules.

5. Streptavidin-HRP is then added to amplify the signal. Streptavidin is also negatively-charged molecule which binds to the Biotin, while HRP is an enzyme. Further amplification is achieved by adding Biotin, and then again adding S-HRP. Leaving biotin on the sample too long will cause unspecific binding to other less-negative molecules, reducing the specificity of the signal.

6. Finally, DAB chromagen is added and acts like a substrate for HRP. Positive staining for the antigen will cause a brown color change (can be instantaneous). If the activated chromagen is left on the samples too long the background will become brown. Stop the reaction by immersing slides in dH2O as soon as the positive cells have become brown, and minimal background has stained.

**General Instructions:**

1. Each container holds approximately 225-250mL of solution.

2. "wet" chamber: Place wet towels along the bottom of a common slide box. Close lid.

3. 1M PBS: dilute 10M PBS stock solution in dH2O (100ml 10M PBS:1000ml dH2O)

4. PBS-Tween: add 0.5ml Tween for every 1L of 1M PBS (Tween is a detergent)

5. Ammonium-H2O: dilute 0.5ml Ammonium Hydroxide (Menconi) (***Toxic!***) in 500 ml tap water.

6. 1M TRIS pH 8: prepare both 1M HCl Tris (acid) and 1M Base Tris (Basic) solving in d-water the powder, with a ratio 1l H2O: 1 weight in grams of the Formula Weight (FW, found on the box of the salts). Then mix the two solution adding acid to base until the needed pH is reached.

7. Citrate...

Items to be placed in *ice* when not in immediate use:

1. TNB
2. Primary Antibody
3. Secondary Antibody
4. Streptavidin-HRP *(light sensitive, wrap in foil!)*
5. Biotin
6. DAB dissolved in PBS

**Staining instructions:**

**DAY 1:**

1. Warm slides on heat plate (for at least 30'-1h), Temp. between 50- 60 °C

(NEVER > 60°C to prevent denaturation!)

1. Label slides with a xylene and Etoh resistant pen or regular lead pencil.
2. Deparrafinize with 2 washes of xylene (5min each)
3. Hydrate slides with an Etoh series, diluting Etoh in ddH2O. 100%(2mins)-95% (2mins)-85%(1min)-70%(1min)
4. dH2O rinse 1minute
5. Immerse in Xylene for 3x, 10 min each
6. REHYDRATION: immerse in alcohol baths of decreasing concentrations:

   (a) (100%, 100%, 90%, 70%, 70%, 50%) for 5min each.

Change the alcohol solution every 2 immersions

1. Wash in PBS: 3 times, 10 min each
2. Immerse slides in [30% H2O2] solution (diluted in methanol), *in dark*, for 20mins – methanol dilution: 25 ml of 30% H2O2 in 225 ml methanol
3. Wash in PBS for 3 times, 5 mins each

**CD-31 / CD45→** *SURFACE* ANTIGEN RETRIVAL

1. Prepare a water bath at 37 °C (start beforehand)
2. Prepare a [0.2M] Tris-H2O solution: dilute 1M Tris (basic pH=8.0) with dH2O 1ml:5ml (50 ml Tris in 200 ml dH2O).
3. Place [0.2M] Tris-H2O solution in water bath to equalize temperature before adding proteinase and slides.
4. Add 90$\mu$l of Proteinase K for every 50ml to Tris H2O solution *just before* immersion of slides.
5. Places slides in water bath: 20 mins
6. Wash in PBS 3 times, 5mins each

**Ki67→** *INTERNAL* ANTIGEN RETRIVAL

1. Immerse slides in citrate (pH=6. 10mM) and microwave slides until solution begins to boil (breaking cell membranes to expose antigen).
2. STOP microwave, and allow container to rest for 5-6 minutes.
3. Microwave slides again until solution begins to boil.
4. STOP microwave, and allow to *rest* until solution reaches room temperature (at least 20 minutes).
5. Wash in PBS 3 times, 5min each

→ SPECIFIC ANTIGEN ENHANCING:

1. Chose 1-2 sections per slide to stain. Wipe off other sections.
2. Dry the area around desired sections.
3. Draw a circle around the remaining sections with a marker (green, located in refrigerator)
4. Add 100-150$\mu$l TNB (allow to defrost beforehand), to sections and leave in wet chamber for 30mins at room temperature.
5. Shake off the agent
6. replace slides in wet chamber, and pipette the primary antibody (1$\mu$l:100$\mu$l in TNB for CD31, 1 : 200 for Ki67), approx. 70-80$\mu$l pipetted onto each section
7. leave in fridge overnight at 4°C

**DAY 2:**

1. Prepare PBS-Tween solution (as per above instructions)
2. Wash in PBS-Tween: 3x, 5min each
3. As you place slides in wet chamber, pipet secondary antibody (60-70$\mu$l) onto each section, then leave 1 hour at room temperature
   (a) Biotinlated Secondary Antibody: 1$\mu$l antibody:200$\mu$l in TNB
4. Wash in PBS-Tween, 3x, 5min each

AMPLIFICATION OF SIGNAL:

1. As you place slides in wet chamber, pipet Streptavidin-HRP (60-70$\mu$l) onto each section, then leave 30 min at room temperature
   (a) Streptavidin-HRP: 1$\mu$l:100$\mu$l in TNB

2. Wash in PBS-Tween, 3x, 5min each

3. Replace slides in wet chamber. Pipette Biotin on slides (1$\mu$l:50$\mu$l in amplification dilutant located in fridge), approx. 60-70$\mu$l pipetted onto each section. Biotin should remain *on each slide for **ONLY 4 minutes!*** **Important:** Be sure to notice the time as you pipette so that the Biotin is not left on too long!

4. After the 4 min, place slides in PBS-Tween, and wash 3x, 5 min each.

5. Repeat the amplification with streptavidin-HRP: As you place slides in wet chamber, pipette Streptavidin-HRP (60-70$\mu$l) onto each section, then leave 30 min at room temperature

6. Wash in PBS-Tween, 3x, 5min each

ACTIVATION:

1. Prepare chromagen agent:

   (a) Dissolve 1/2 a tablet of DAB (located in fridge, ***very toxic***) in 5mL PBS

   (b) Only activate 2-3 mL of this solution at one time.

      i. To activate chromagen, add 1$\mu$l 30% H2O2 per 1 mL DAB/PBS solution.

2. Also have two containers of dH20 prepared.

3. Bring slides (in PBS-Tween chamber), dH20 containers, and activated DAB solution to light microscope.

4. Place slide on microscope under 10x magnification,

5. Activation is often instantaneous. Therefore, once a few drops (approx 3 drops) of activated DAB solution ***(Toxic!)*** is evenly placed on sections, look under microscope and STOP the reaction once the positive-staining structures are darkened (brown) by placing slide in *dH20.* **Important:** Waiting too long to STOP reaction will cause the background to stain as well!

COUNTERSTAIN:

1. Fill 1 container with Hematoxylin; make sure there is no layer of film on top (Hematoxylin can be reused- but after a film starts to form, it should only be used 5 or 6 more times). If there is a film filter the Hematoxylin (remove the film).
2. Fill another container with tap water.
3. Immerse slides in Hematoxylin for 1 min.
4. Immerse slides in water for a few seconds, change water immediately at least one time.
5. Leave slides in the container with constant water flow (not too strong) for at least 10 min.
6. Fill one container with Ammonium-H2O as per above instructions.
7. After the 10 min in water, dip slides in Ammonium-H2O 10 times.
8. Put them back in tap water.

COVERSLIPS:

1. Dehydrate tissue with 70% (1 min) 85% (1 min) 100% (1min) 100% (3mins) make sure slide labeled area is covered with 100%. There should be no H2O molecules on the slide or labels of the slides
2. Rinse in Xylene to remove PapPen 2x 5 minutes
3. Cover Slip with Permanent mount. Push air bubbles out from beneath the slide with a pipette tip (*very important:* small air bubbles will appear *much* larger under a microscope!)
4. Place slides on aluminum foil to dry

# Appendix B

# Protocol for Manufacture of Collagen-GAG Scaffold

### C.1. Collagen-Glycosaminoglycan (CG) Suspension Protocol

**SUPPLIES**

1. 3.6 gm type I microfibrillar bovine tendon collagen (Integra LifeSciences, Inc., placeCityPlainsboro, StateNJ); store at 4°C.
2. 2991.3 ml distilled, deionized water
3. 8.7 ml Glacial Acetic Acid (Mallinckrodt Chemical Co., placeCityParis, StateKY)
4. 0.32 gm Chondroitin 6-sulfate from shark cartilage (Cat. No. C-4383, Sigma-Aldrich Chemical Co., placeCitySt. Louis, ,StateMO); store at 4°C.

**EQUIPMENT**

1. Suspension cooling system (Brinkman cooler model RC-2T, Brinkman Co., placeCityWestbury, StateNY)

2. Suspension mixer (Ultra Turrax T18 Overhead blender, IKA Works, Inc., placeCityWilmington, StateNC)

3. Peristaltic pump (Manostat Cassette Pump, Cat. No. 75-500-000, placeCityManostat, State-New York, NY)

**PROCEDURE**

1. Turn on the cooling system (Brinkman model RC-2T) for the blender (Ultra Turrax T18 Overhead blender, IKA Works) and allow the mixing chamber to cool to 4°C (~30 minutes).

2. Prepare a 0.05 M acetic acid (HOAc) (pH 3.2) solution: add 8.7 ml HOAc (Glacial Acetic Acid, Mallinckrodt Chemical Co.) to 2991.3 ml of distilled, deionized water in the chemical fume hood. This solution has a shelf life of approximately 1 week.

3. Blend 3.6 gm of microfibrillar bovine tendon collagen with 600 ml of 0.05 M acetic acid at 15,000 rpm (Blender Setting: 3.25) for 90 minutes at 4°C.

4. Prepare the chondroitin 6-sulfate solution: dissolve 0.32 gm chondroitin 6-sulfate (from shark cartilage: Cat. No. C-4384, Sigma-Aldrich) in 120 ml of 0.05 M acetic acid.

5. Calibrate the peristaltic pump (Manostat Cassette Pump, Cat. No. 75-500-000) to 120 ml per 15 minutes.

6. Add the 120 ml chondroitin 6-sulfate solution dropwise to the blending collagen dispersion over 15 minutes using the peristaltic pump, while maintaining the blender at 15,000 rpm (Blender Setting: 3.25) and 4°C.

7. Blend the collagen-GAG suspension an additional 90 minutes at 15,000 rpm (Blender Setting: 3.25) at 4°C.

8. Degas the collagen-GAG suspension in a vacuum flask for 60+ minutes until bubbles are no longer present in the solution.

9. Store the suspension in a capped bottle at 4°C; it will keep for up to four months.

10. If collagen-GAG suspension has been stored for more than one week, re-blend it for fifteen minutes at 10,000 rpm (Blender Setting: 2) at 4°C and degas again.

C.2. **Collagen-GAG Scaffold Fabrication: Constant Cooling Lyophilization Protocol – Long Version**

**REFERENCE:** (O'Brien, Harley, et al., 2004; O'Brien, Harley, et al., 2005)

**SUPPLIES**

§ Type I collagen-glycosaminoglycan suspension (67.25 ml/sheet)

§ 5" x 5", 18 gauge 304 stainless steel pan (VirTis Inc., Gardiner, NY)

§ 0.05 M acetic acid

**EQUIPMENT**

§ Genesis freeze dryer (VirTis)

**PROCEDURE**

1. Turn on the freeze dryer (VirTis Genesis): Check that the vacuum oil level is at least 2/3, the oil appears clean, and that the vacuum pump is properly vented (either outside or into a chemical fume hood).

Plug the condenser drain valve and close the condenser and main chamber door.

Turn the main ***Power*** switch on.

Turn the ***Condenser*** switch on.

Set the ***SV*** gauge to 20°C and turn on the ***Freeze*** and ***Heat*** switches

You need to allow approximately 60 minutes for the freeze dryer temperature to stabilize and for the condenser to reach a cold enough temperature to continue.

2. Degas the CG suspension in a vacuum flask (Pressure: ~50 mTorr). Degas approximately twice the required volume to allow appropriate removal of all air bubbles. The length of time needed to degas the suspension varies from 30 – 90 min. depending on the total volume being degassed and the length of time the entire volume of suspension was degassed immediately following mixing.

3. Clean the stainless steel pan (VirTis) with ethanol or 0.05 M acetic acid and wipe the inside with Kim-Wipes to remove all dust and any remaining CG content from the previous run. When cleaning and handling the pan, do not touch the inside of the pan with your bare hands. Use gloves.

Allow the pan to air dry.

4. Pipet 67.25 ml of the degassed CG suspension into each pan.

5. Remove any air bubbles introduced into the suspension during the pipetting step using a 200 $\mu$l pipette tip. Drag the bubbles to the edge of the pan, allowing them to stick to the edge. Place the pan into the freeze dryer.

6. Check the appropriate program is selected using the Wizard controller. Press the button under ***Program X*** (X = 1 – 12) (Button #1) on the digital display. Select the appropriate program number using the ***Up*** and ***Down*** keys and then press the ***Edit*** key. Check the program variables (Temperature, Time, Ramp/Hold) against those detailed below. If the progression is incorrect, correct the values. Use the outer two buttons to scroll left or right through the program and the inner two keys to change the value of the selected criteria to match the desired program.

**Program 2**

Ramp to – – 40°C. Total time from start to sublimation: ˜135 minutes

Mean pore size: 95.9 ± 12.3 $\mu$m

Percent porosity: 0.994

Specific surface area (S.A./Vol): 0.00748 $\mu$m

**Freeze dryer program to fabricate CG scaffolds with a 96 $\mu$m mean pore size:**

| Freezing Step | Temperature, °C | Time, min | R/H |
|---|---|---|---|
| **1(start)** | 20 | 5 | H |
| **2("'ramping"')** | −40 | 65 | R |
| **3("'annealing"')** | −40 | > 60 | H |

NOTE: In all cases, **Step 3** should run for at least 60 minutes, but it is given a longer time in case you are delayed in returning. It is acceptable for that step to run longer than 60 minutes, since the solidification process will be complete by that point.

1. After confirming the program, press the two middle keys on the Wizard together to end the

editing step. Select the ***Save*** option from the menu displayed after ending the editing step. The Wizard screen should return to the original screen seen at start-up.

2. Turn off the ***Freeze*** and ***Heat*** buttons, turn the ***Auto*** button on, and press the ***Start*** key. The program should start running. Leave the program to run for the specified length of time.

3. At the end of the 60 minute annealing period, cancel the program. Press the inner two buttons on the wizard controller together, and then when prompted press the outer two keys. Turn off the ***Auto*** switch, then turn on the ***Freeze*** and ***Heat*** switches and set the ***SV*** to the appropriate freezing temperature (-10, -20, -30, or –40°C).

4. Turn on the ***Vacuum*** switch. Make sure the seal on the condenser and main chamber doors is tight and put pressure on the door to the main chamber until a vacuum pressure registers on the Wizard control screen (typically ~1900 mTorr).

5. When the vacuum pressure reaches below 300 mTorr, raise the temperature in the ***SV*** display to 0°C. Allow the freeze dryer to run for 17 hours at 0°C and a pressure <300 mTorr.

6. After 17 hours, raise the value of the ***SV*** control to 200°C. Wait for the chamber temperature to equilibrate to 20°C (temperature displayed in the ***PV*** display). Turn off the ***Vacuum*** switch and turn on the ***Chamber Release*** switch. Wait for the pressure to equilibrate to atmospheric pressure. Remove the pan from the main chamber.

7. Turn off the freeze dryer:

   Turn off the ***Chamber Release*** switch

   Turn off the ***Freeze*** and ***Heat*** switches

   Turn off the ***Condenser*** Switch

   Turn off the ***Power*** Switch

   Open the condenser door, unplug the condenser drain line allow condense to drain.

8. Remove the CG scaffold from the pan with gloved hands. Place the scaffold into an aluminum foil packet and store it in a dessicator.

9. Wash the stainless steel pan with ethanol or 0.05 M acetic acid and wipe down with Kim-Wipes to remove any portion of the scaffold that may have torn during removal. Return the pan to storage.

10. Make a notation on the run sheet attached to the front of the freeze dryer in order to keep track of the total number of runs between oil changes. When a row is completely checked off (8 freeze dryer runs), change the oil.

### C.4. Dehydrothermal Crosslinking Protocol

**REFERENCE:** (Yannas and Tobolsky, 1967; Yannas, Lee, et al., 1989; Harley, Spilker, et al., 2004)

**EQUIPMENT**

§ Isotemp vacuum oven (Model 201, Fisher Scientific, Hanover Park, IL)

**PROCEDURE**

1. Place the collagen-GAG scaffold into an aluminum foil packet. Leave the packet open at the top.

2. Select the appropriate processing conditions. The following processing conditions are those that are typically utilized:

DHT105/24 (Cross-linking temperature: 105°C for Cross-linking time: 24 hours) is the accepted laboratory standard crosslinking technique and is the default crosslinking applied to collagen-GAG scaffolds unless otherwise noted.

1. Place the packet into vacuum oven (Isotemp Model 201, Fisher Scientific) maintained at the desired temperature. Open the "*Vacuum*" knob (turn the knob counterclockwise) and close the "*Purge*" knob (turn the knob clockwise).

2. Turn on the vacuum pump. Wait until the vacuum has been obtained (nearly full scale on the vacuum oven dial).

3. At the end of the processing period, turn off the vacuum and vent the chamber by closing the "Vacuum" knob (clockwise) and opening the "Purge" knob (counterclockwise). Once the vacuum has completely vented, open the vacuum oven door and immediately seal the aluminum foil bag(s). The scaffold is now crosslinked and considered sterile; to maintain sterility, handle the scaffold from this point on using aseptic techniques.

4. Store the scaffold in a dessicator. Crosslinked scaffolds can remain indefinitely in a dessicator prior to use.

# Appendix C

# H&E Stain (Day 3 Post-Surgery)

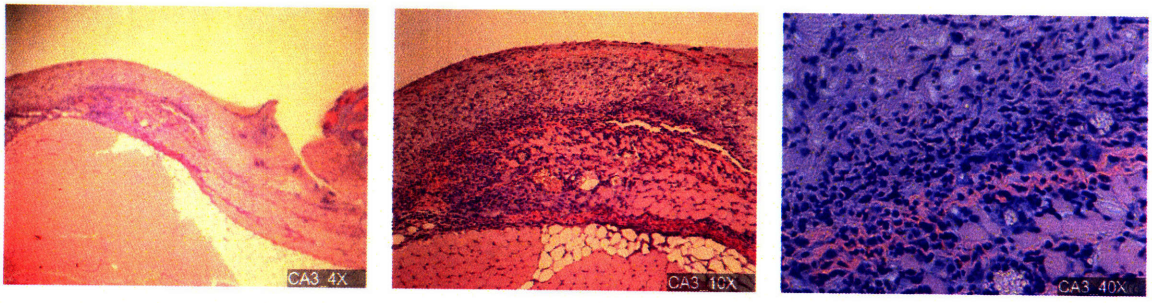


(a) 4X (b) 10X (c) 40X

Figure C-1: **Animal CA3 (Untreated Control Group with scaffold)**

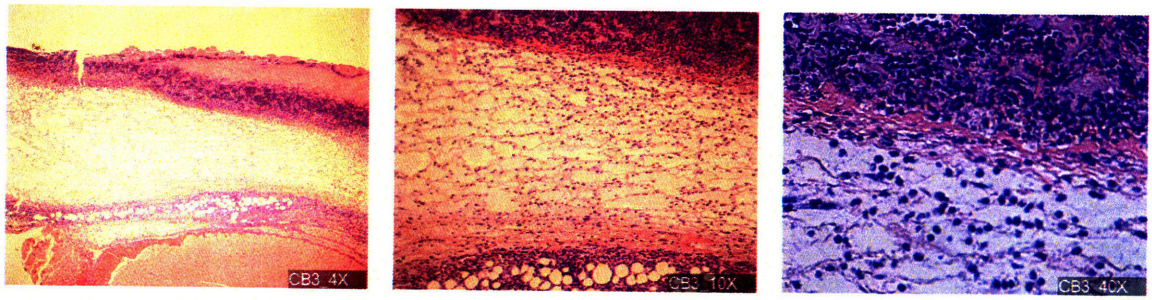


(a) 4X (b) 10X (c) 40X

Figure C-2: **Animal CB3 (Untreated Control Group with scaffold)**

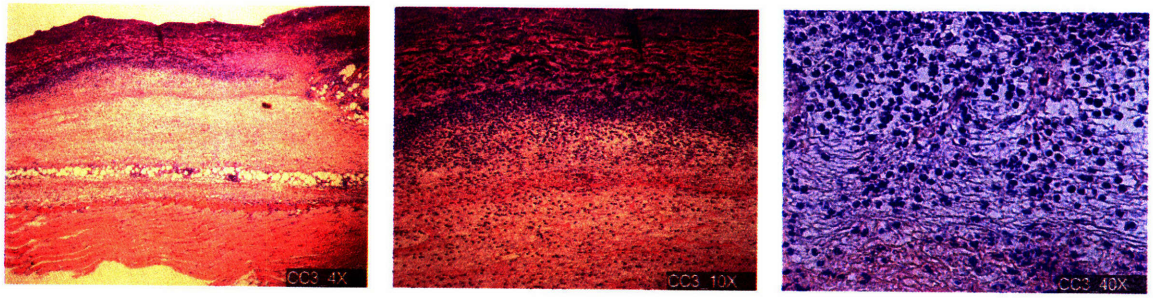


(a) 4X (b) 10X (c) 40X

Figure C-3: **Animal CC3 (Untreated Control Group with scaffold)**

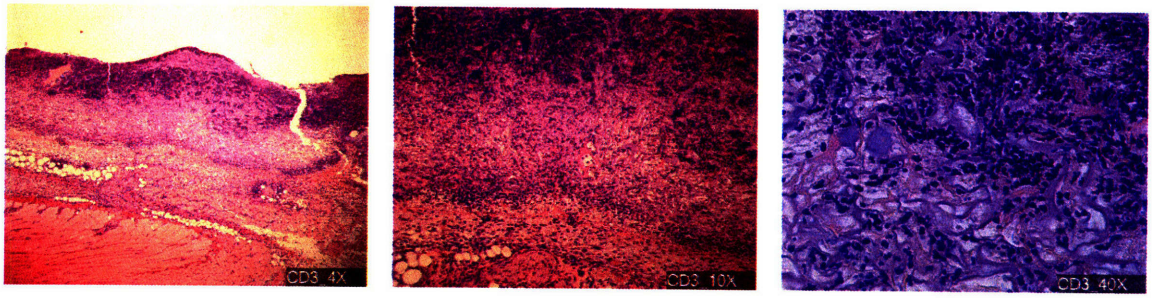


(a) 4X (b) 10X (c) 40X

Figure C-4: **Animal CD3 (Untreated Control Group with scaffold)**

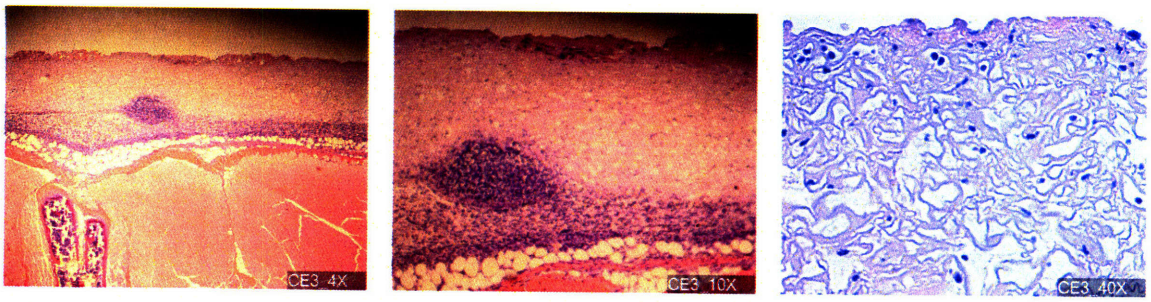


(a) 4X (b) 10X (c) 40X

Figure C-5: **Animal CE3 (Untreated Control Group with scaffold)**

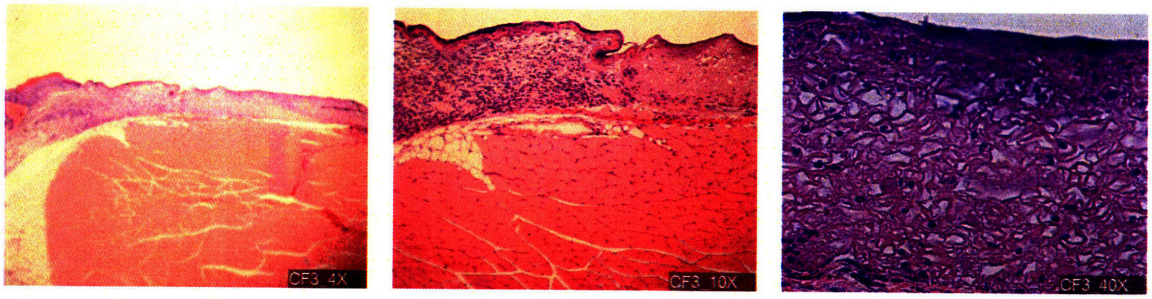


(a) 4X (b) 10X (c) 40X

Figure C-6: **Animal CF3 (Untreated Control Group with scaffold)**

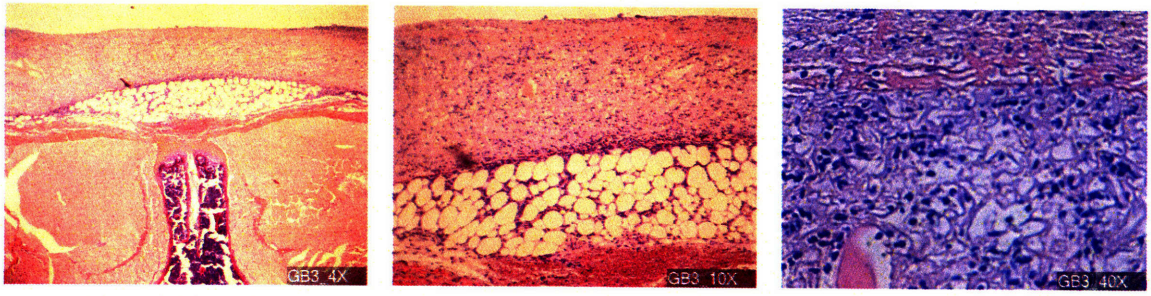


(a) 4X (b) 10X (c) 40X

Figure C-7: **Animal GB3 (GCSF with scaffold)**

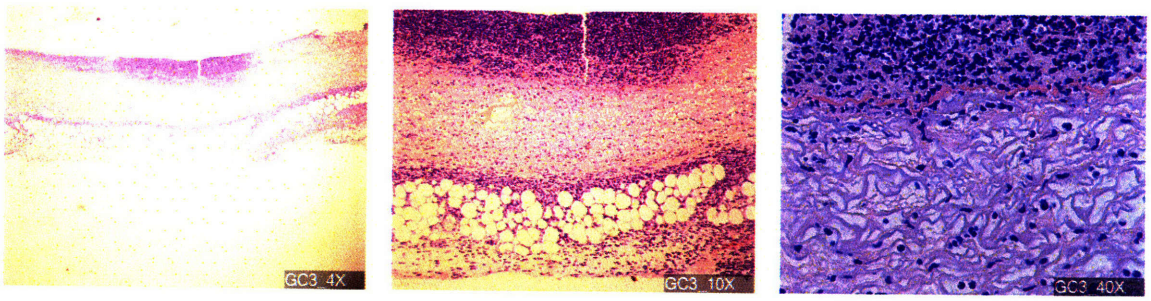


(a) 4X (b) 10X (c) 40X

Figure C-8: **Animal GC3 (GCSF with scaffold)**

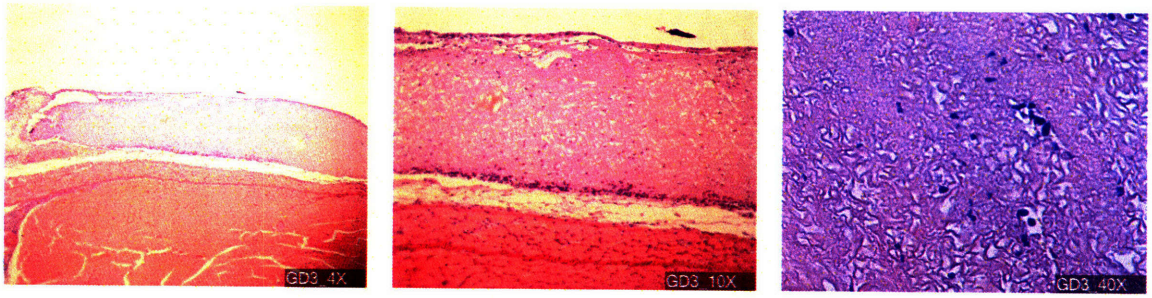


(a) 4X (b) 10X (c) 40X

Figure C-9: **Animal GD3 (GCSF with scaffold)**

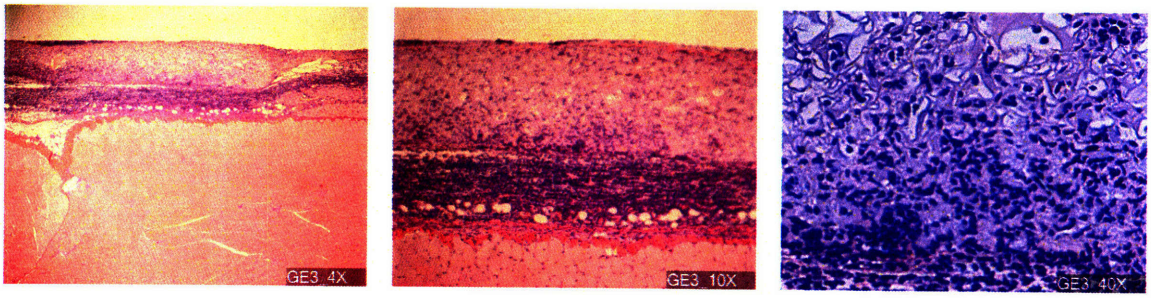


(a) 4X (b) 10X (c) 40X

Figure C-10: **Animal GE3 (GCSF with scaffold)**

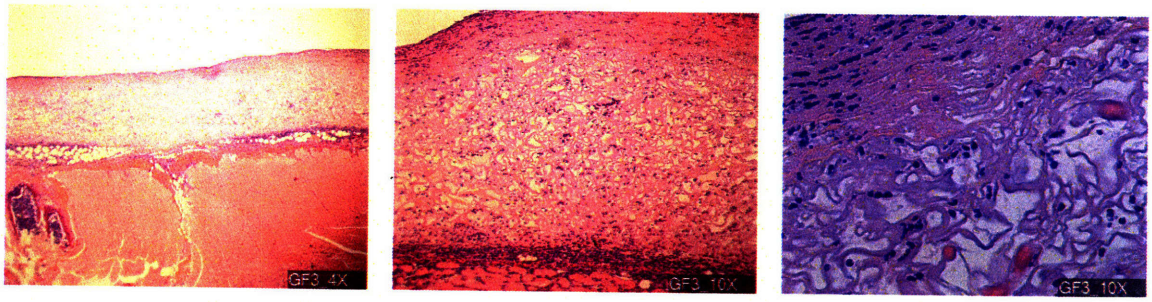


(a) 4X (b) 10X (c) 40X

Figure C-11: **Animal GF3 (GCSF with scaffold)**

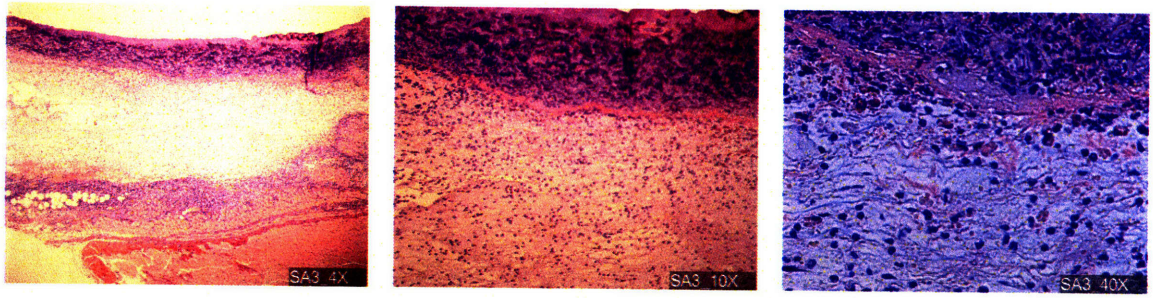


(a) 4X (b) 10X (c) 40X

Figure C-12: **Animal SA3 (SDF-1 with scaffold)**

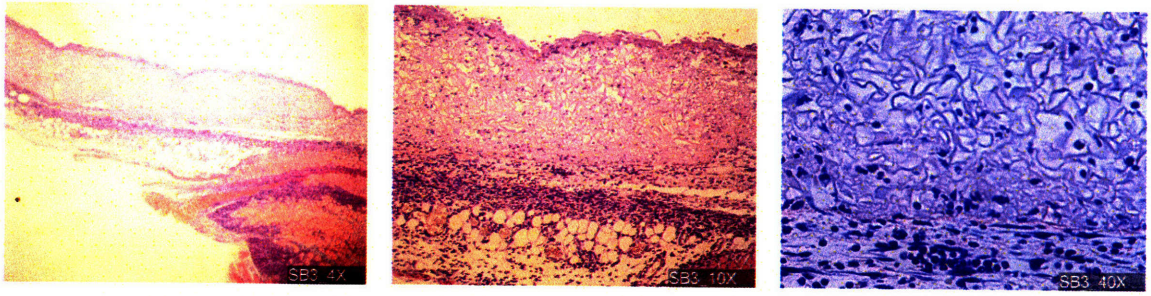


(a) 4X (b) 10X (c) 40X

Figure C-13: **Animal SB3 (SDF-1 with scaffold)**

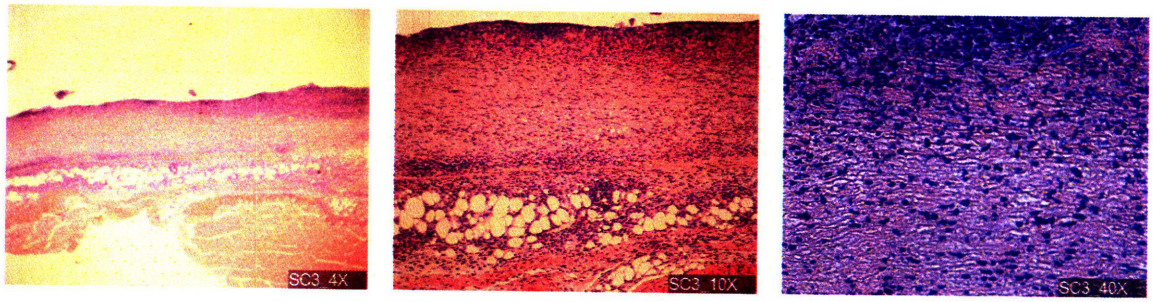


(a) 4X (b) 10X (c) 40X

Figure C-14: **Animal SC3 (SDF-1 with scaffold)**

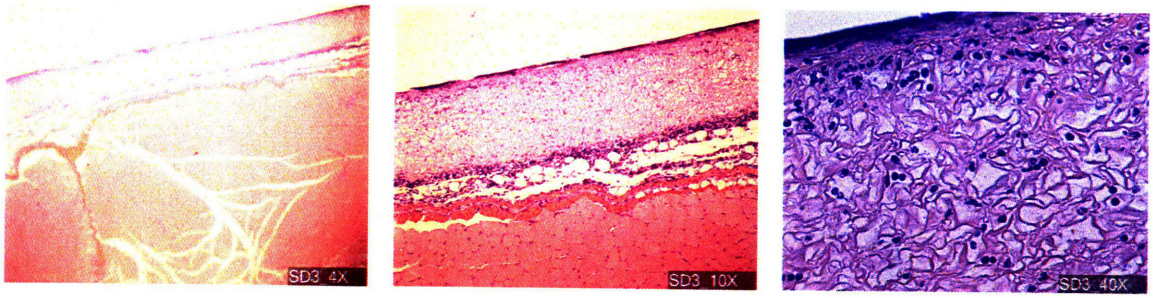


(a) 4X (b) 10X (c) 40X

Figure C-15: **Animal SD3 (SDF-1 with scaffold)**

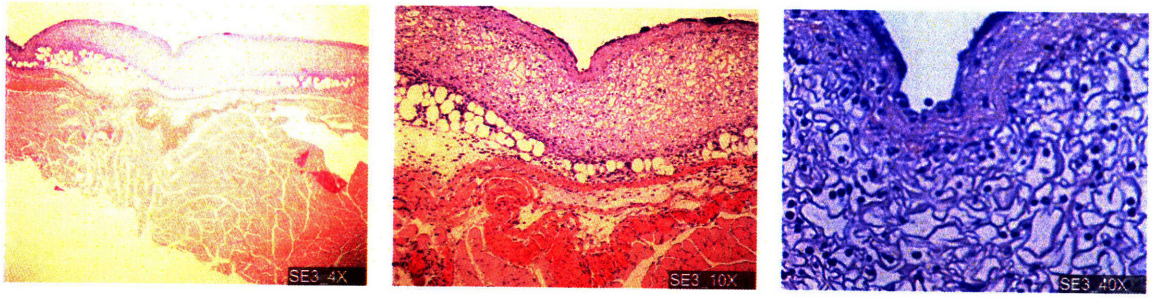


(a) 4X (b) 10X (c) 40X

Figure C-16: **Animal SE3 (SDF-1 with scaffold)**

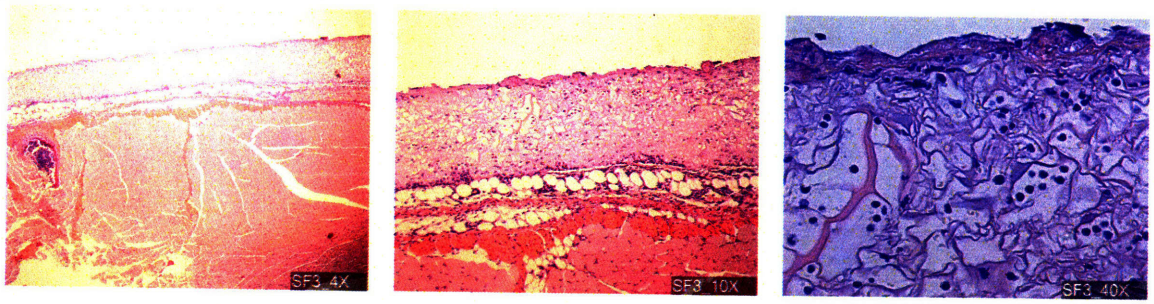


(a) 4X (b) 10X (c) 40X

Figure C-17: **Animal SF3 (SDF-1 with scaffold)**


(a) 4X (b) 10X (c) 40X

Figure C-18: **Animal SGA3 (GCSF + SDF-1 with scaffold)**

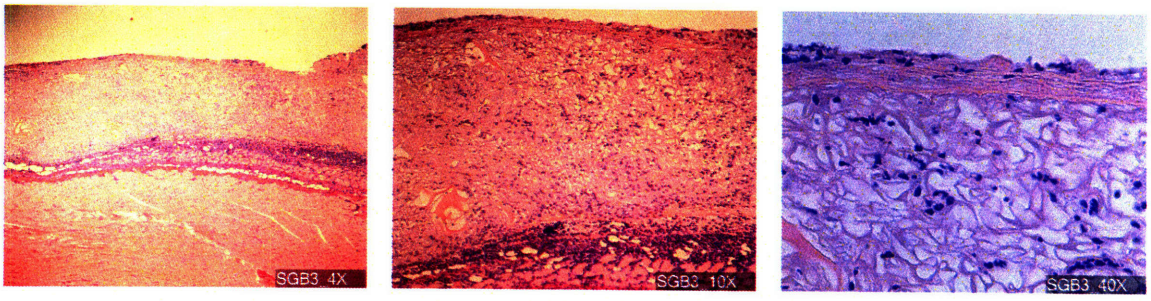


(a) 4X (b) 10X (c) 40X

Figure C-19: **Animal SGB3 (GCSF + SDF-1 with scaffold)**

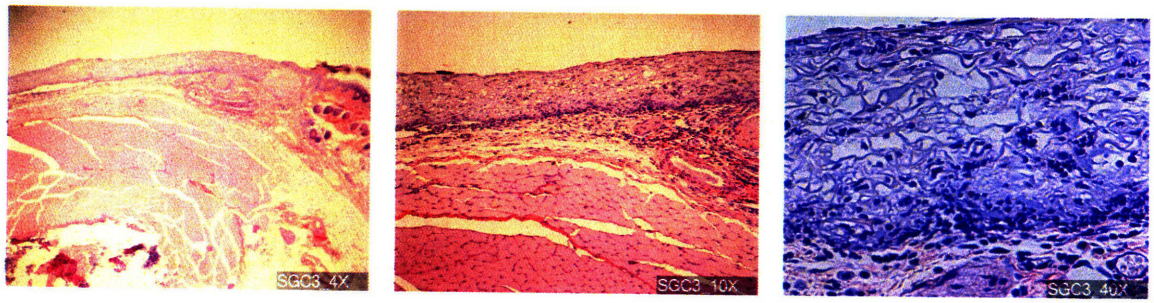


(a) 4X (b) 10X (c) 40X

Figure C-20: **Animal SGC3 (GCSF + SDF-1 with scaffold)**

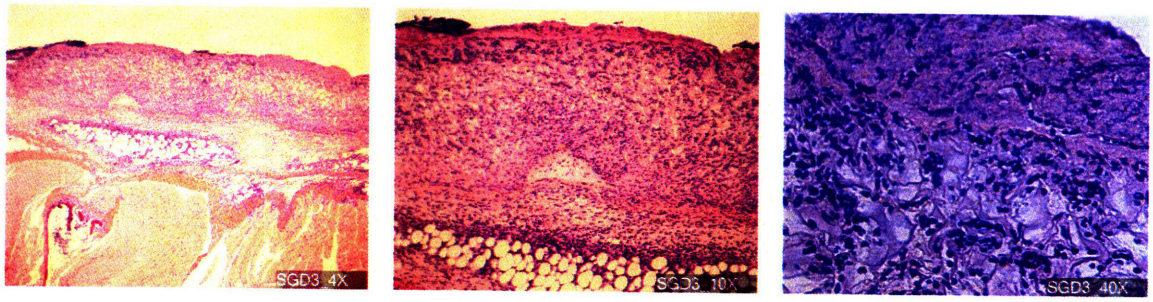


(a) 4X (b) 10X (c) 40X

Figure C-21: **Animal SGD3 (GCSF + SDF-1 with scaffold)**

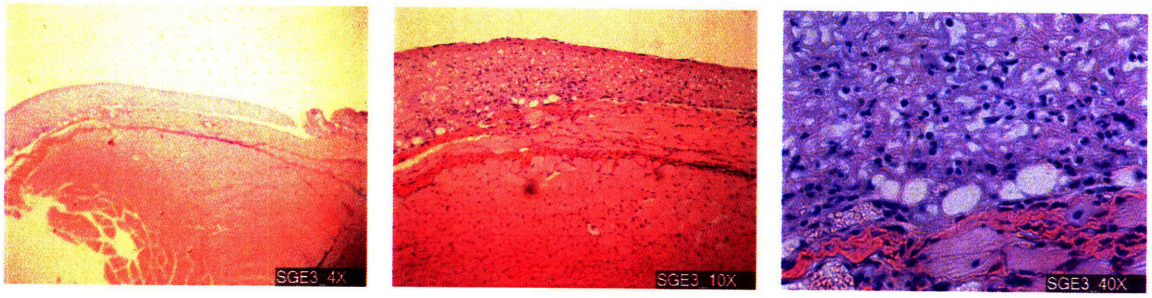


(a) 4X (b) 10X (c) 40X

Figure C-22: **Animal SGE3 (GCSF + SDF-1 with scaffold)**

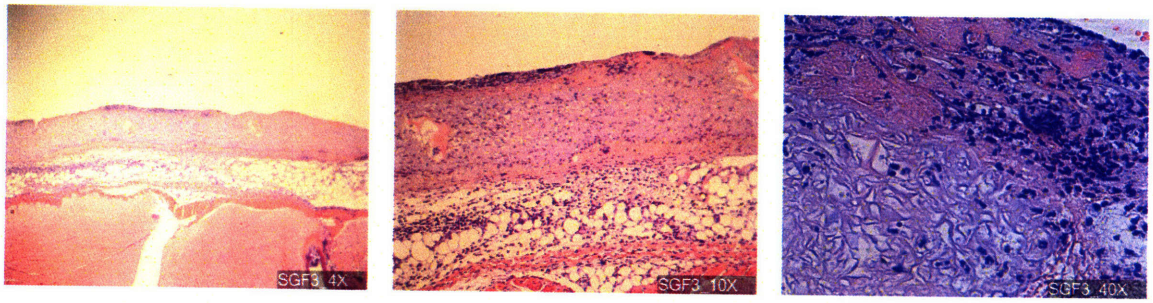


(a) 4X (b) 10X (c) 40X

Figure C-23: **Animal SGF3 (GCSF + SDF-1 with scaffold)**

# Appendix D

# H&E Stain (Day 18 Post-Surgery)

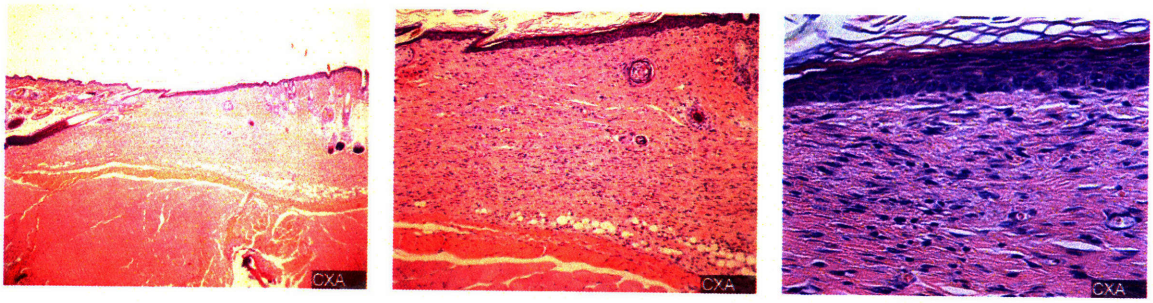


(a) 4X (b) 10X (c) 40X

Figure D-1: **Animal CXA (Untreated Control Group with scaffold)**

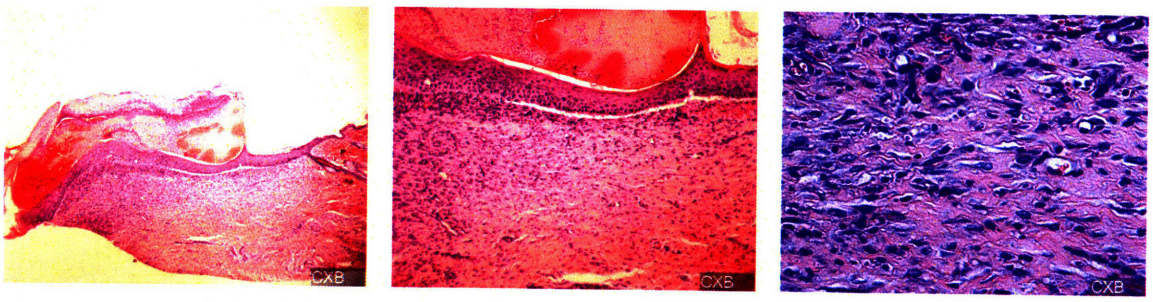


(a) 4X (b) 10X (c) 40X

Figure D-2: **Animal CXB (Untreated Control Group with scaffold)**

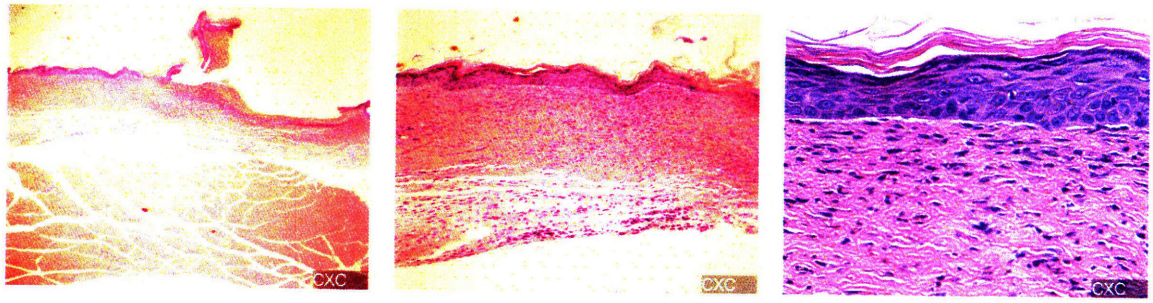


(a) 4X (b) 10X (c) 40X

Figure D-3: **Animal CXC (Untreated Control Group with scaffold)**

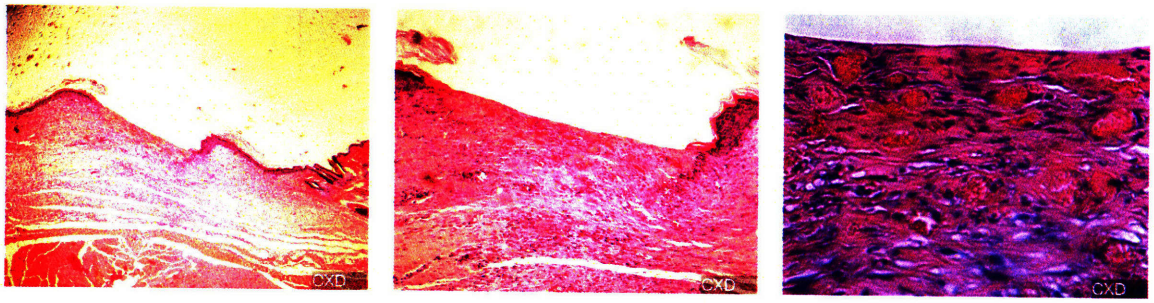


(a) 4X (b) 10X (c) 40X

Figure D-4: **Animal CXD (Untreated Control Group with scaffold)**

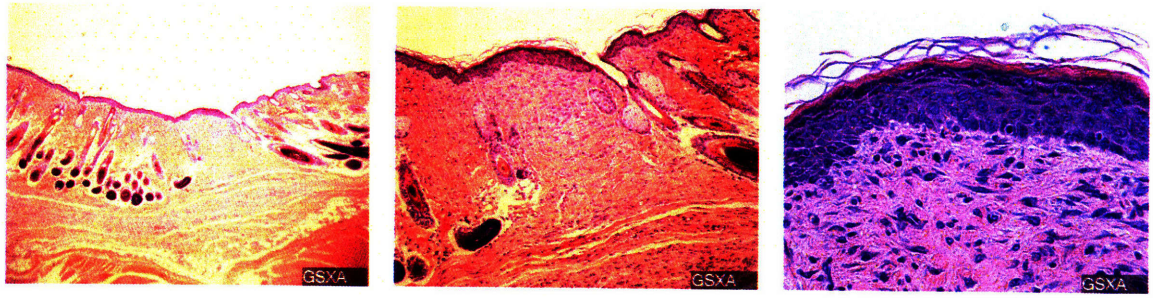


(a) 4X (b) 10X (c) 40X

Figure D-5: **Animal GSXA (GCSF + SDF-1 Group with scaffold)**

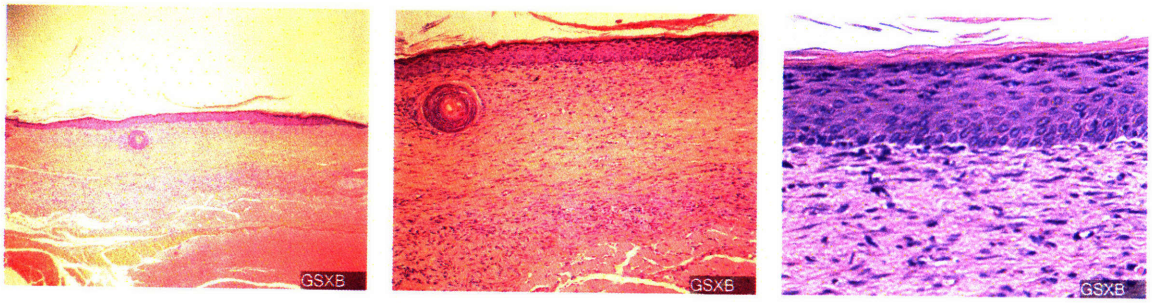


(a) 4X (b) 10X (c) 40X

Figure D-6: **Animal GSXB (GCSF + SDF-1 Group with scaffold)**

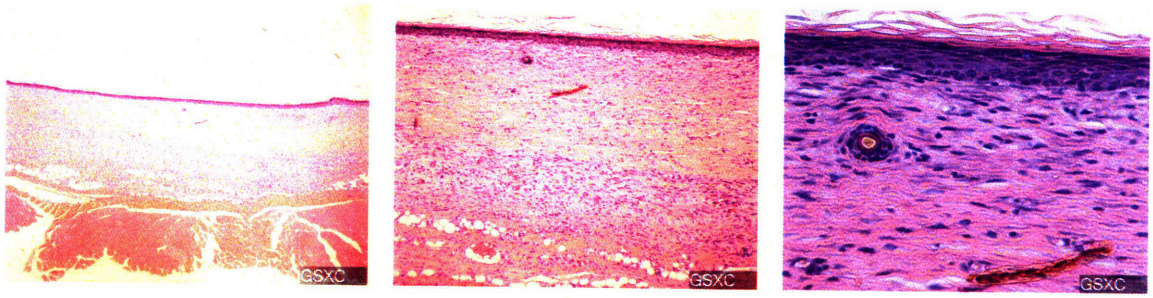


(a) 4X (b) 10X (c) 40X

Figure D-7: **Animal GSXC (GCSF + SDF-1 Group with scaffold)**

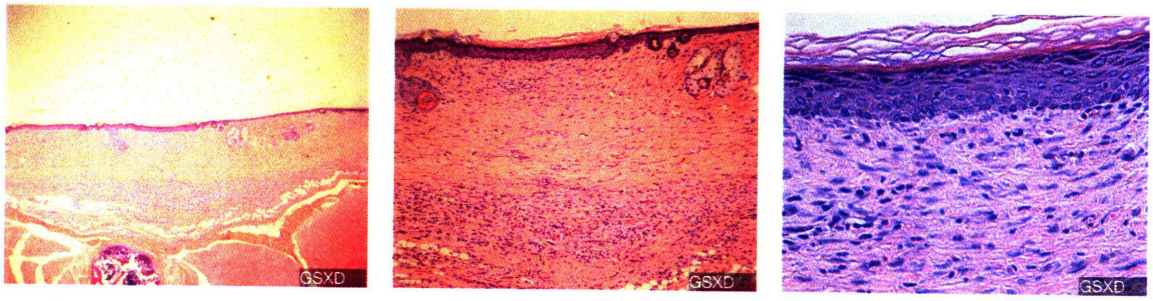


(a) 4X (b) 4X (c) 4X

Figure D-8: **Animal GSXD (GCSF + SDF-1 Group with scaffold)**

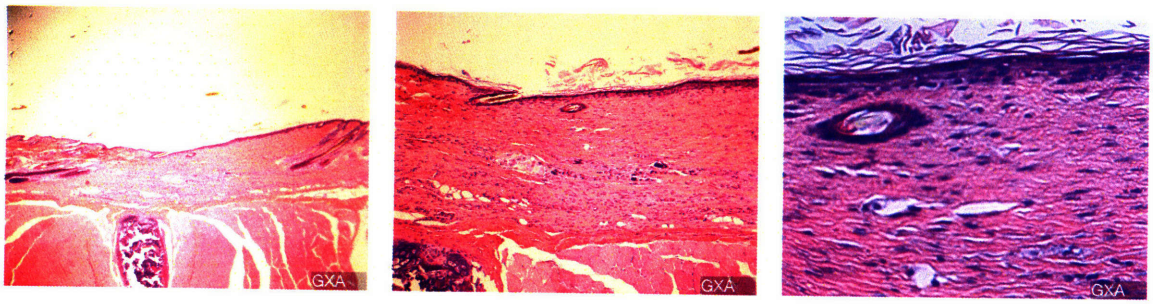


(a) 4X (b) 10X (c) 40X

Figure D-9: **Animal GXA (GCSF Group with scaffold)**

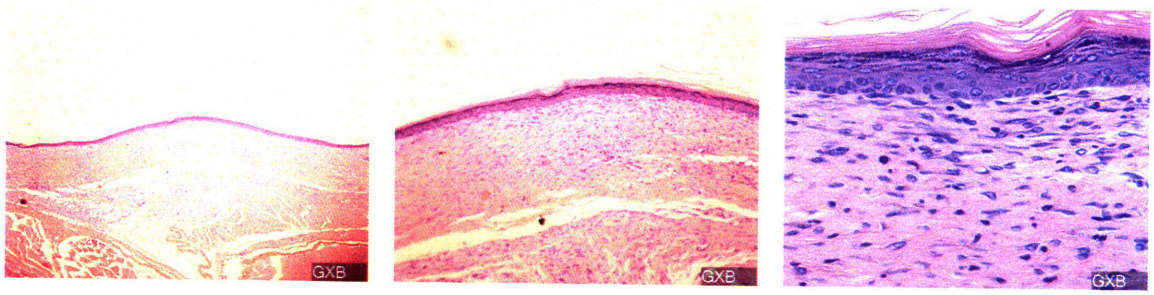


(a) 4X (b) 10X (c) 40X

Figure D-10: **Animal GXB (GCSF Group with scaffold)**

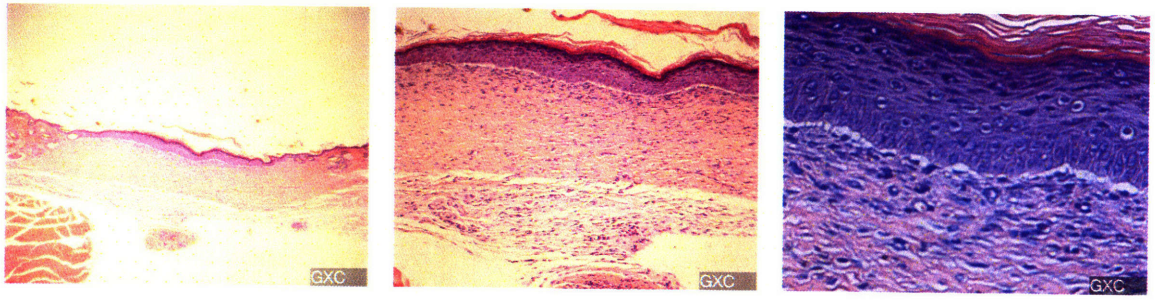


(a) 4X (b) 10X (c) 40X

Figure D-11: **Animal GXC (GCSF Group with scaffold)**

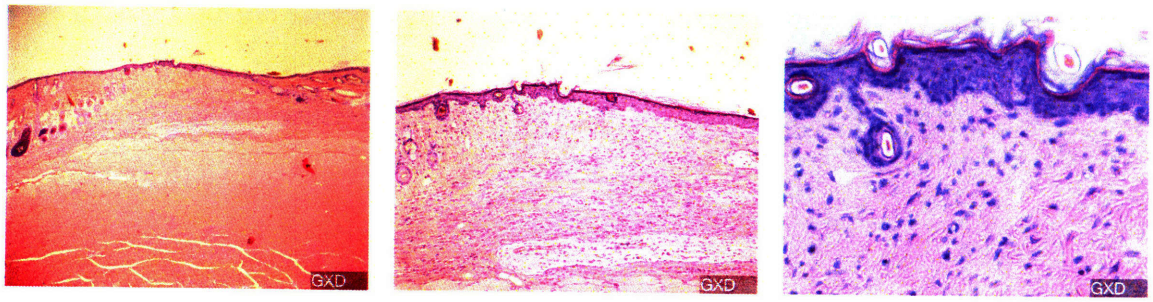


(a) 4X (b) 10X (c) 40X

Figure D-12: **Animal GXD (GCSF Group with scaffold)**

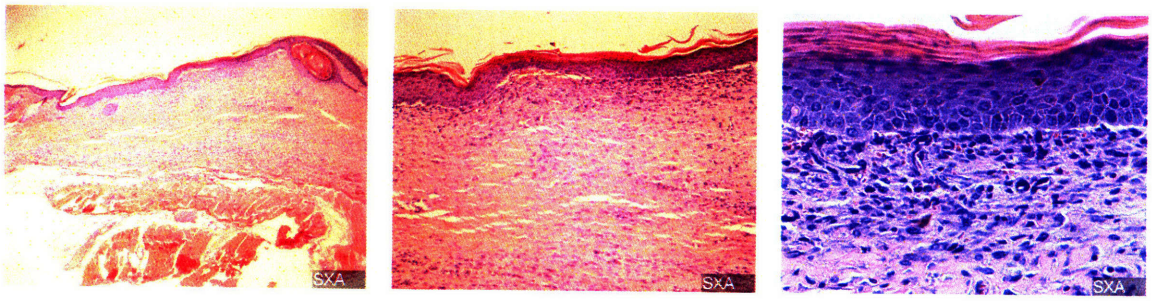


(a) 4X (b) 10X (c) 40X

Figure D-13: **Animal SXA (SDF-1 Group with scaffold)**

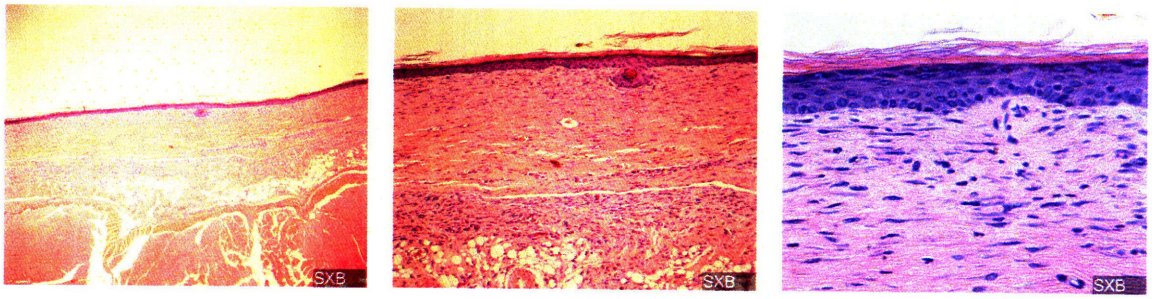


(a) 4X (b) 10X (c) 40X

Figure D-14: **Animal SXB (SDF-1 Group with scaffold)**

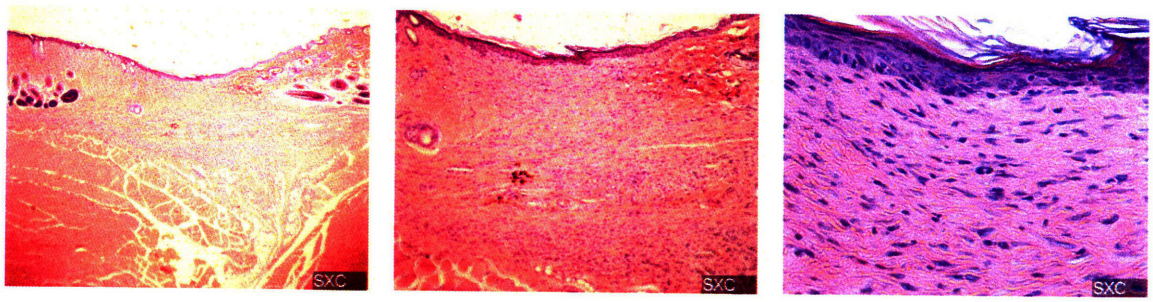


(a) 4X (b) 10X (c) 40X

Figure D-15: **Animal SXC (SDF-1 Group with scaffold)**

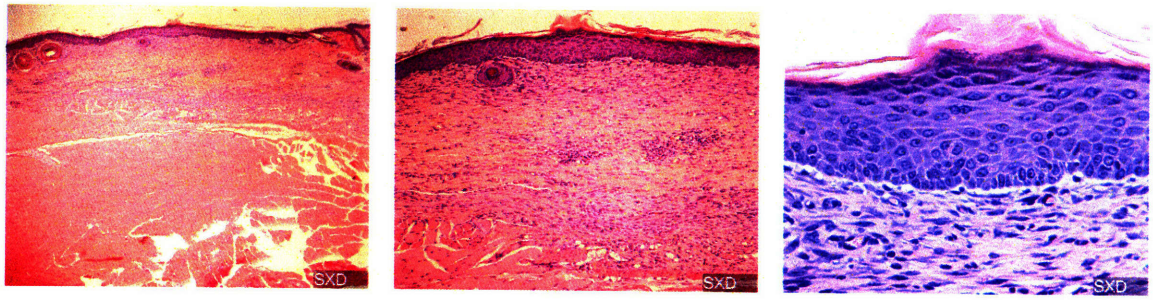


(a) 4X (b) 10X (c) 40X

Figure D-16: **Animal SXD (SDF-1 Group with scaffold)**

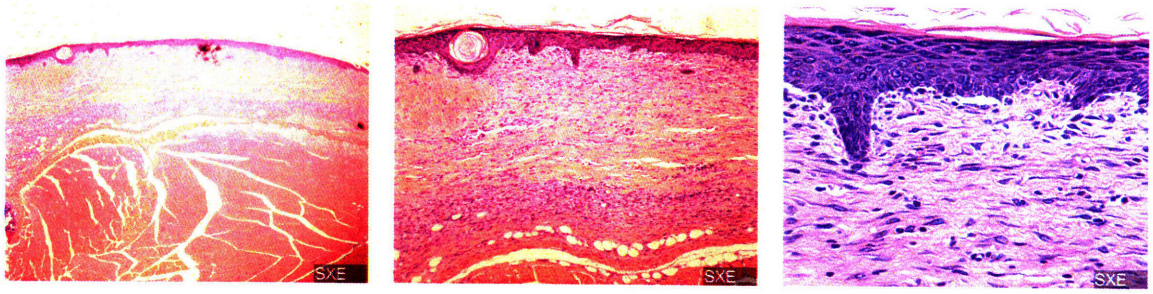


(a) 4X (b) 10X (c) 40X

Figure D-17: **Animal SXE (SDF-1 Group with scaffold)**

# Appendix E

# Masson's Trichrome Stain (Day 18 Post-Surgery)

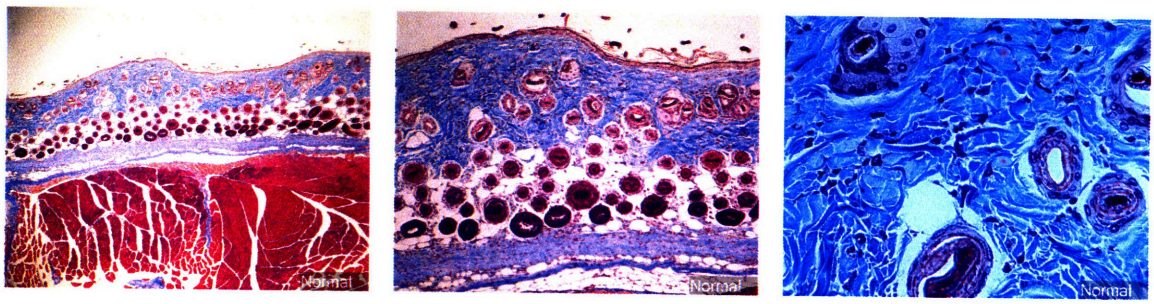


(a) 4X (b) 10X (c) 40X

Figure E-1: **Normal Uninjured Dermis Region**

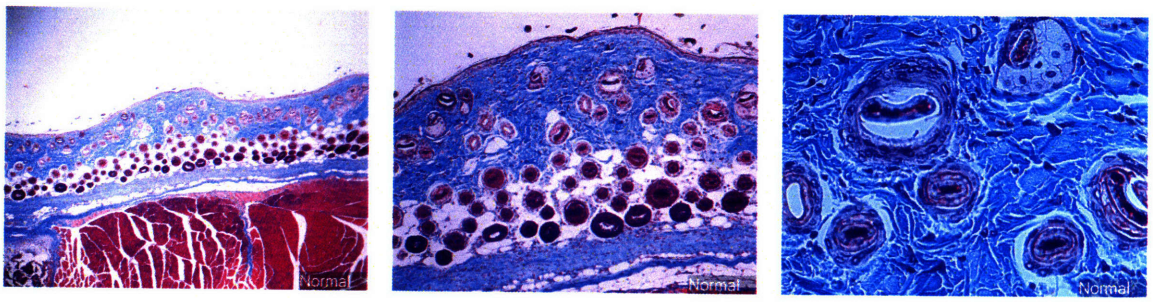


(a) 4X (b) 10X (c) 40X

Figure E-2: **Normal Uninjured Dermis Region**

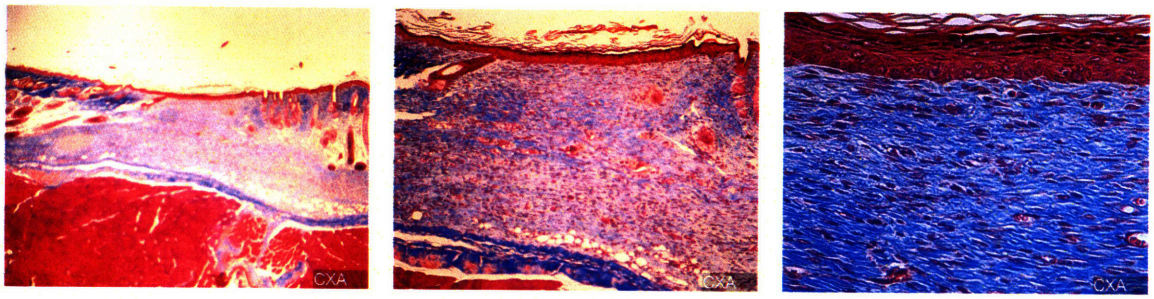


(a) 4X (b) 10X (c) 40X

Figure E-3: **Animal CXA (Untreated Control Group with scaffold)**

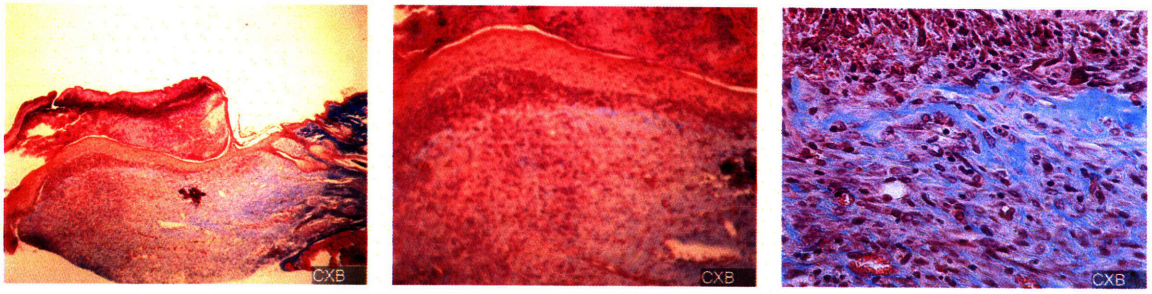


(a) 4X (b) 10X (c) 40X

Figure E-4: **Animal CXB (Untreated Control Group with scaffold)**

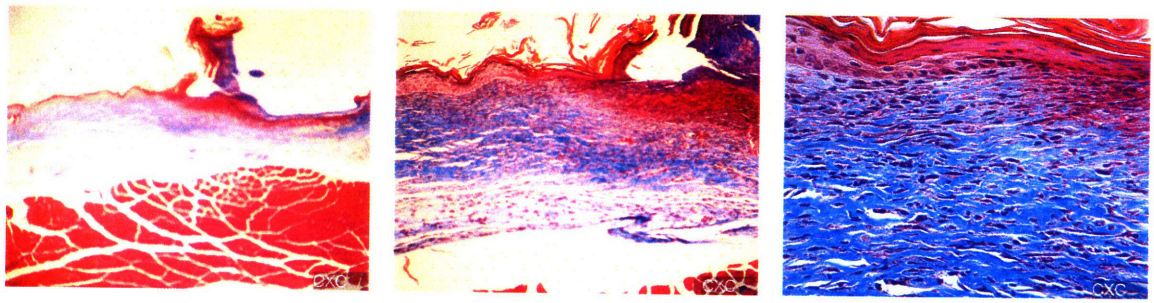


(a) 4X (b) 10X (c) 40X

Figure E-5: **Animal CXC (Untreated Control Group with scaffold)**

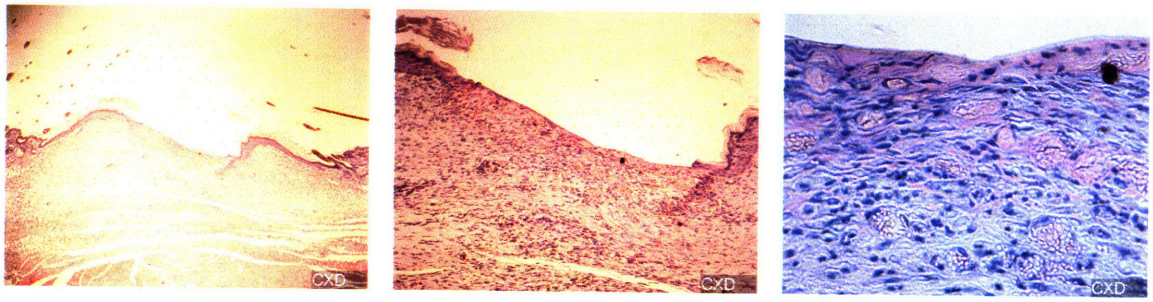


(a) 4X (b) 10X (c) 40X

Figure E-6: **Animal CXD (Untreated Control Group with scaffold)**

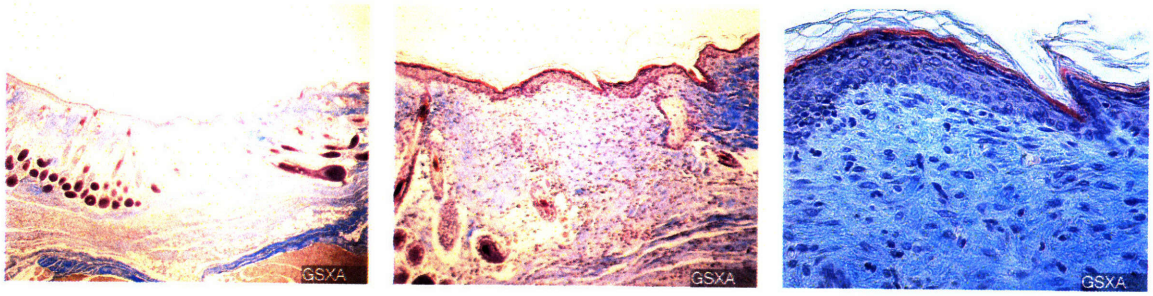


(a) 4X (b) 10X (c) 40X

Figure E-7: **Animal GSXA (GCSF + SDF-1 with scaffold)**

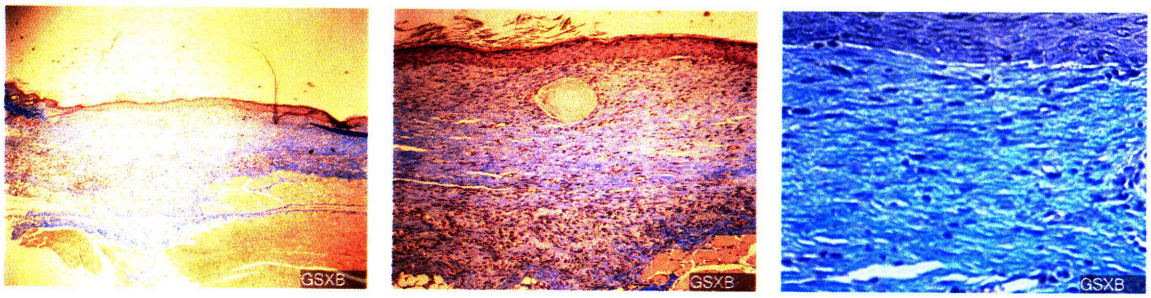


(a) 4X (b) 10X (c) 40X

Figure E-8: **Animal GSXB (GCSF + SDF-1 with scaffold)**

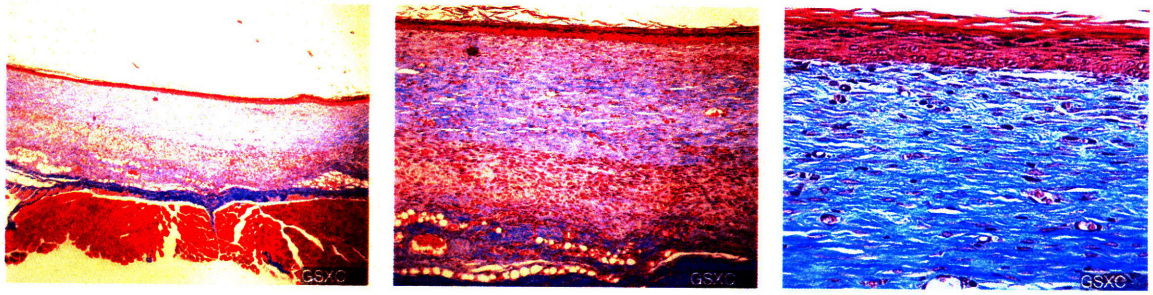


(a) 4X (b) 10X (c) 40X

Figure E-9: **Animal GSXC (GCSF + SDF-1 with scaffold)**

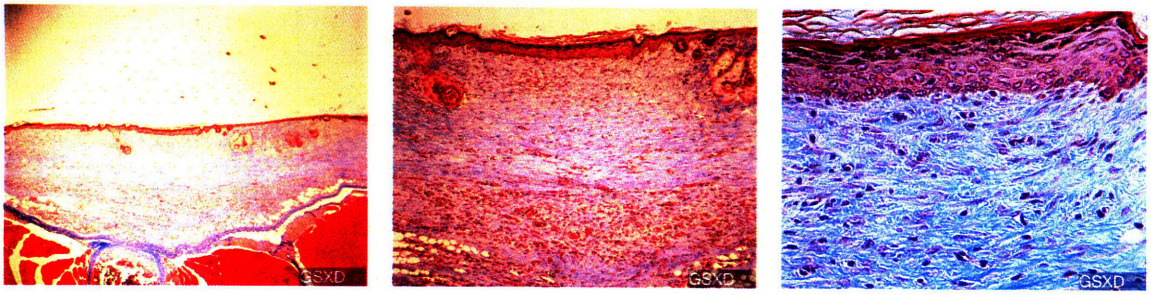


(a) 4X (b) 10X (c) 40X

Figure E-10: **Animal GSXD (GCSF + SDF-1 with scaffold)**

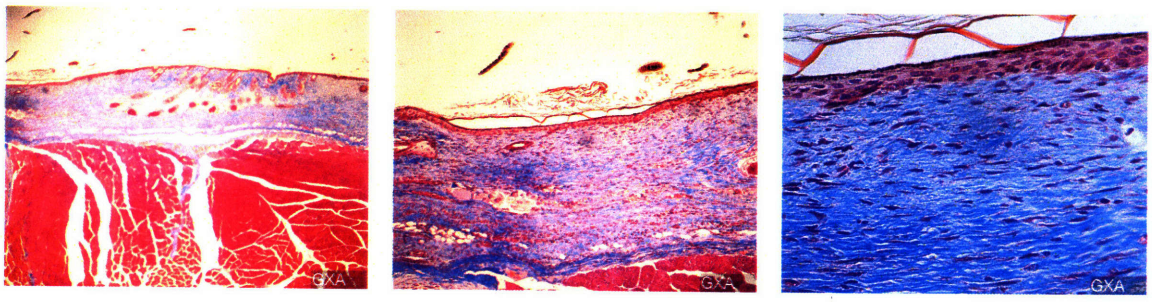


(a) 4X (b) 10X (c) 40X

Figure E-11: **Animal GXA (GCSF with scaffold)**

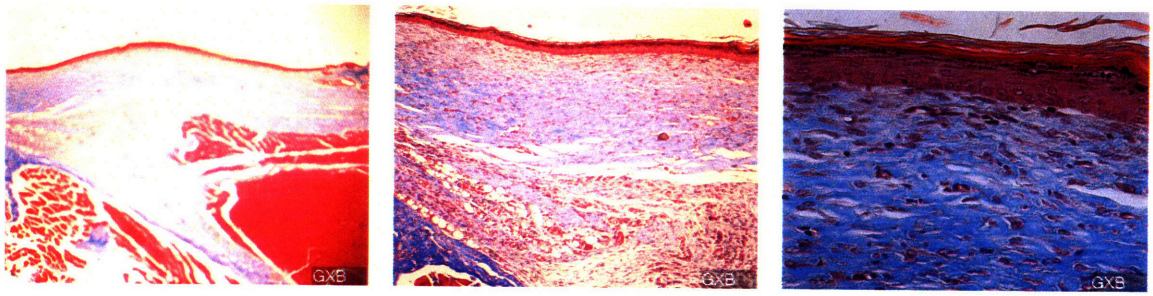


(a) 4X (b) 10X (c) 40X

Figure E-12: **Animal GXB (GCSF with scaffold)**

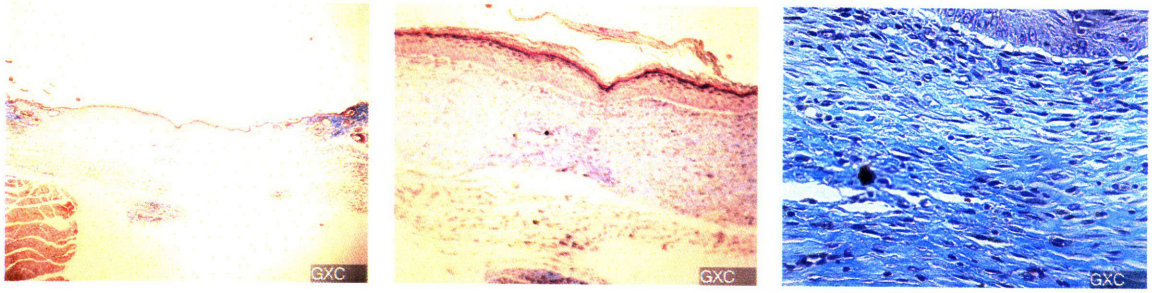


(a) 4X (b) 10X (c) 40X

Figure E-13: **Animal GXC (GCSF with scaffold)**

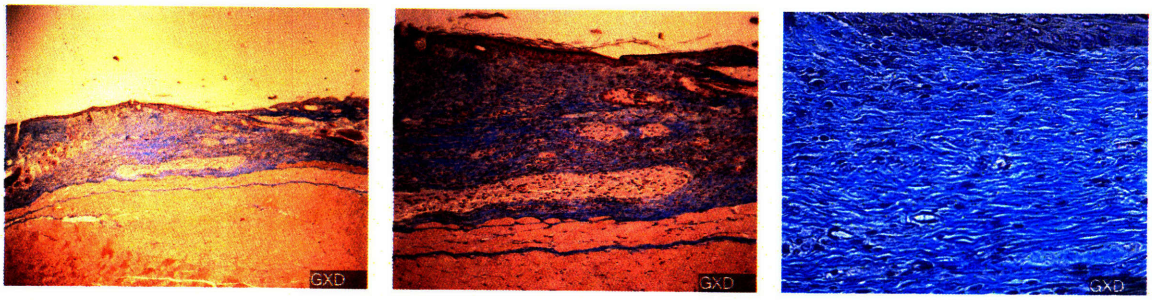


(a) 4X (b) 10X (c) 40X

Figure E-14: **Animal GXD (GCSF with scaffold)**

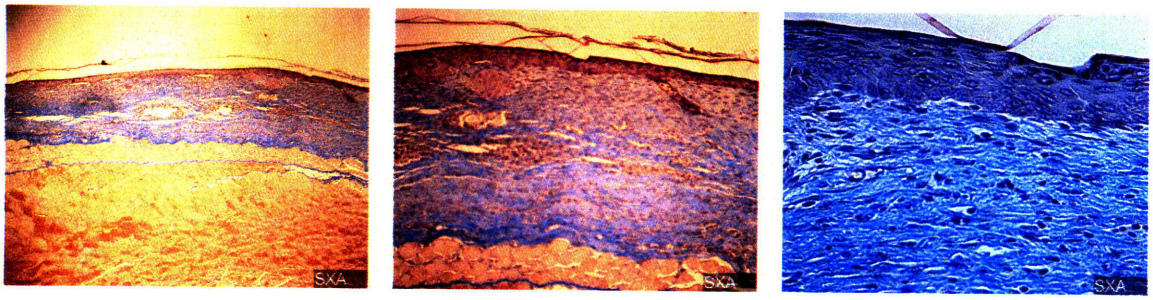


(a) 4X (b) 10X (c) 40X

Figure E-15: **Animal SXA (SDF-1 with scaffold)**

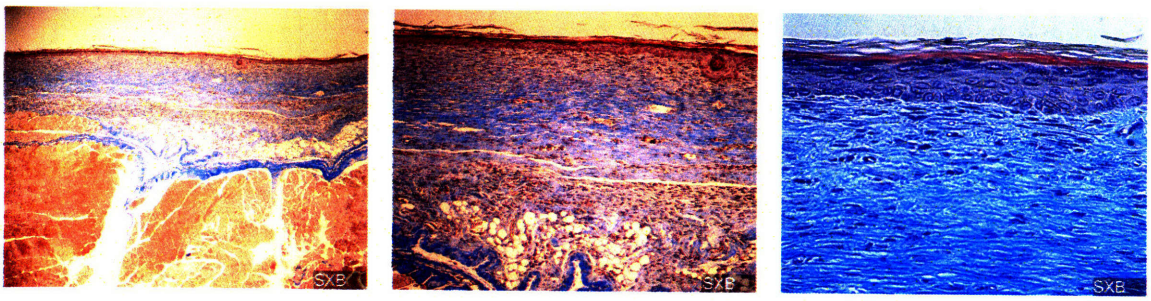


(a) 4X (b) 10X (c) 40X

Figure E-16: **Animal SXB (SDF-1 with scaffold)**

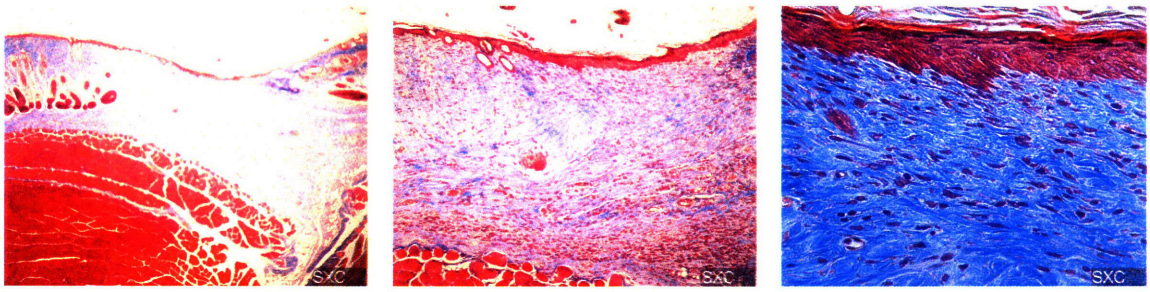


(a) 4X (b) 10X (c) 40X

Figure E-17: **Animal SXC (SDF-1 with scaffold)**

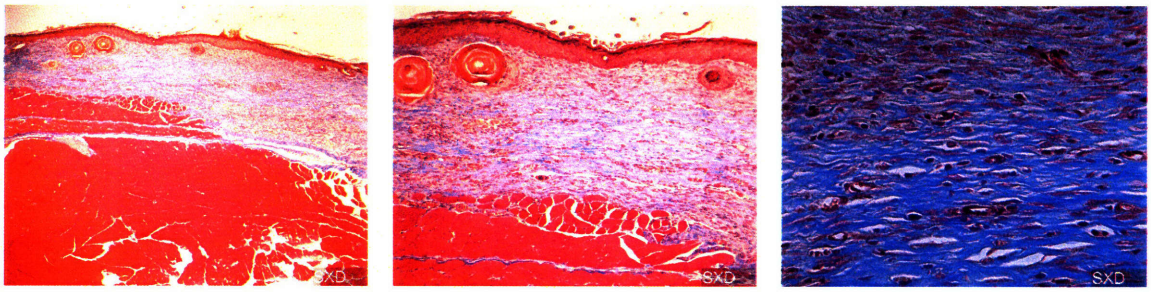


(a) 4X (b) 10X (c) 40X

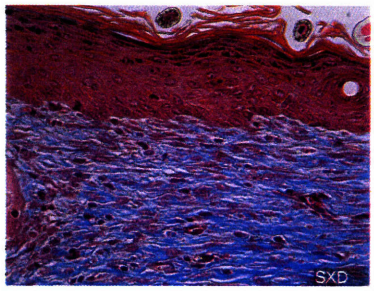


(d) 40X

Figure E-18: **Animal SXD (SDF-1 with scaffold)**

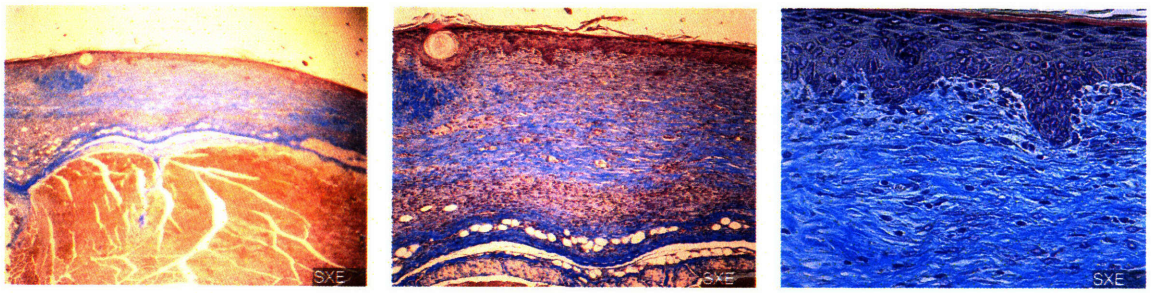


(a) 4X (b) 10X (c) 40X

Figure E-19: **Animal SXE (SDF-1 with scaffold)**

# Appendix F

# Polarized Light Microscopy (Day 18 Post-Surgery)

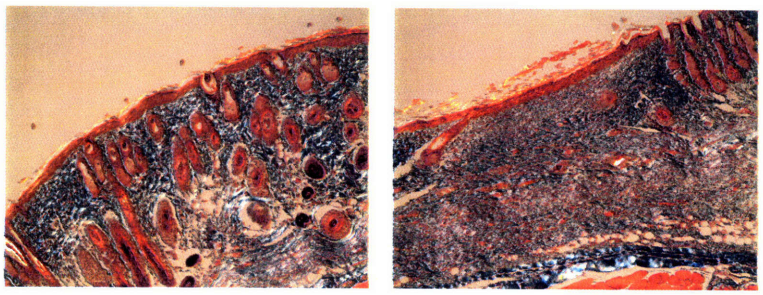

(a) 10X (b) 10X

Figure F-1: **Animal CXA (Untreated Control Group with scaffold)**

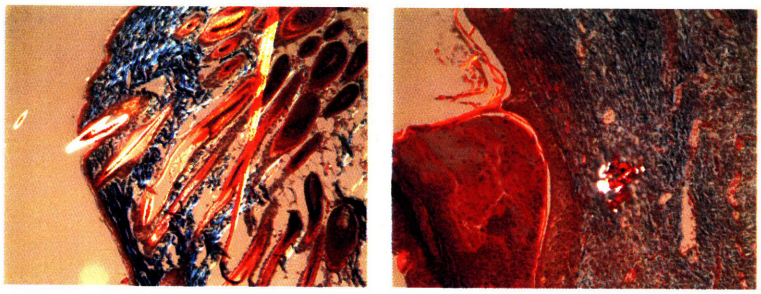

(a) 10X (b) 10X

Figure F-2: **Animal CXB (Untreated Control Group with scaffold)**

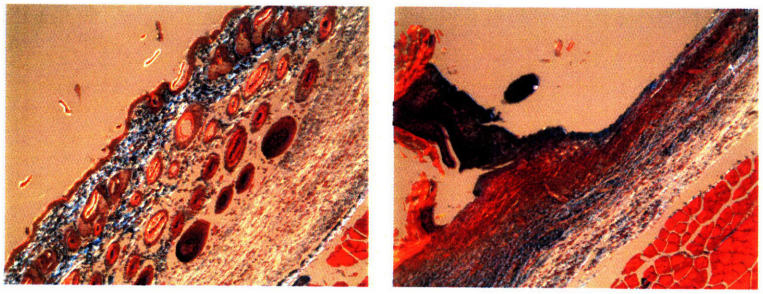

(a) 10X (b) 10X

Figure F-3: **Animal CXC (Untreated Control Group with scaffold)**

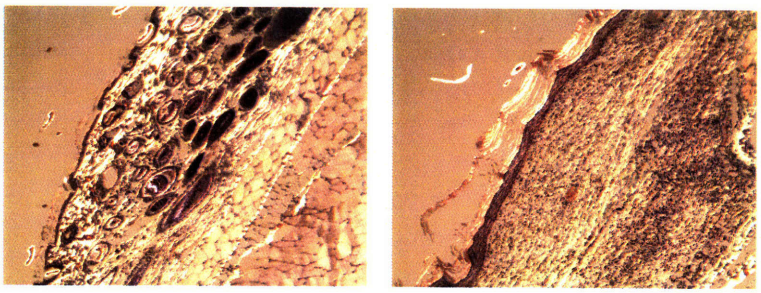

(a) 10X (b) 10X

Figure F-4: **Animal CXD (Untreated Control Group with scaffold)**

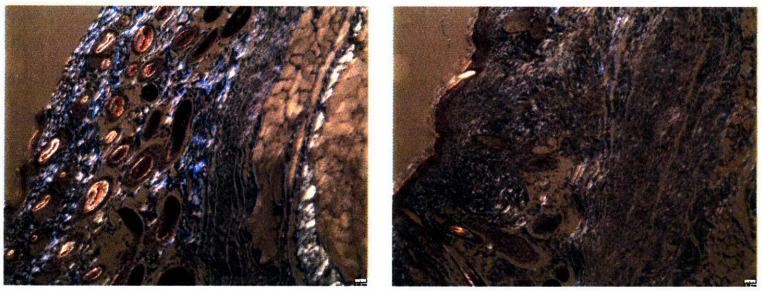

(a) 10X (b) 10X

Figure F-5: **Animal GSXA (GCSF + SDF-1 with scaffold)**

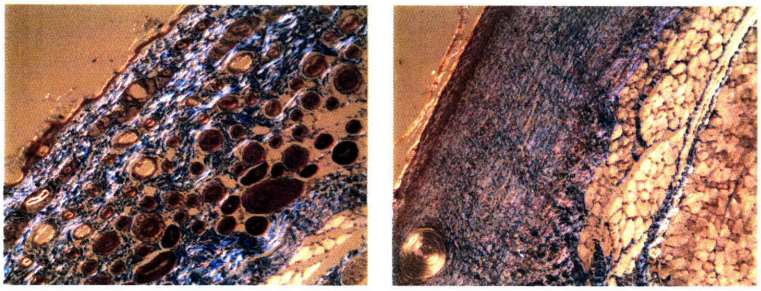

(a) 10X (b) 10X

Figure F-6: **Animal GSXB (GCSF + SDF-1 with scaffold)**

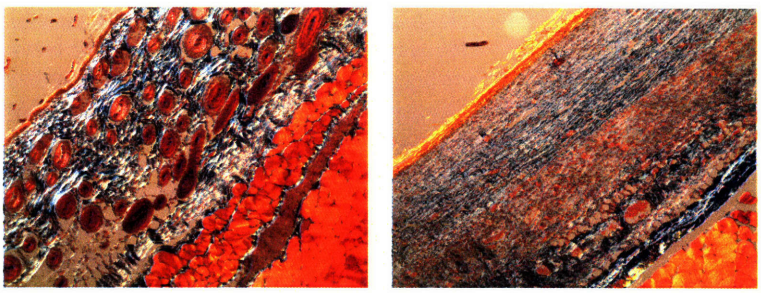

(a) 10X (b) 10X

Figure F-7: **Animal GSXC (GCSF + SDF-1 with scaffold)**

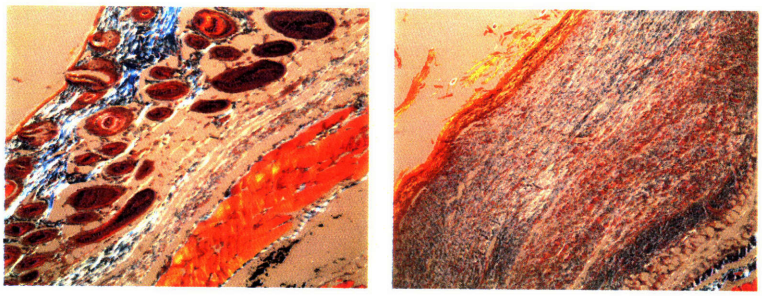

(a) 10X (b) 10X

Figure F-8: **Animal GSXD (GCSF + SDF-1 with scaffold)**

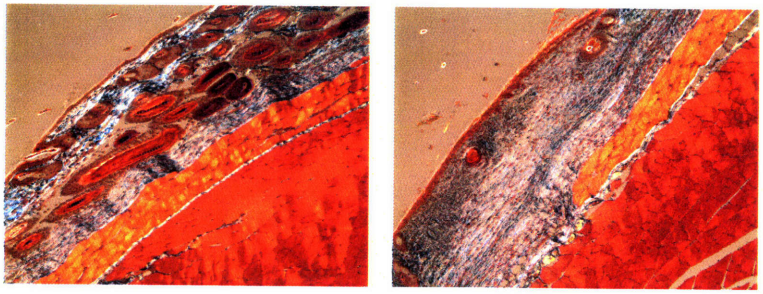

(a) 10X (b) 10X

Figure F-9: **Animal GXA (GCSF with scaffold)**

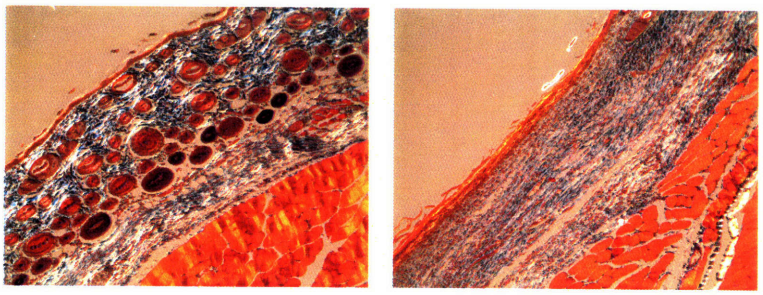

(a) 10X (b) 10X

Figure F-10: **Animal GXB (GCSF with scaffold)**

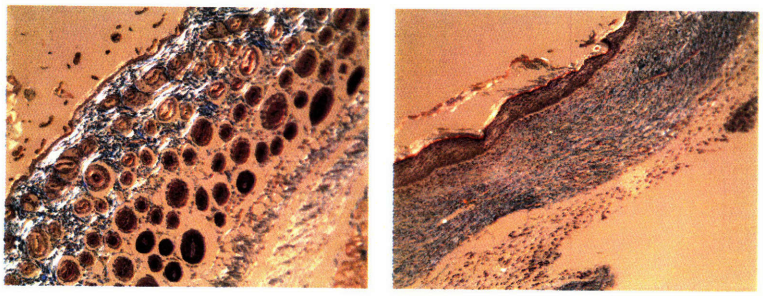

(a) 10X (b) 10X

Figure F-11: **Animal GXC (GCSF with scaffold)**

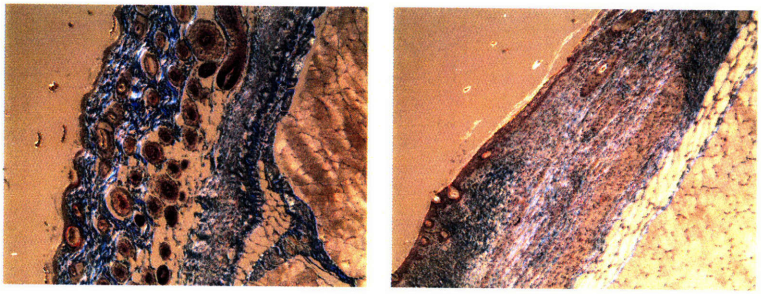

(a) 10X (b) 10X

Figure F-12: **Animal GXD (GCSF with scaffold)**

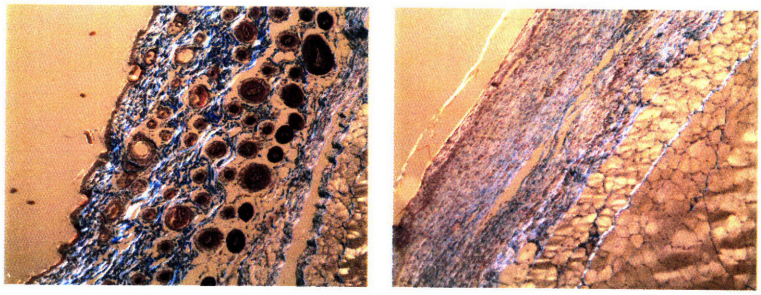

(a) 10X (b) 10X

Figure F-13: **Animal SXB (SDF-1 with scaffold)**

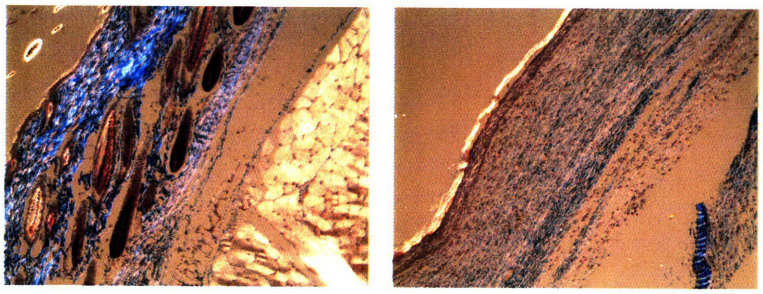

(a) 10X (b) 10X

Figure F-14: **Animal SXB (SDF-1 with scaffold)**

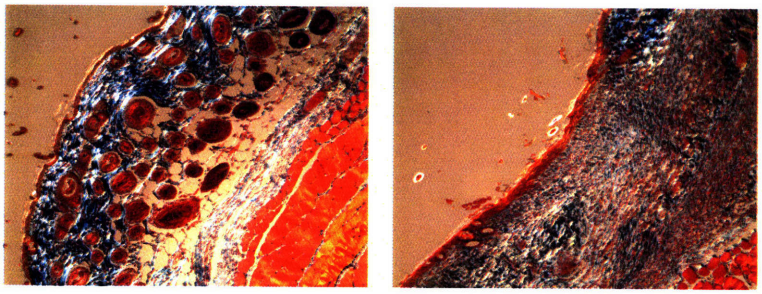

(a) 10X (b) 10X

Figure F-15: **Animal SXC (SDF-1 with scaffold)**

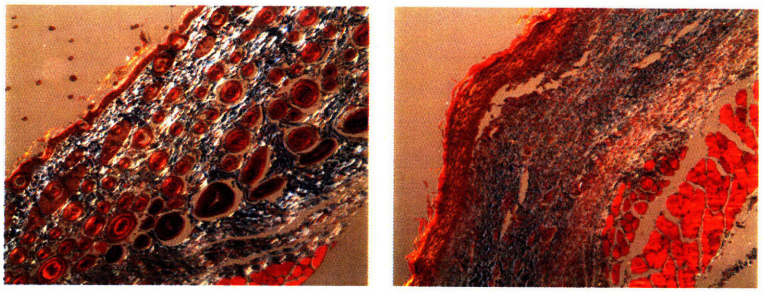

(a) 10X (b) 10X

Figure F-16: **Animal SXD (SDF-1 with scaffold)**

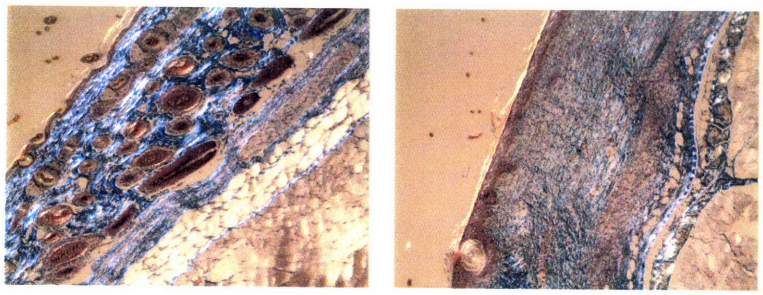

(a) 10X

(b) 10X

Figure F-17: **Animal SXE (SDF-1 with scaffold)**

# Appendix G

# Masson's Trichrome Stain (Day 18 Post-Surgery)

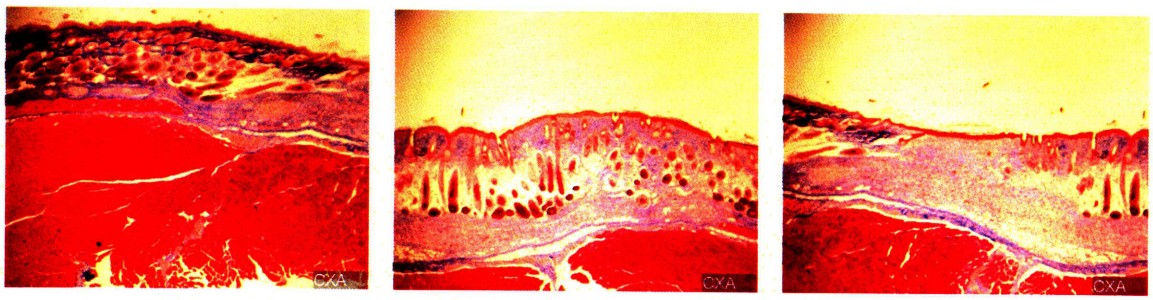


(a) 4X (b) 4X (c) 4X

Figure G-1: **Animal CXA (Untreated Control Group with scaffold)**

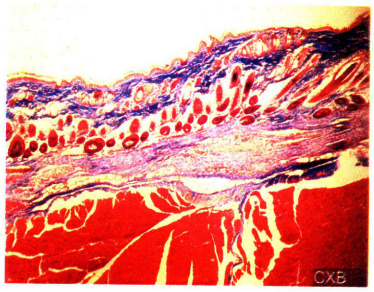


(a) 4X

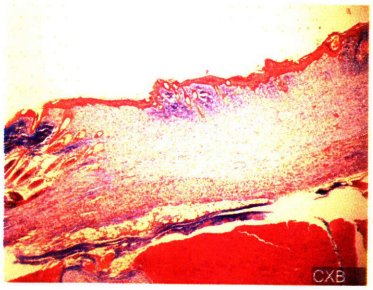


(b) 4X

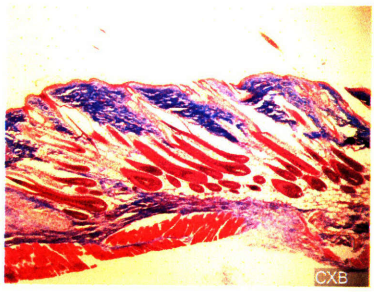


(c) 4X

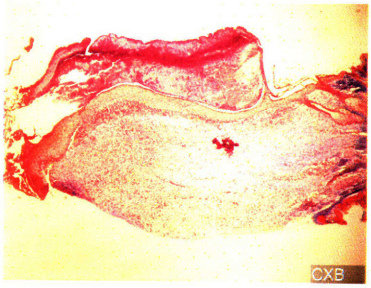


(d) 4X

Figure G-2: **Animal CXB (Untreated Control Group with scaffold)**

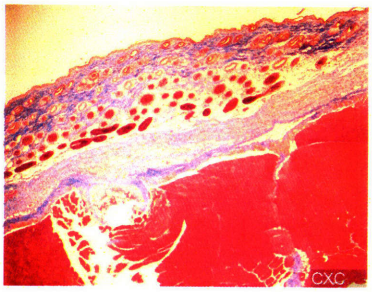


(a) 4X

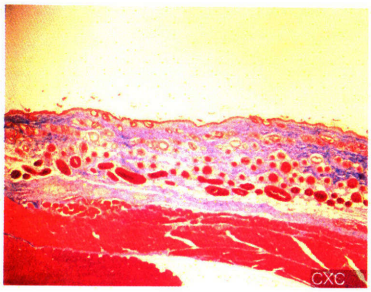


(b) 4X

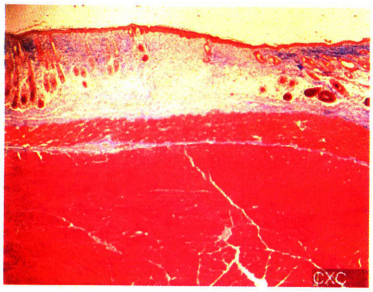


(c) 4X

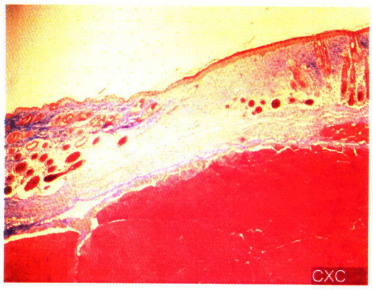


(d) 4X

Figure G-3: **Animal CXC (Untreated Control Group with scaffold)**

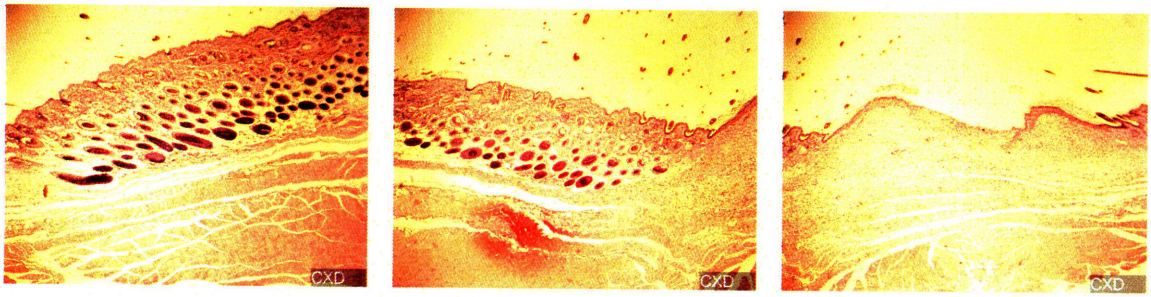


(a) 4X (b) 4X (c) 4X

Figure G-4: **Animal CXD (Untreated Control Group with scaffold)**

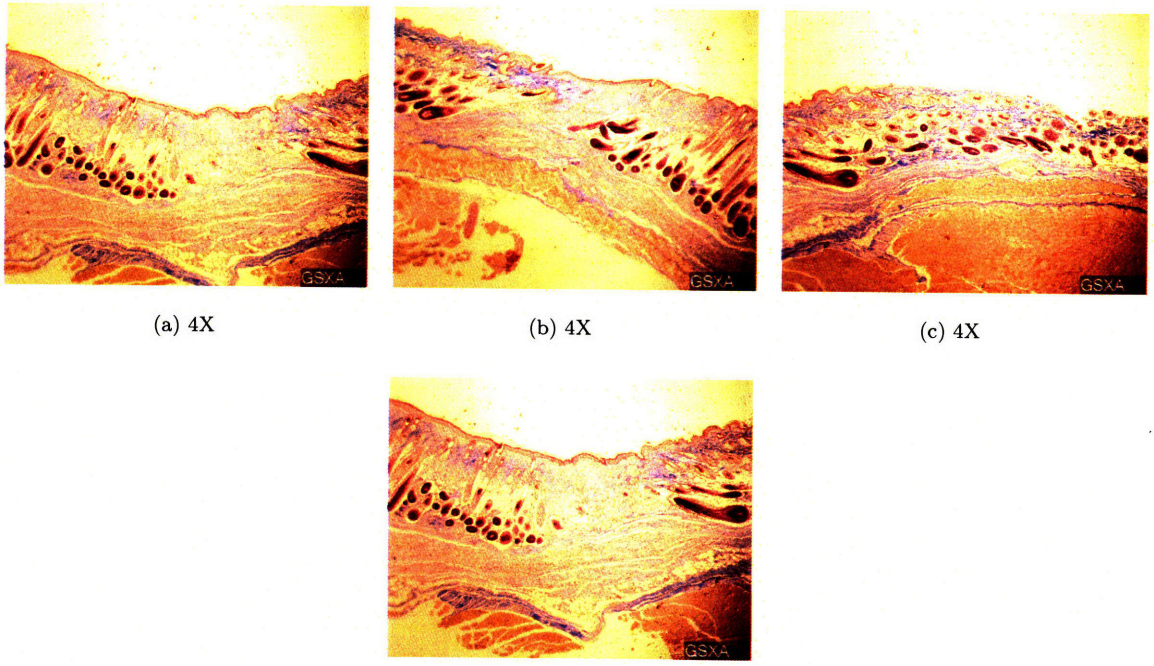


(a) 4X (b) 4X (c) 4X

(d) 4X

Figure G-5: **Animal GSXA (GCSF + SDF-1 with scaffold)**

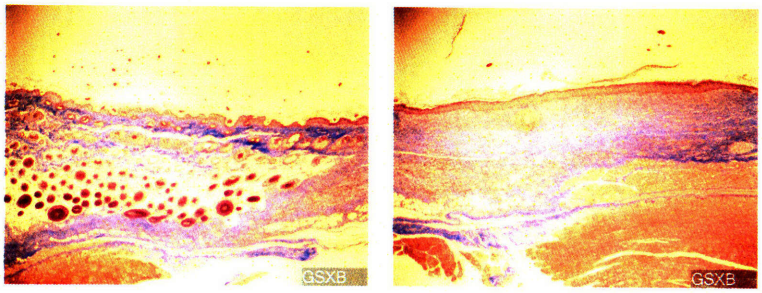


(a) 4X (b) 4X

Figure G-6: **Animal GSXB (GCSF + SDF-1 with scaffold)**

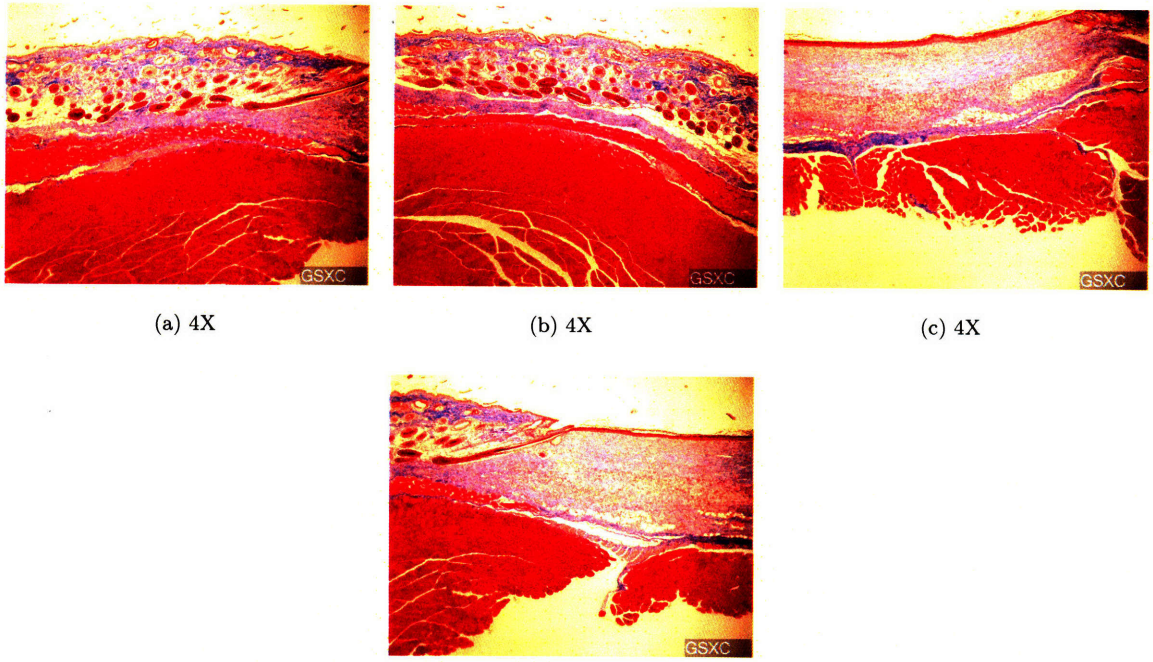


(a) 4X (b) 4X (c) 4X

(d) 4X

Figure G-7: **Animal GSXC (GCSF + SDF-1 with scaffold)**

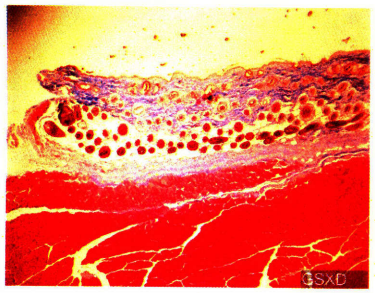


(a) 4X

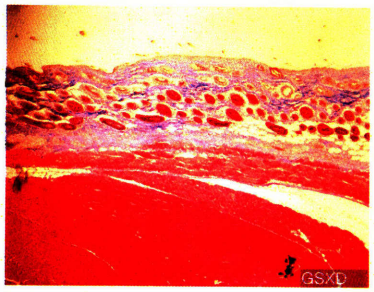


(b) 4X

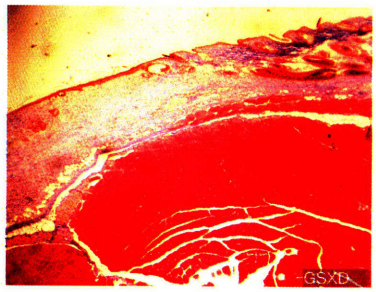


(c) 4X

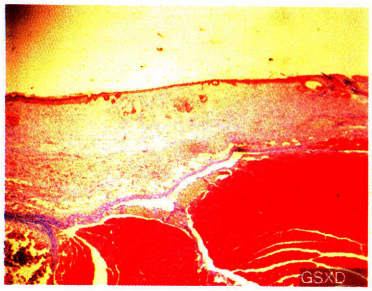


(d) 4X

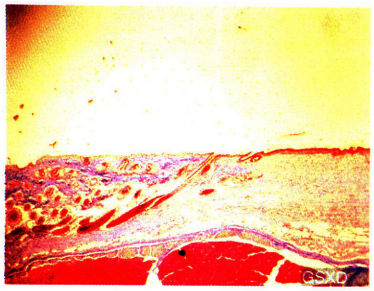


(e) 4X

Figure G-8: **Animal GSXD (GCSF + SDF-1 with scaffold)**

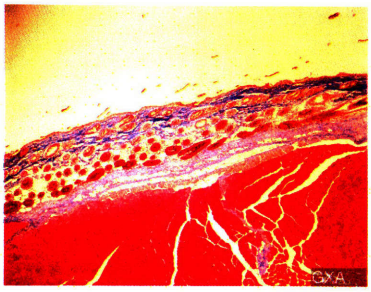


(a) 4X

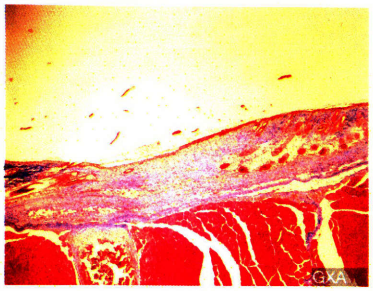


(b) 4X

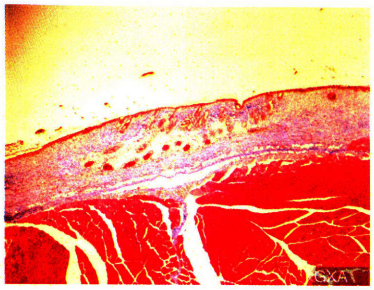


(c) 4X

Figure G-9: **Animal GXA (GCSF with scaffold)**

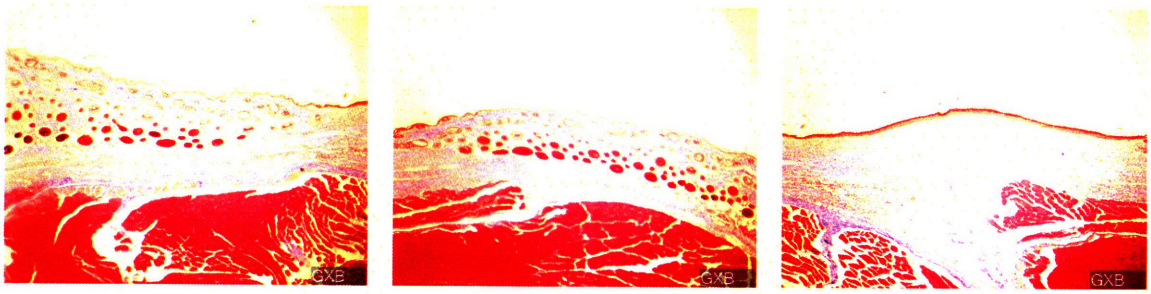


(a) 4X (b) 4X (c) 4X

Figure G-10: **Animal GXB (GCSF with scaffold)**

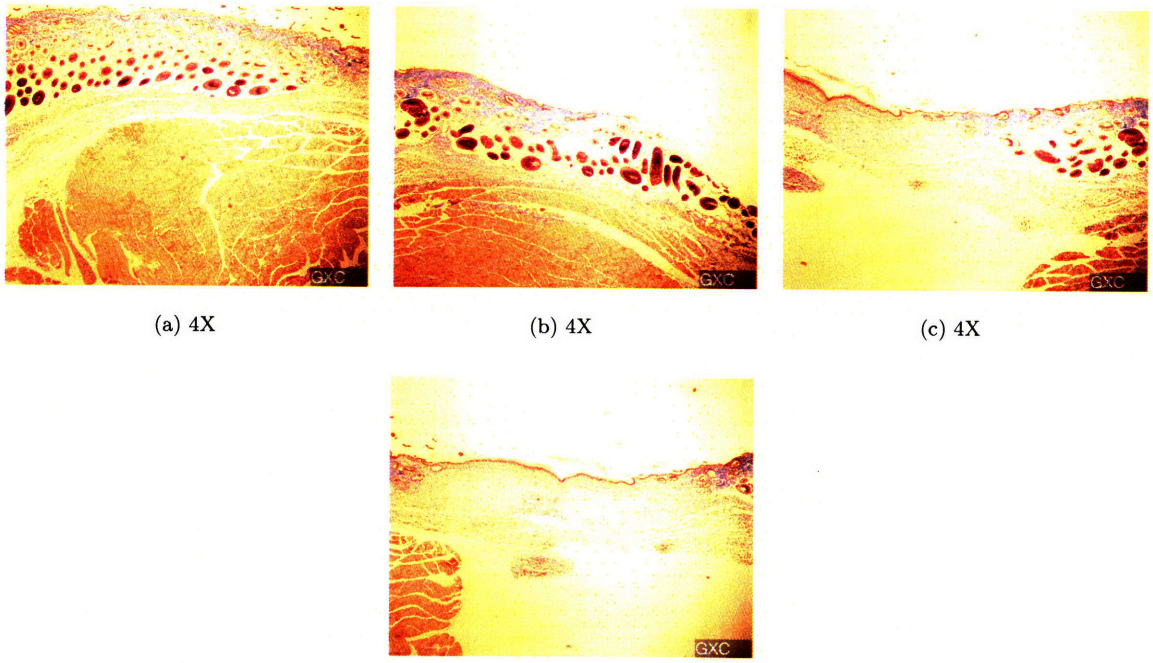


(a) 4X (b) 4X (c) 4X

(d) 4X

Figure G-11: **Animal GXC (GCSF with scaffold)**

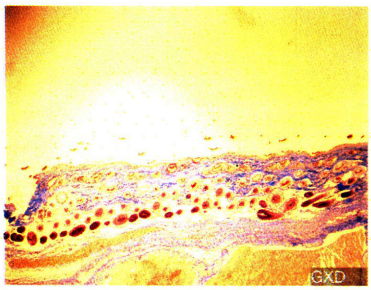


(a) 4X

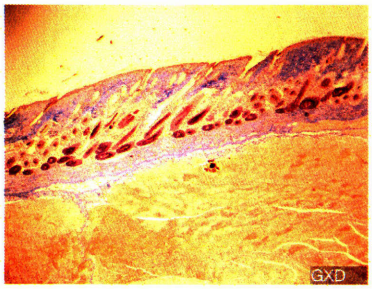


(b) 4X

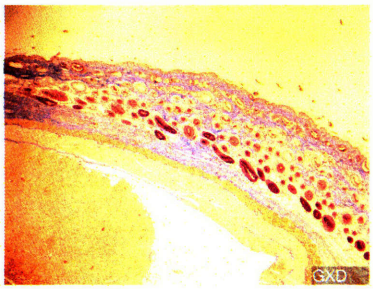


(c) 4X

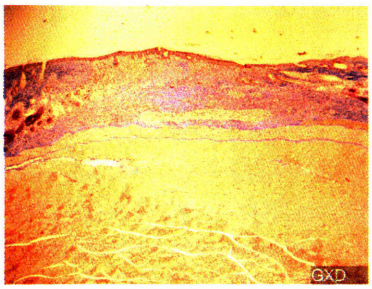


(d) 4X

Figure G-12: **Animal GXD (GCSF with scaffold)**

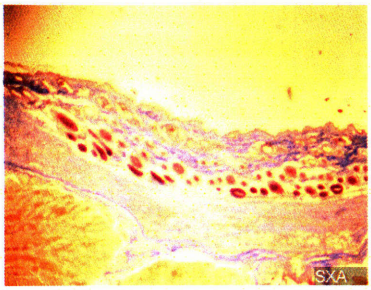


(a) 4X

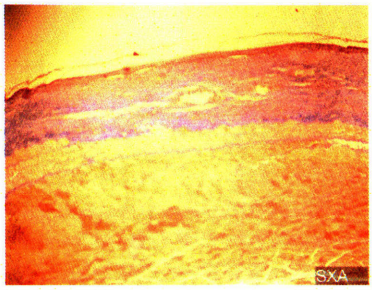


(b) 4X

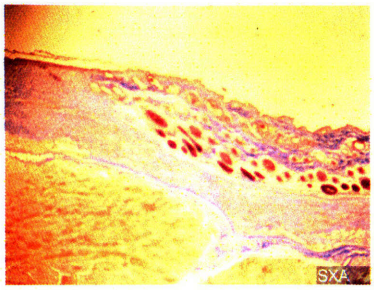


(c) 4X

Figure G-13: **Animal SXA (SDF-1 with scaffold)**

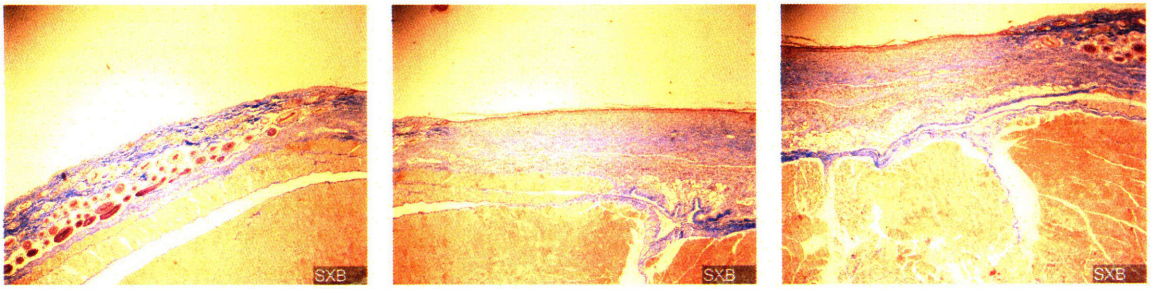


(a) 4X (b) 4X (c) 4X

Figure G-14: **Animal SXB (SDF-1 with scaffold)**

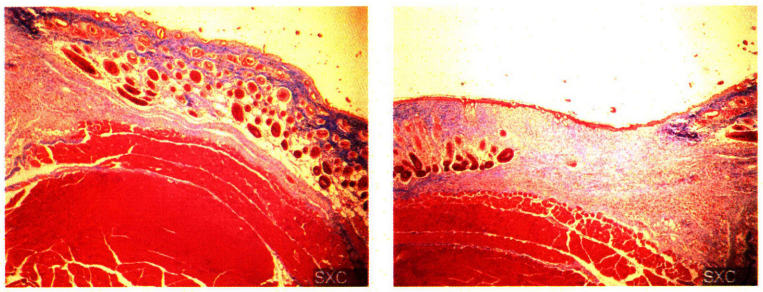


(a) 4X (b) 4X

Figure G-15: **Animal SXC (SDF-1 with scaffold)**

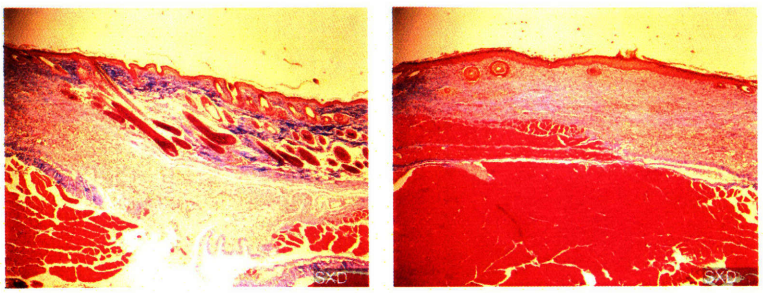


(a) 4X (b) 4X

Figure G-16: **Animal SXD (SDF-1 with scaffold)**

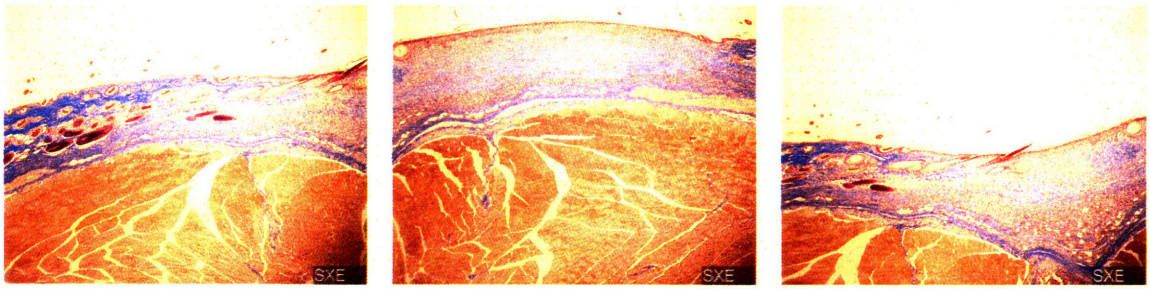


(a) 4X (b) 4X (c) 4X

Figure G-17: **Animal SXE (SDF-1 with scaffold)**

| Group Type | Closure Day | Animal Name | Contraction Distance Left Side (Pixels) | Contraction Distance Right Side (Pixels) | Contraction Distance Total (Pixels) | Neoepidermis/Reepithelialization Distance (Pixels) | Contraction Distance Average (mm) | Contraction Distance STD. DEV | Neoepidermis/Reepithelialization Distance Average (mm) | Neoepidermis/Reepithelialization Distance STD. DEV | Observations |
|---|---|---|---|---|---|---|---|---|---|---|---|
| Control | | CXA | 817 523 | 1943 207 | 2760 730 | 435 097 | 5 993 | 0 808 | 1 0099 | 0 8291 | |
| | | CXB | 1681 36 | 1812 697 | 3494 277 | 0 000 | | | | | |
| | | CXC | 1543 829 | 1931 723 | 3477 362 | 1086 207 | | | | | Normal dermis with hair growing in side of reepithelialized area (the normal dermis resembles the neoepidermis area) |
| | | CXD | 1086 383 | 1308 823 | 2965 836 | 671 891 | | | | | |
| GCSF | 16 | GXA | 1904 332 | 1132 931 | 3037 483 | 815 349 | 6 241 | 0 809 | 2 1050 | 0 7407 | |
| | | GXB | 1408 46 | 1520 856 | 2929 316 | 1654 791 | | | | | |
| | | GXC | 1548 226 | 2215 313 | 3758 541 | 1232 341 | | | | | |
| | | GXD | 2184 316 | 1520 846 | 3705 164 | 827 420 | | | | | |
| GCSF+SDF-1 | 17 | GSXA | 1242 434 | 1974 08 | 3216 514 | 960 804 | 5 476 | 2 531 | 3 0482 | 0 9002 | |
| | | GSXB | 1154 718 | 0 | 1154 718 | 1642 106 | | | | | |
| | | GSXC | 1454 985 | 1500 907 | 2955 892 | 2058 829 | | | | | |
| | | GSXD | 2210 896 | 2245 927 | 4456 825 | 1858 113 | | | | | |
| SDF-1 | 16 | SXA | 1009 889 | 1598 968 | 2608 857 | 2105 889 | 3 178 | 0 945 | 3 3693 | 1 2324 | |
| | | SXB | 1002 419 | 606 849 | 1609 268 | 2367 876 | | | | | |
| | | SXC | 0 | 1479 158 | 1479 158 | 739 475 | | | | | |
| | | SXD | 0 | 1486 423 | 1486 423 | 1671 261 | | | | | |
| | | SXE | 1367 981 | 0 | 1367 981 | 2198 993 | | | | | |

NOTE: In 4X, 1mm = 538 pixels

| Contraction Distance (Length) | | | | |
|---|---|---|---|---|
| | Control | GCSF | GCSF+SDF-1 | SDF-1 |
| Average | 3 993478 16 | 6 241356911 | 5 47581 2732 | 3 178173978 |
| Standard Deviation | 0 807879252 | 0 808975156 | 2 531468193 | 0 945232706 |

| RESULTS | | |
|---|---|---|
| p-value | Group comparison types | Stat value |
| p<0.05 is significant | Control versus SDF-1 | 0 001884851 |
| | Control versus GCSF+SDF-1 | 0 748722393 |
| | Control versus GCSF | 0 679813878 |
| | GCSF versus GCSF+SDF-1 | 0 398540615 |
| | GCSF versus SDF-1 | 0 001243799 |
| | SDF-1 versus GCSF+SDF-1 | 0 166571896 |

| Neoepidermis/Re-epithelialization Distance (Length) | | | | |
|---|---|---|---|---|
| | Control | GCSF | GCSF+SDF-1 | SDF-1 |
| Average | 1 009881108 | 2 104972584 | 3 048186803 | 3 369261 71 |
| Standard Deviation | 0 829144384 | 0 740712 48 | 0 900173 58 | 1 23250 7858 |

| RESULTS | | |
|---|---|---|
| p-value | Group comparison types | Stat value |
| p<0.05 is significant | Control versus SDF-1 | 0 011434033 |
| | Control versus GCSF+SDF-1 | 0 015943 7029 |
| | Control versus GCSF | 0 096589 7230 |
| | GCSF versus GCSF+SDF-1 | 0 158572 0139 |
| | GCSF versus SDF-1 | 0 109873 2173 |
| | SDF-1 versus GCSF+SDF-1 | 0 885317 4803 |

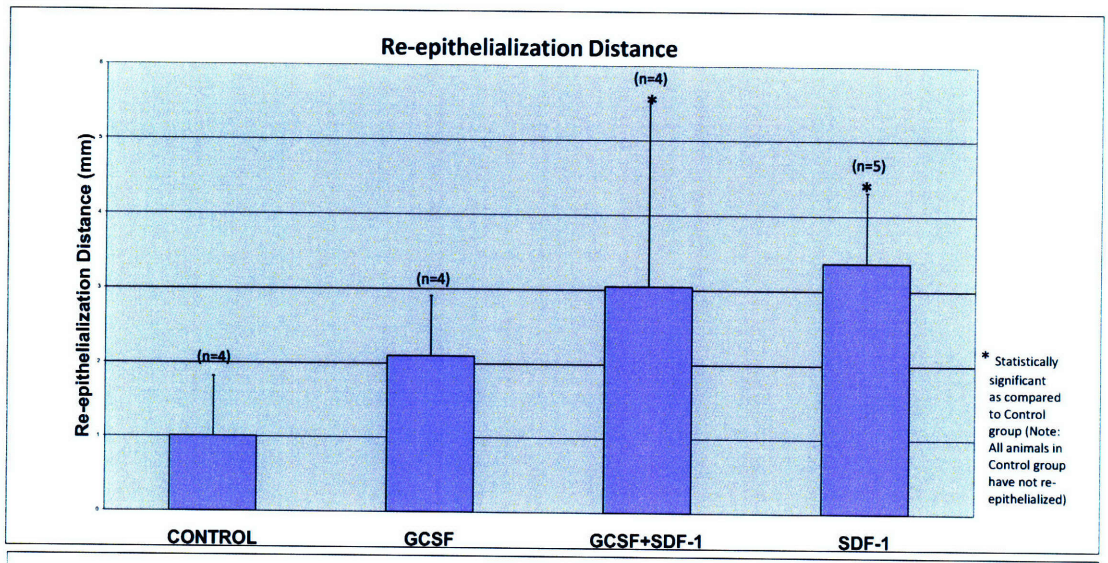


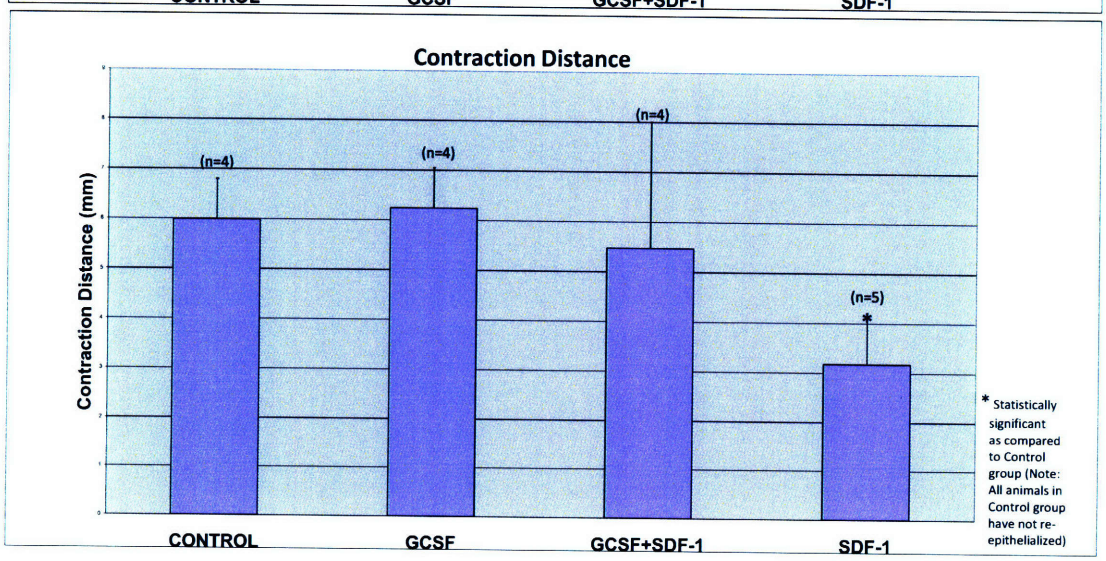

# Appendix H

# Ki67 Stain (Day 3 Post-Surgery)

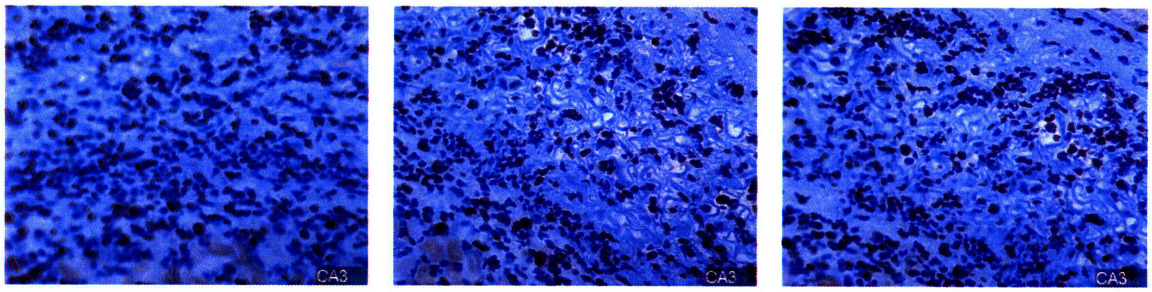


(a) 40X (b) 40X (c) 40X

Figure H-1: **Animal CA3 (Untreated Control Group with scaffold)**

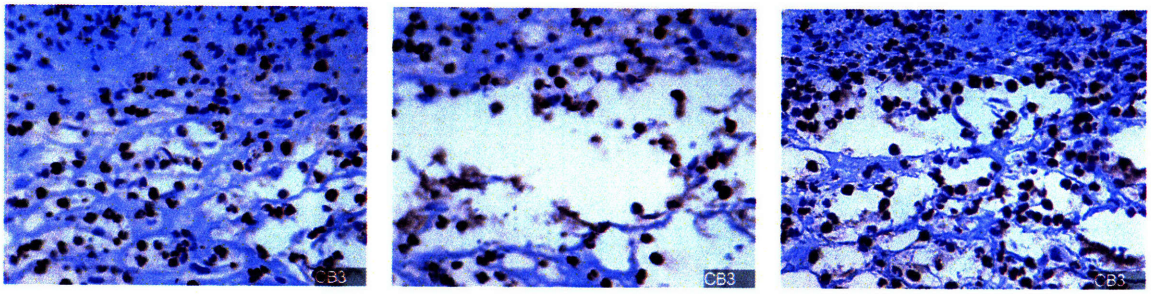


(a) 40X (b) 40X (c) 40X

Figure H-2: **Animal CB3 (Untreated Control Group with scaffold)**

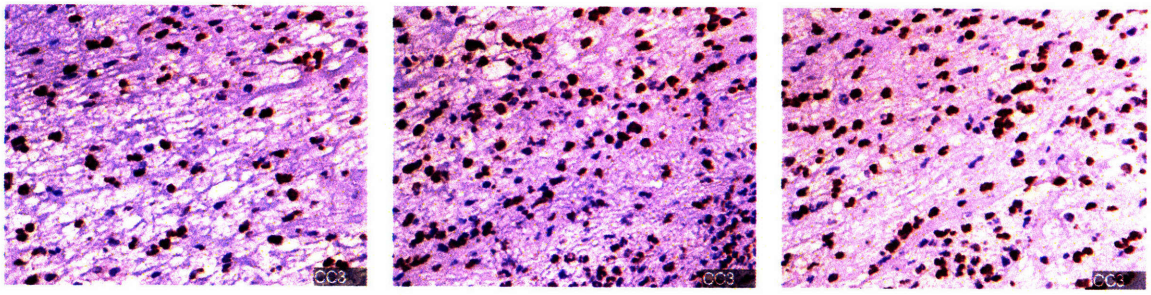


(a) 40X (b) 40X (c) 40X

Figure H-3: **Animal CC3 (Untreated Control Group with scaffold)**

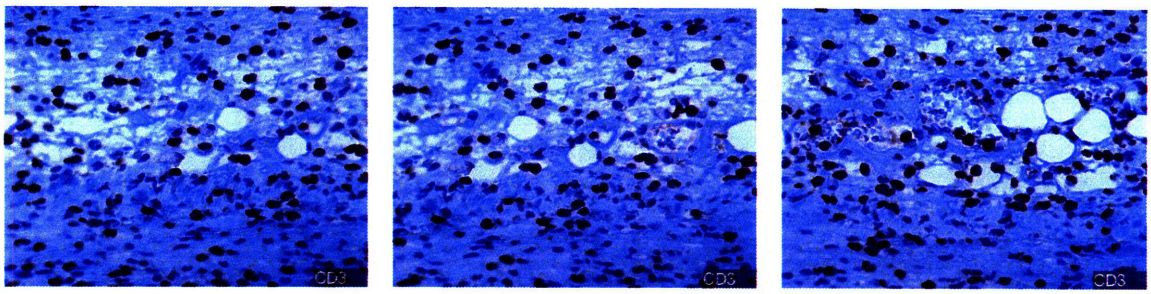


(a) 40X (b) 40X (c) 40X

Figure H-4: **Animal CD3 (Untreated Control Group with scaffold)**

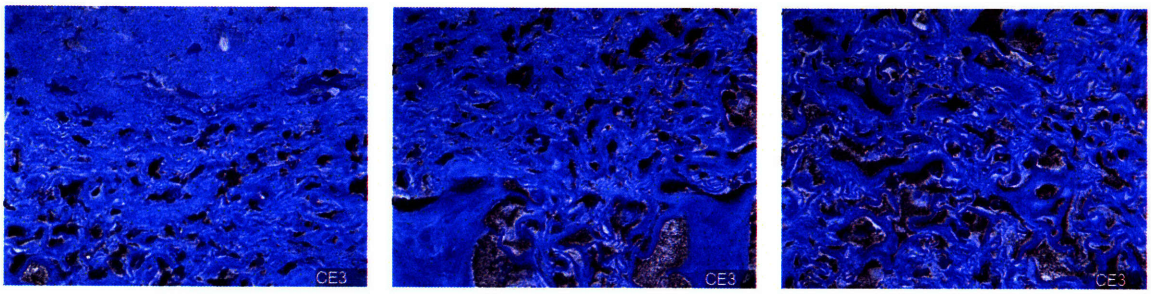


(a) 40X (b) 40X (c) 40X

Figure H-5: **Animal CE3 (Untreated Control Group with scaffold)**

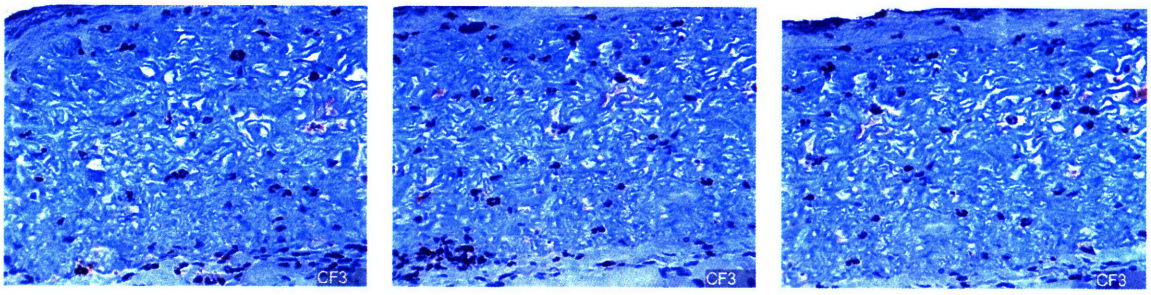


(a) 40X (b) 40X (c) 40X

Figure H-6: **Animal CF3 (Untreated Control Group with scaffold)**

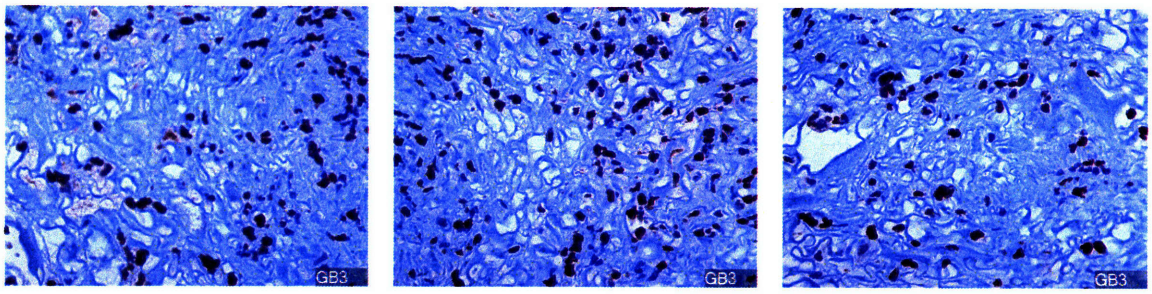


(a) 40X (b) 40X (c) 40X

Figure H-7: **Animal GB3 (GCSF with scaffold)**

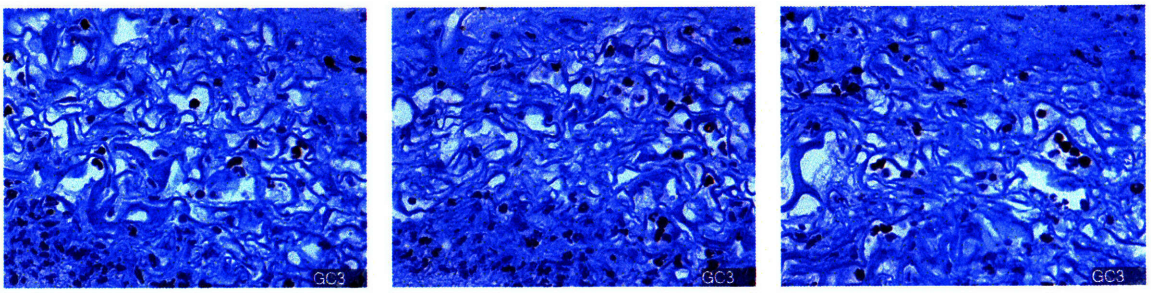


(a) 40X (b) 40X (c) 40X

Figure H-8: **Animal GC3 (GCSF with scaffold)**

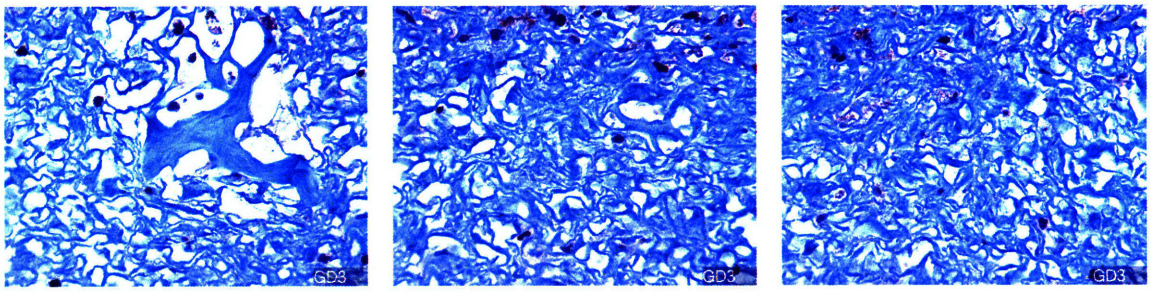


(a) 40X (b) 40X (c) 40X

Figure H-9: **Animal GD3 (GCSF with scaffold)**

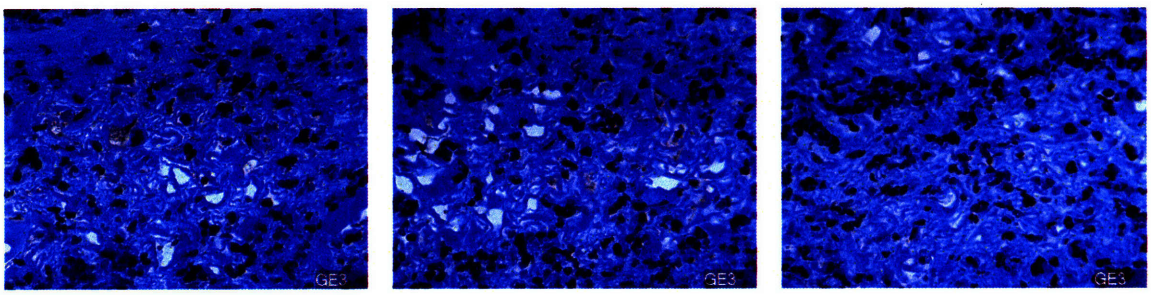


(a) 40X (b) 40X (c) 40X

Figure H-10: **Animal GE3 (GCSF with scaffold)**

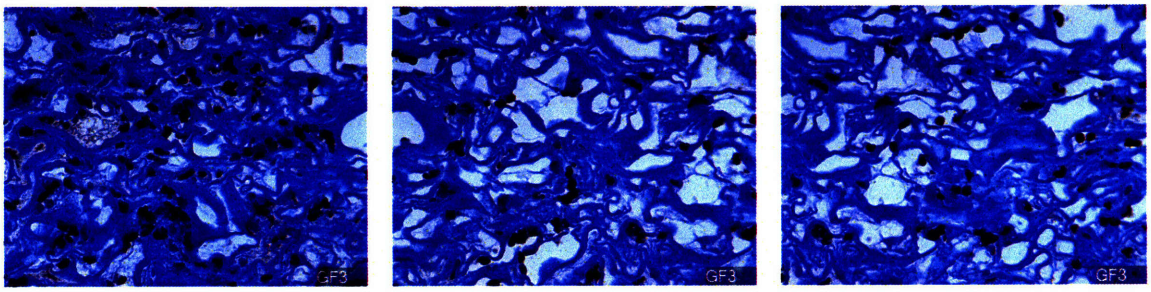


(a) 40X (b) 40X (c) 40X

Figure H-11: **Animal GF3 (GCSF with scaffold)**

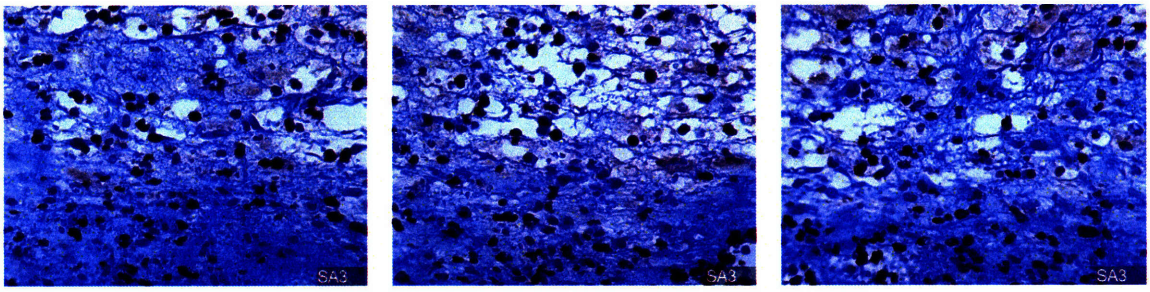


(a) 40X (b) 40X (c) 40X

Figure H-12: **Animal SA3 (SDF-1 with scaffold)**

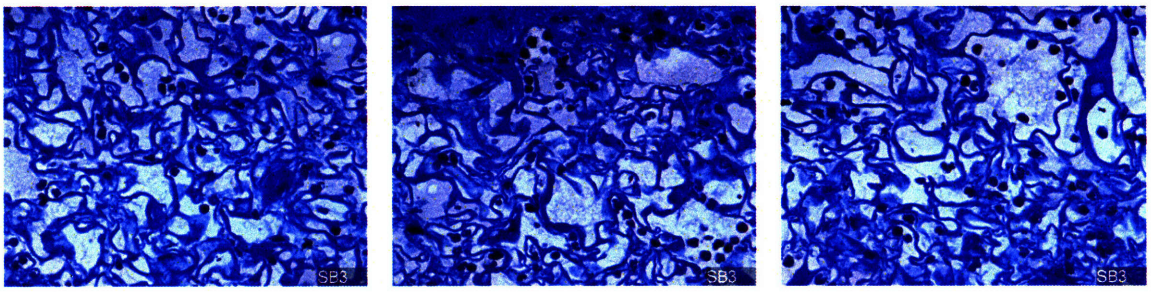


(a) 40X (b) 40X (c) 40X

Figure H-13: **Animal SB3 (SDF-1 with scaffold)**

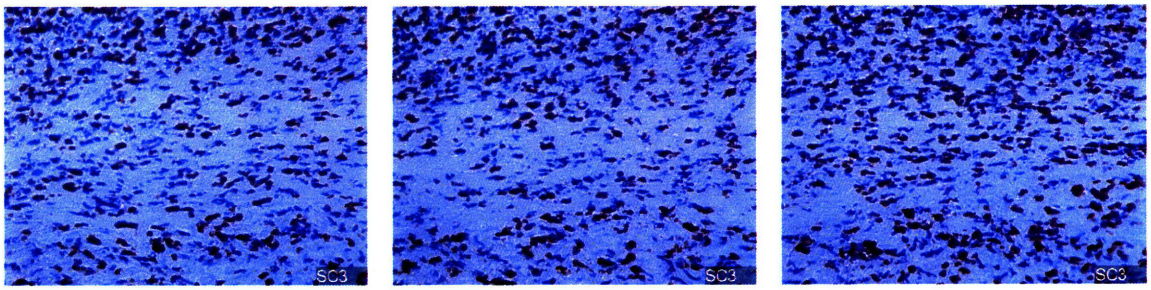


(a) 40X (b) 40X (c) 40X

Figure H-14: **Animal SC3 (SDF-1 with scaffold)**

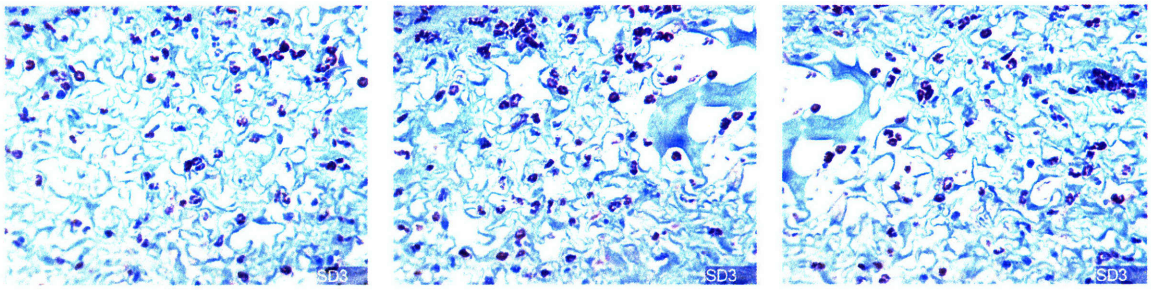


(a) 40X (b) 40X (c) 40X

Figure H-15: **Animal SD3 (SDF-1 with scaffold)**

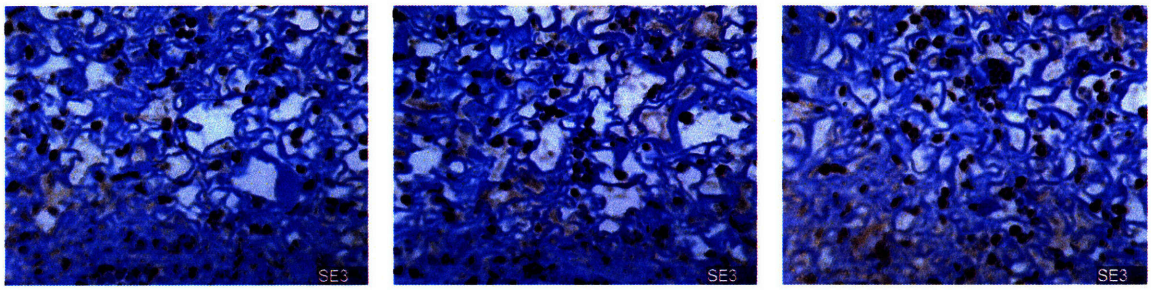


(a) 40X (b) 40X (c) 40X

Figure H-16: **Animal SE3 (SDF-1 with scaffold)**

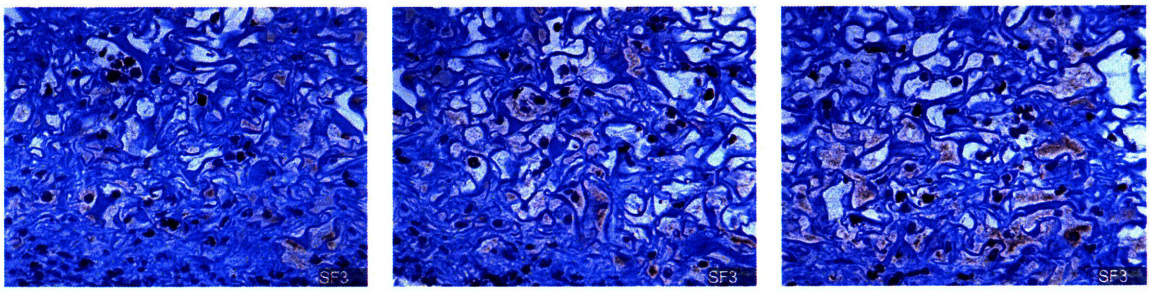


(a) 40X (b) 40X (c) 40X

Figure H-17: **Animal SF3 (SDF-1 with scaffold)**

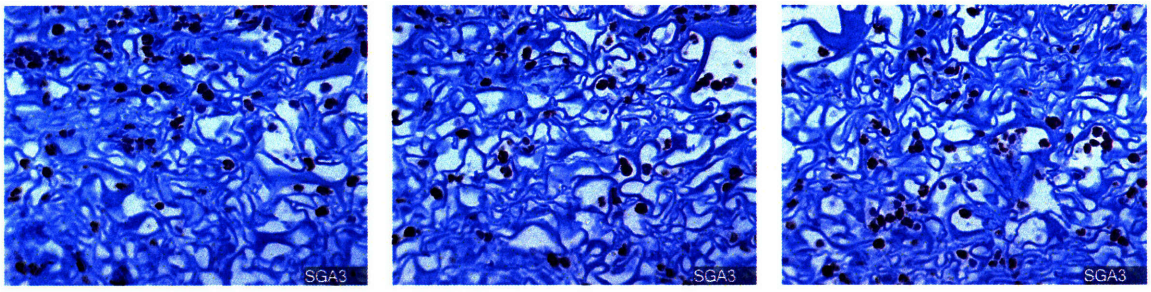


(a) 40X (b) 40X (c) 40X

Figure H-18: **Animal SGA3 (GCSF + SDF-1 with scaffold)**

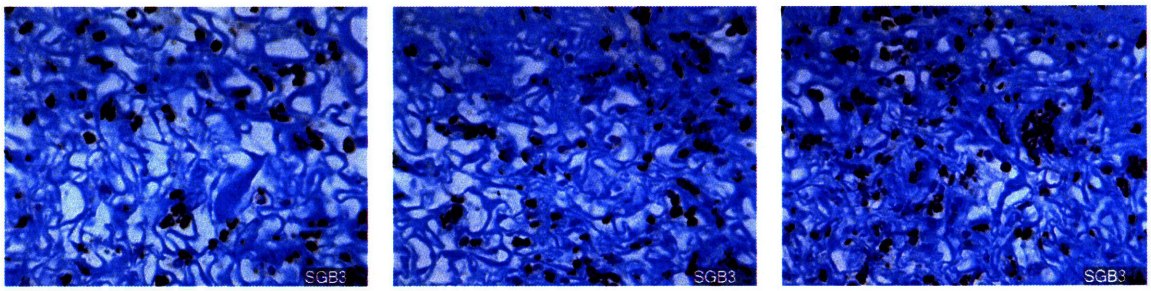


(a) 40X (b) 40X (c) 40X

Figure H-19: **Animal SGB3 (GCSF + SDF-1 with scaffold)**

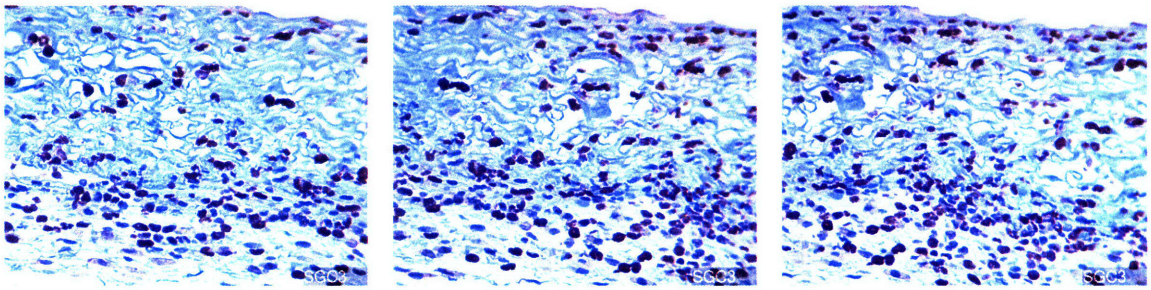

(a) 40X (b) 40X (c) 40X

Figure H-20: **Animal SGC3 (GCSF + SDF-1 with scaffold)**

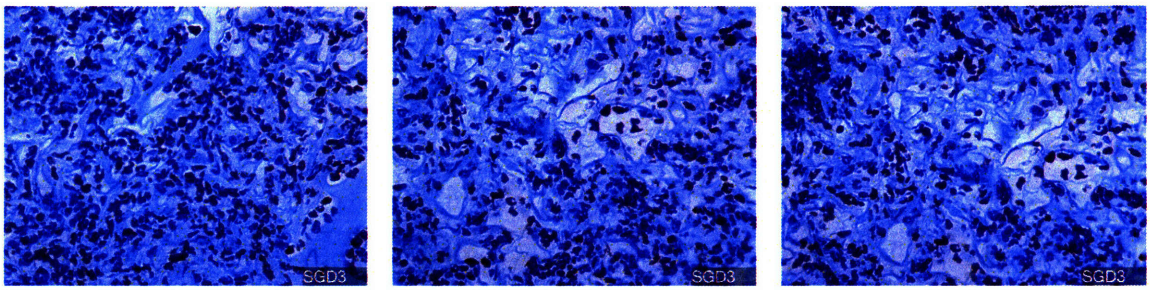


(a) 40X (b) 40X (c) 40X

Figure H-21: **Animal SGD3 (GCSF + SDF-1 with scaffold)**

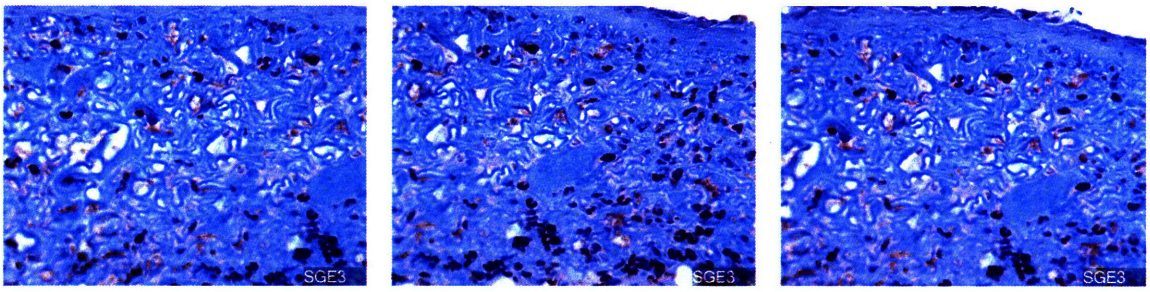


(a) 40X (b) 40X (c) 40X

Figure H-22: **Animal SGE3 (GCSF + SDF-1 with scaffold)**

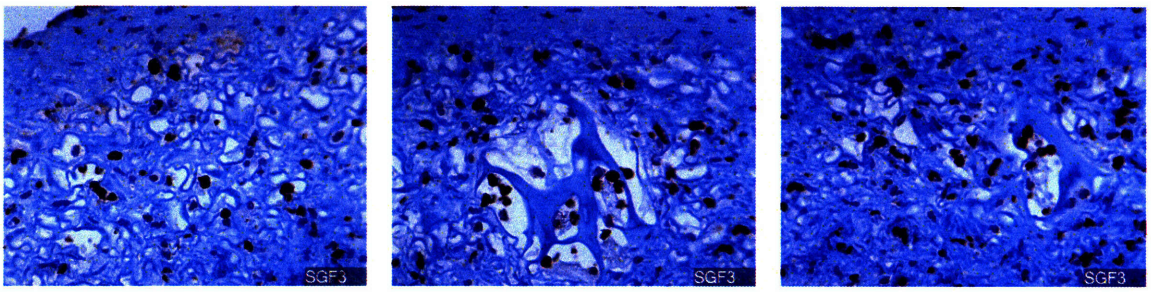


(a) 40X (b) 40X (c) 40X

Figure H-23: **Animal SGF3 (GCSF + SDF-1 with scaffold)**

| Name | Middle Ki67+ cells | Middle Ki67- cells | Total number of Middle cells | Middle Proliferation Rate of Ki67+ | Left Ki67+ cells | Left Ki67- cells | Total number of Left cells | Left Proliferation Rate of Ki67+ | Right Ki67+ cells | Right Ki67- cells | Total number of Right cells | Right Proliferation Rate of Ki67+ | Total Proliferation Rate | Average | Standard Deviation | P Value (Treated group versus Control) | P Result (p<0.05 is significant) |
|---|---|---|---|---|---|---|---|---|---|---|---|---|---|---|---|---|---|
| CA3 | 170 | 143 | 313 | 54.31309904 | 193 | 153 | 346 | 55.78034682 | 226 | 144 | 370 | 61.08108108 | 57.05817565 | 57.07609219 | 11.92647739 | | |
| CB3 | 79 | 20 | 99 | 79.7979798 | 124 | 65 | 189 | 65.60846561 | 120 | 62 | 182 | 65.93406593 | 70.44683711 | | | | |
| CC3 | 58 | 101 | 159 | 36.47798742 | 99 | 48 | 147 | 67.34693878 | 70 | 57 | 127 | 55.11811024 | 52.98101214 | | | | |
| CD3 | 88 | 94 | 182 | 48.35164835 | 92 | 95 | 187 | 49.19786096 | 116 | 78 | 194 | 59.79381443 | 52.44777458 | | | | |
| CE3 | 36 | 12 | 48 | 75 | 52 | 16 | 68 | 76.47058824 | 22 | 15 | 37 | 59.45945946 | 70.3100159 | | | | |
| CF3 | 39 | 66 | 105 | 37.14285714 | 31 | 45 | 76 | 40.78947368 | 27 | 41 | 68 | 39.70588235 | 39.21273773 | | | | |
| | | | | | | | | | | | | | | | | | |
| GB3 | 89 | 47 | 136 | 65.44117647 | 78 | 25 | 103 | 75.72815534 | 73 | 36 | 109 | 66.97247706 | 69.38060296 | 67.25769906 | 18.20797581 | 0.32038905 | Not significant |
| GC3 | 40 | 59 | 99 | 40.4040404 | 28 | 63 | 91 | 30.76923077 | 28 | 39 | 67 | 41.79104478 | 37.65477198 | | | | |
| GD3 | 11 | 4 | 15 | 73.33333333 | 9 | 2 | 11 | 81.81818182 | 6 | 7 | 13 | 46.15384615 | 67.1017871 | | | | |
| GE3 | 141 | 38 | 179 | 78.77094972 | 124 | 59 | 183 | 67.75956284 | 166 | 42 | 208 | 79.80769231 | 75.44606829 | | | | |
| GF3 | 55 | 8 | 63 | 87.3015873 | 99 | 23 | 122 | 81.14754098 | 44 | 4 | 48 | 91.66666667 | 86.70526498 | | | | |
| | | | | | | | | | | | | | | | | | |
| SA3 | 63 | 34 | 97 | 64.94845361 | 56 | 48 | 104 | 53.84615385 | 75 | 41 | 116 | 64.65517241 | 61.14992662 | 75.50955257 | 15.28269611 | 0.043538871 | Significant |
| SB3 | 31 | 7 | 38 | 81.57894737 | 42 | 4 | 46 | 91.30434783 | 31 | 10 | 41 | 75.6097561 | 82.8310171 | | | | |
| SC3 | 104 | 86 | 190 | 54.73684211 | 106 | 119 | 225 | 47.11111111 | 125 | 65 | 190 | 65.78947368 | 55.8791423 | | | | |
| SD3 | 65 | 12 | 77 | 84.41558442 | 61 | 7 | 68 | 89.70588235 | 61 | 12 | 73 | 83.56164384 | 85.8943702 | | | | |
| SE3 | 64 | 5 | 69 | 92.75362319 | 75 | 4 | 79 | 94.93670886 | 90 | 1 | 91 | 98.9010989 | 95.53047698 | | | | |
| SF3 | 36 | 10 | 46 | 78.26086957 | 32 | 34 | 66 | 48.48484848 | 31 | 4 | 35 | 88.57142857 | 71.77238221 | | | | |
| | | | | | | | | | | | | | | | | | |
| SGA3 | 47 | 2 | 49 | 95.91836735 | 48 | 8 | 56 | 85.71428571 | 47 | 7 | 54 | 87.03703704 | 89.55656337 | 69.17711097 | 14.81017849 | 0.151480824 | Not significant |
| SGB3 | 84 | 21 | 105 | 80 | 72 | 7 | 79 | 91.13924051 | 93 | 52 | 145 | 64.13793103 | 78.42572385 | | | | |
| SGC3 | 136 | 73 | 209 | 65.07177033 | 96 | 45 | 141 | 68.08510638 | 140 | 80 | 220 | 63.63636364 | 65.59774678 | | | | |
| SGD3 | 120 | 57 | 177 | 67.79661017 | 37 | 148 | 185 | 20 | 144 | 131 | 275 | 52.36363636 | 46.72008218 | | | | |
| SGE3 | 85 | 26 | 111 | 76.57657658 | 38 | 17 | 55 | 69.09090909 | 38 | 13 | 51 | 74.50980392 | 73.39242986 | | | | |
| SGF3 | 40 | 33 | 73 | 54.79452055 | 32 | 23 | 55 | 58.18181818 | 69 | 28 | 97 | 71.13402062 | 61.37011978 | | | | |

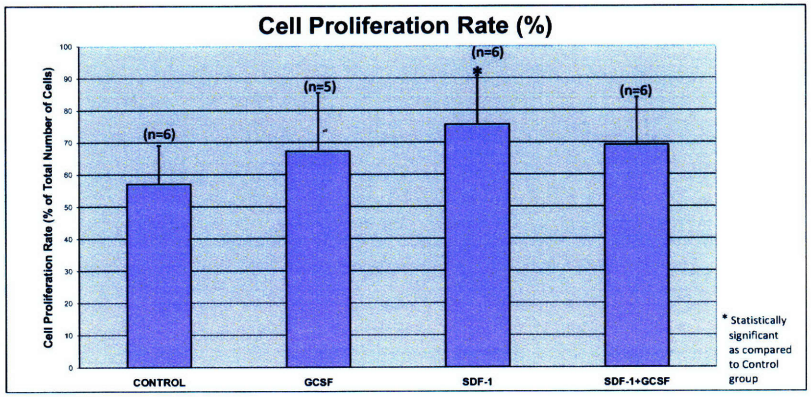


## Cell Proliferation Rate (Ki67+)

| | Control | GCSF | SDF-1 | SDF-1+GCSF |
|---|---|---|---|---|
| Average | 57.07609219 | 67.25769906 | 75.50955257 | 69.17711097 |
| Standard Deviation | 11.92647739 | 18.20797581 | 15.28269611 | 14.81017849 |

| RESULTS | | |
|---|---|---|
| p-value | Group comparison types | ttest value |
| p<0.05 is significant | Control versus SDF-1 | 0.043538707 |
| | Control versus GCSF+SDF-1 | 0.151480241 |
| | Control versus GCSF | 0.320389501 |
| | GCSF versus GCSF+SDF-1 | 0.854761958? |
| | GCSF versus SDF-1 | 0.444699355 |
| | SDF-1 versus GCSF+SDF-1 | 0.482823404? |

# Appendix I

# CD31 Stain (Day 3 Post Surgery)

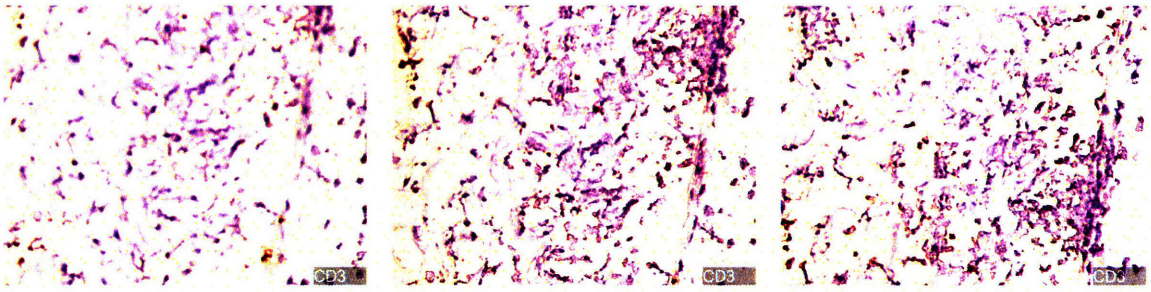


(a) 40X (b) 40X (c) 40X

Figure I-1: **Animal CD3 (Untreated Control Group with scaffold)**

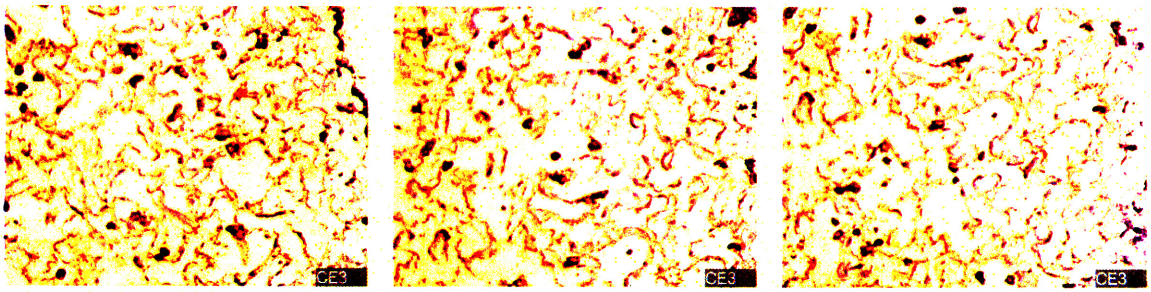


(a) 40X (b) 40X (c) 40X

Figure I-2: **Animal CE3 (Untreated Control Group with scaffold)**

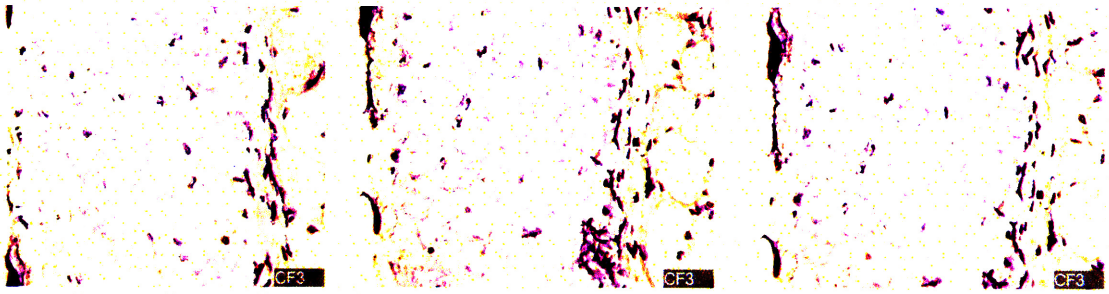


(a) 40X (b) 40X (c) 40X

Figure I-3: **Animal CF3 (Untreated Control Group with scaffold)**

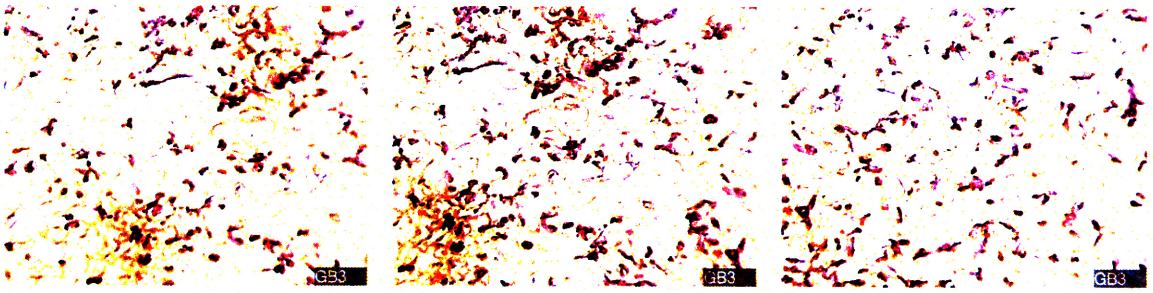


(a) 40X (b) 40X (c) 40X

Figure I-4: **Animal GB3 (GCSF with scaffold)**

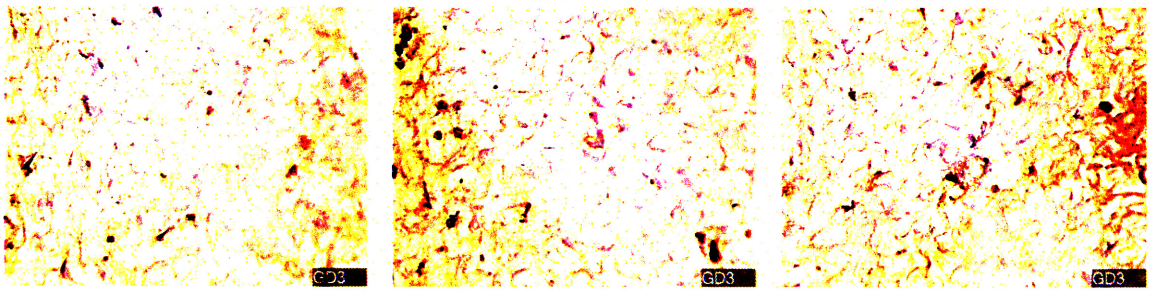


(a) 40X (b) 40X (c) 40X

Figure I-5: **Animal GD3 (GCSF with scaffold)**

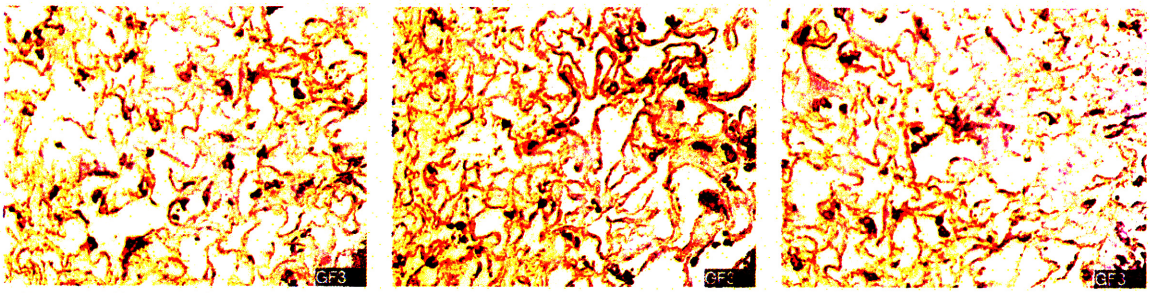


(a) 40X (b) 40X (c) 40X

Figure I-6: **Animal GF3 (GCSF with scaffold)**

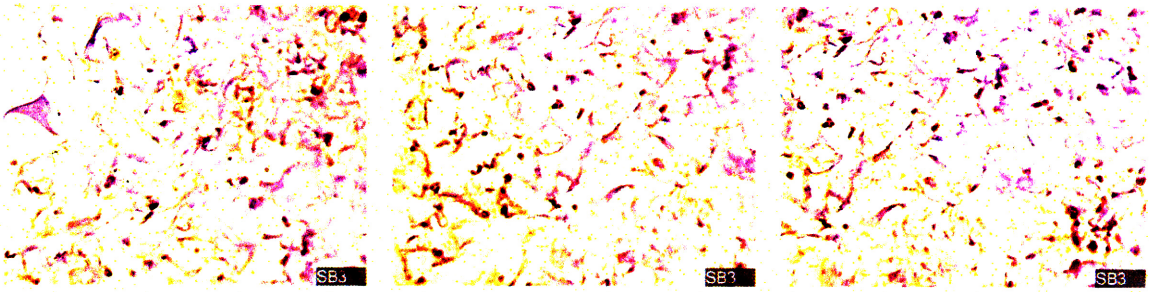


(a) 40X (b) 40X (c) 40X

Figure I-7: **Animal SB3 (SDF-1 with scaffold)**

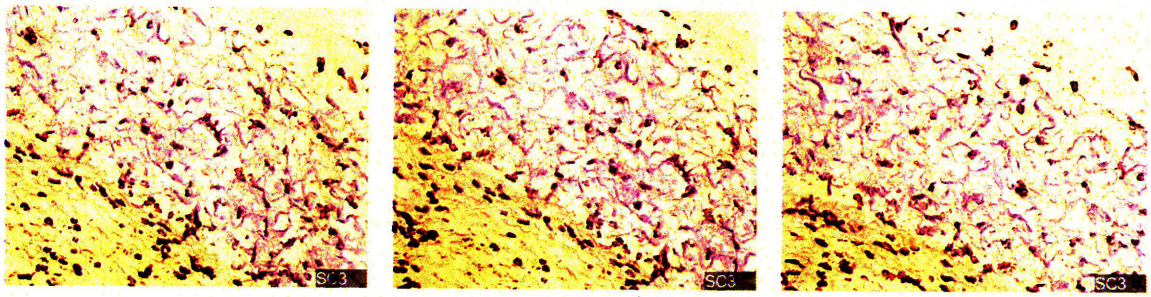


(a) 40X (b) 40X (c) 40X

Figure I-8: **Animal SC3 (SDF-1 with scaffold)**

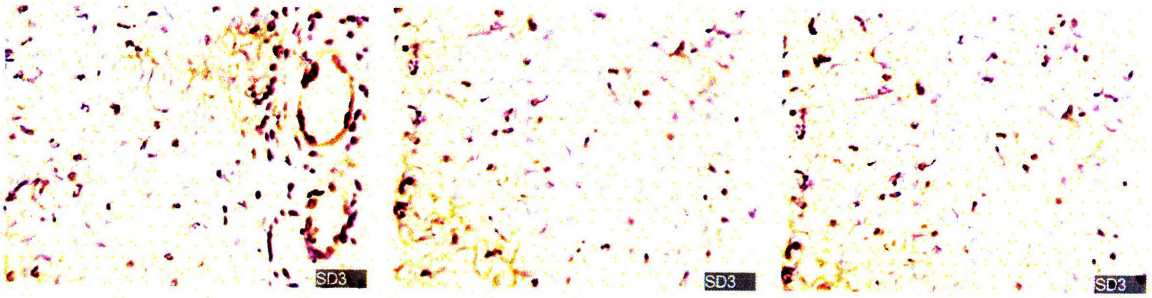


(a) 40X (b) 40X (c) 40X

Figure I-9: **Animal SD3 (SDF-1 with scaffold)**

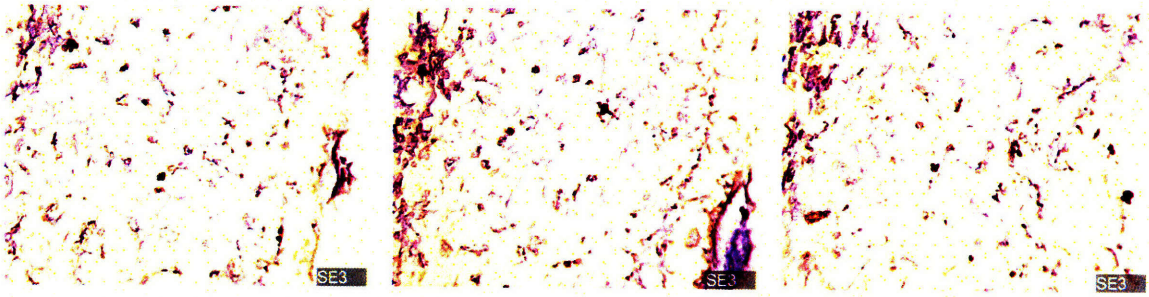


(a) 40X (b) 40X (c) 40X

Figure I-10: **Animal SE3 (SDF-1 with scaffold)**

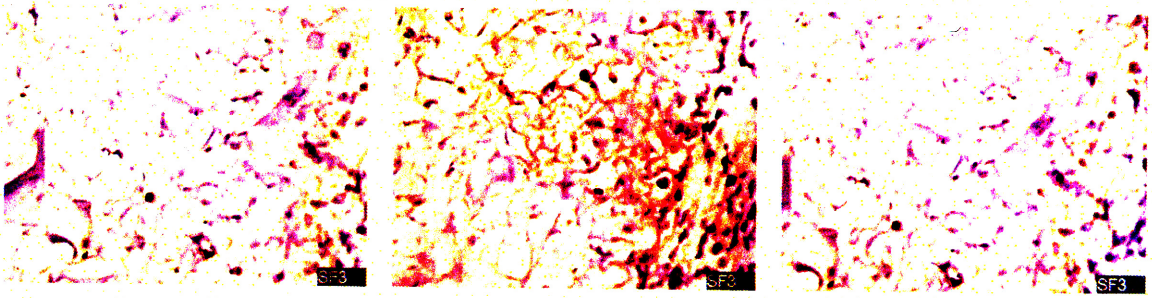


(a) 40X (b) 40X (c) 40X

Figure I-11: **Animal SF3 (SDF-1 with scaffold)**

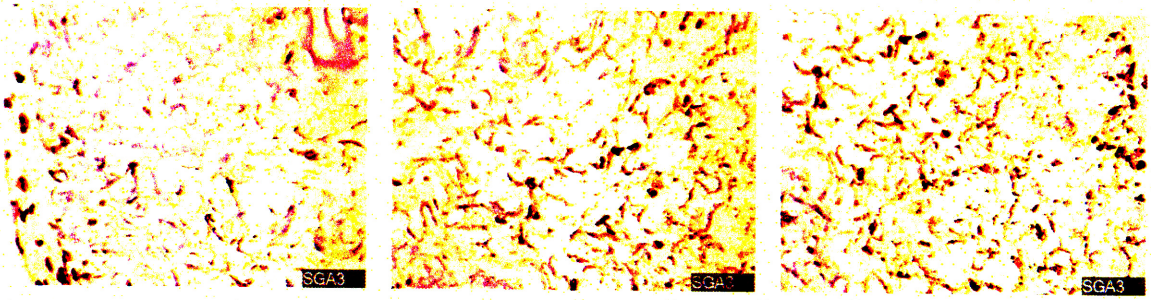


(a) 40X (b) 40X (c) 40X

Figure I-12: **Animal SGA3 (GCSF + SDF-1 with scaffold)**

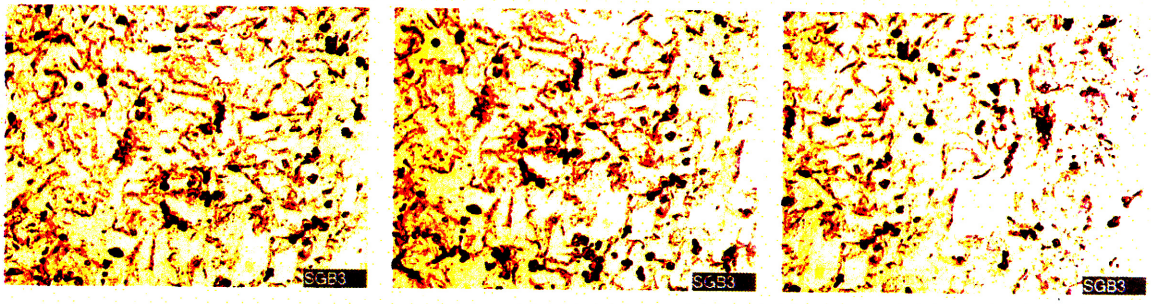


(a) 40X (b) 40X (c) 40X

Figure I-13: **Animal SGB3 (GCSF + SDF-1 with scaffold)**


(a) 40X (b) 40X (c) 40X

Figure I-14: **Animal SGC3 (GCSF + SDF-1 with scaffold)**

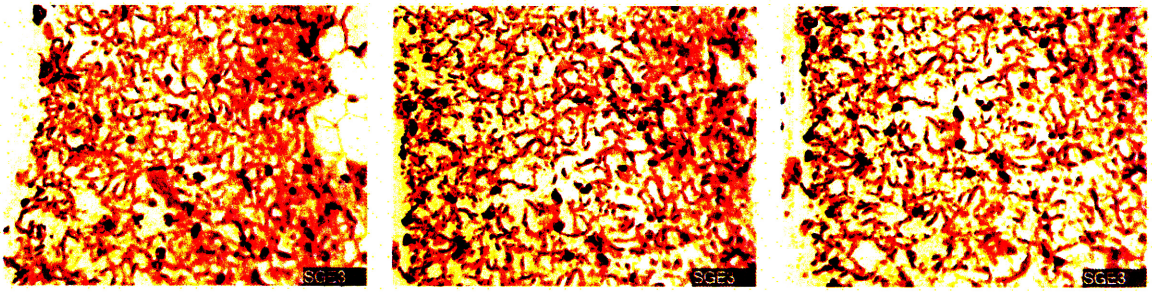


(a) 40X (b) 40X (c) 40X

Figure I-15: **Animal SGE3 (GCSF + SDF-1 with scaffold)**

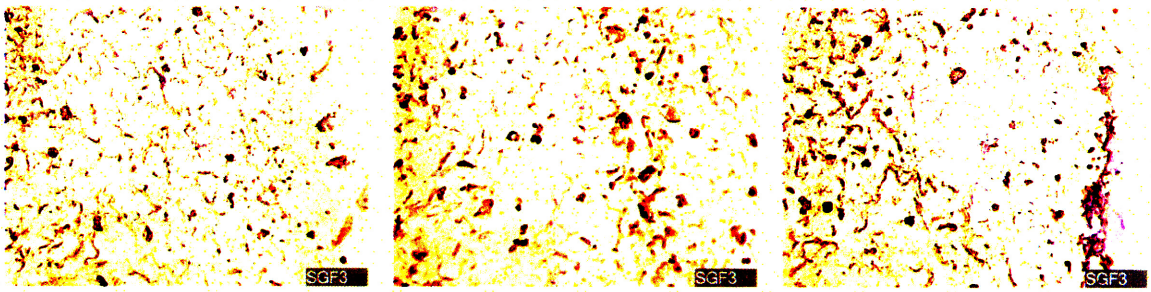


(a) 40X (b) 40X (c) 40X

Figure I-16: **Animal SGF3 (GCSF + SDF-1 with scaffold)**

| Name | Left CD31+ cells | vliddle CD31+ cell | Right CD31+ cells | Total CD31+ cells | Average | Standard Deviation | Observations |
|---|---|---|---|---|---|---|---|
| CA3 | 0 | 0 | 0 | 0 | 5 | 8.148619515 | |
| CB3 | 0 | 0 | 0 | 0 | | | |
| CC3 | 0 | 0 | 0 | 0 | | | |
| CD3 | 4 | 2 | 3 | 9 | | | |
| CE3 | 8 | 5 | 7 | 20 | | | |
| CF3 | 1 | 0 | 0 | 1 | | | |
| | | | | | | | |
| GB3 | 7 | 11 | 6 | 24 | 13.2 | 13.08434179 | |
| GC3 | 0 | 0 | 0 | 0 | | | |
| GD3 | 4 | 7 | 3 | 14 | | | |
| GE3 | 0 | 0 | 0 | 0 | | | |
| GF3 | 9 | 11 | 8 | 28 | | | |
| | | | | | | | |
| SA3 | 0 | 0 | 0 | 0 | 19.16666667 | 15.23701633 | |
| SB3 | 13 | 10 | 7 | 30 | | | |
| SC3 | 5 | 11 | 8 | 24 | | | |
| SD3 | 20 | 10 | 11 | 41 | | | Blood vessels apparent |
| SE3 | 3 | 3 | 2 | 8 | | | |
| SF3 | 3 | 8 | 1 | 12 | | | |
| | | | | | | | |
| SGA3 | 11 | 10 | 16 | 37 | 25.5 | 22.36738697 | |
| SGB3 | 15 | 24 | 23 | 62 | | | |
| SGC3 | 3 | 1 | 2 | 6 | | | |
| SGD3 | 0 | 0 | 0 | 0 | | | |
| SGE3 | 7 | 10 | 6 | 23 | | | |
| SGF3 | 10 | 6 | 9 | 25 | | | |

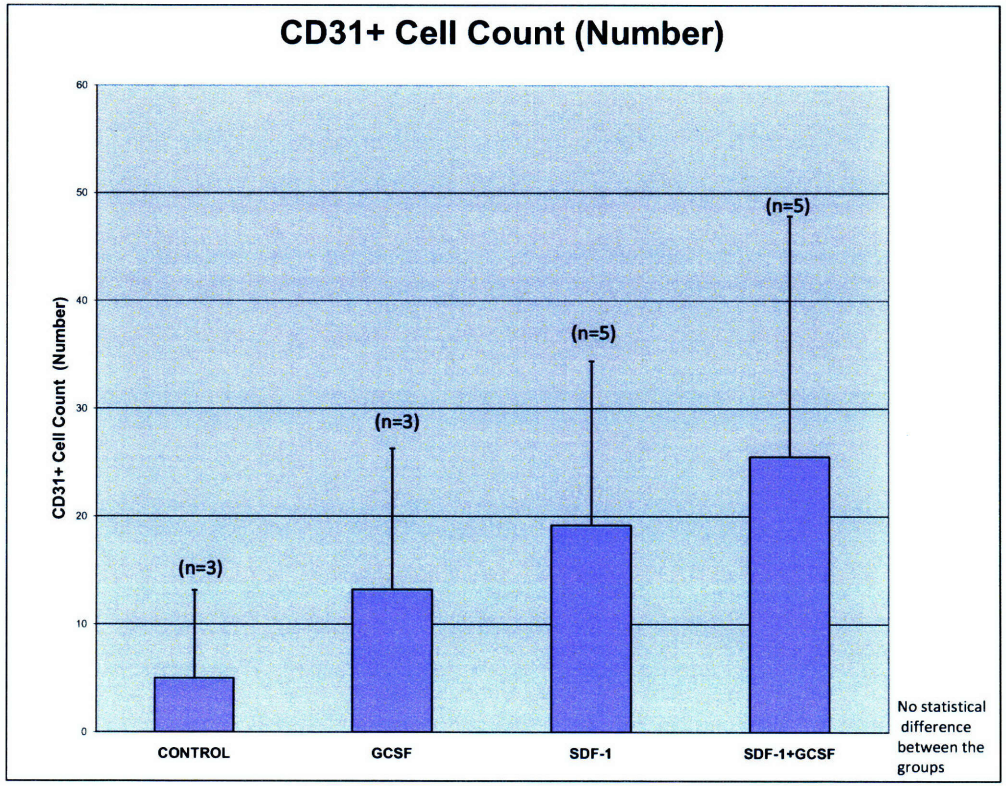


No statistical difference between the groups

| RESULTS | | |
|---|---|---|
| p-value | Group comparison types | ttest value |
| p<0.05 is significant | Control versus SDF-1 | 0.0811505709 |
| | Control versus GCSF+SDF-1 | 0.0772141493 |
| | Control versus GCSF | 0.2657265233 |
| | GCSF versus GCSF+SDF-1 | 0.2887442113 |
| | GCSF versus SDF-1 | 0.5024613281 |

## CD31+ Cell Count

| | Control | GCSF | SDF-1 | SDF-1+GCSF |
|---|---|---|---|---|
| Average | 5 | 13.2 | 19.16667 | 25.5 |
| Standard Deviation | 8.148619515 | 13.08434179 | 15.23702 | 22.36738697 |

# Appendix J

# $\alpha$-SMA Stain (Day 18 Post-Surgery)

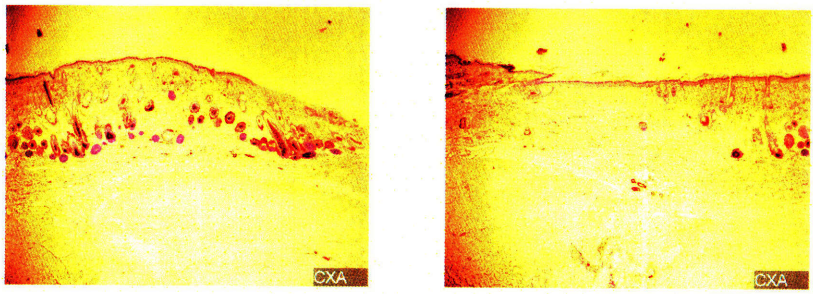


(a) 4X (b) 4X

Figure J-1: **Animal CXA (Untreated Control Group with scaffold)**

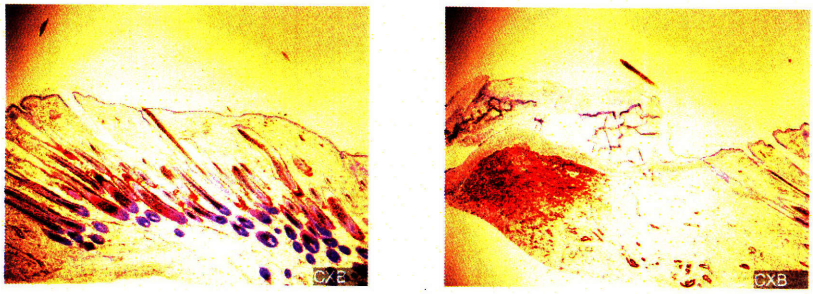


(a) 4X (b) 4X

Figure J-2: **Animal CXB (Untreated Control Group with scaffold)**

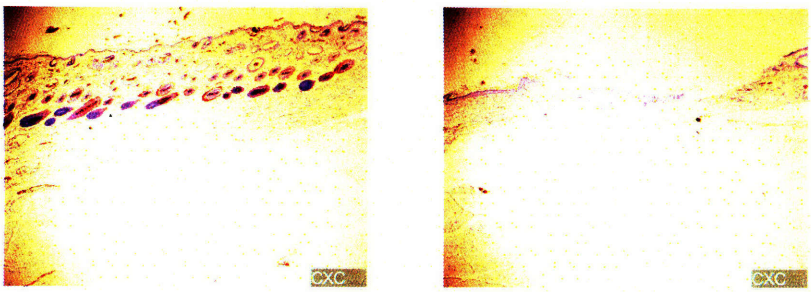


(a) 4X (b) 4X

Figure J-3: **Animal CXC (Untreated Control Group with scaffold)**

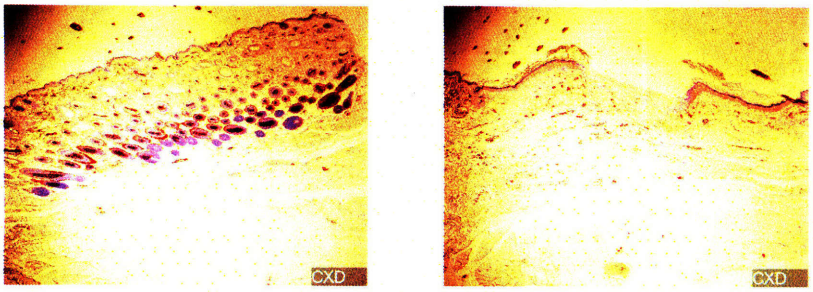


(a) 4X (b) 4X

Figure J-4: **Animal CXC (Untreated Control Group with scaffold)**

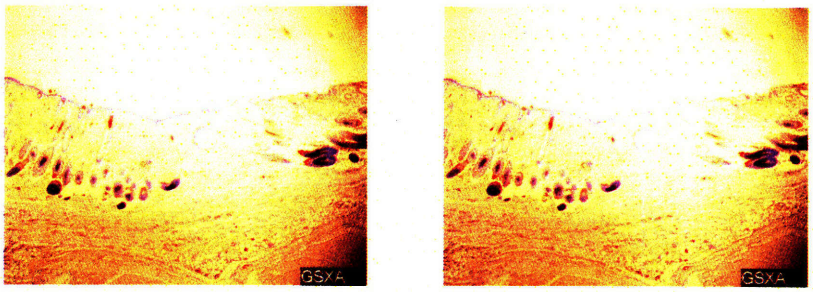


(a) 4X (b) 4X

Figure J-5: **Animal GSXA (GCSF + SDF-1 with scaffold)**

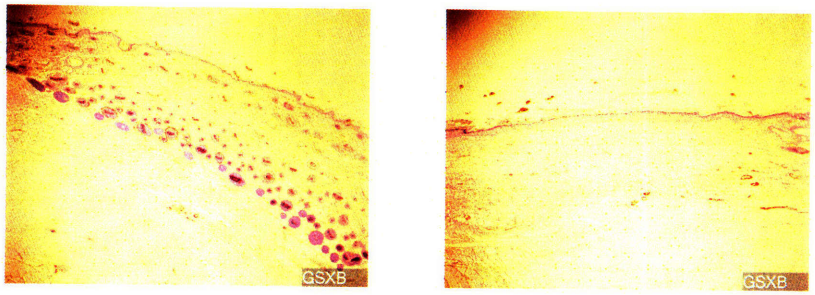


(a) 4X (b) 4X

Figure J-6: **Animal GSXB (GCSF + SDF-1 with scaffold)**

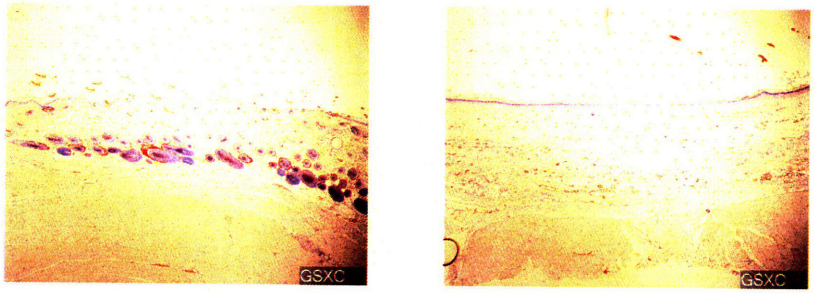


(a) 4X (b) 4X

Figure J-7: **Animal GSXC (GCSF + SDF-1 with scaffold)**

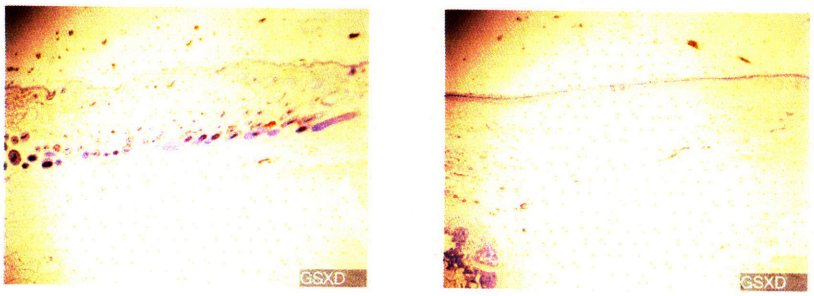


(a) 4X (b) 4X

Figure J-8: **Animal GSXD (GCSF + SDF-1 with scaffold)**

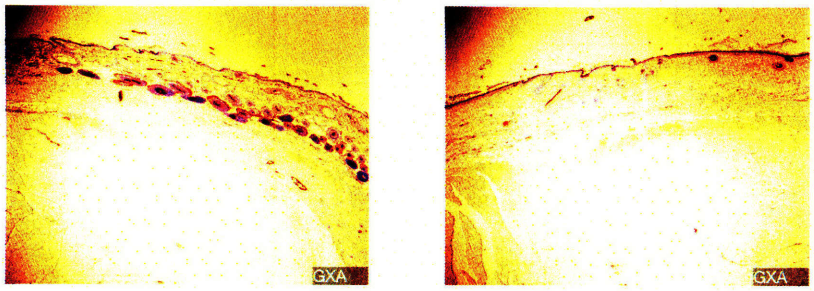


(a) 4X (b) 4X

Figure J-9: **Animal GXA (GCSF with scaffold)**

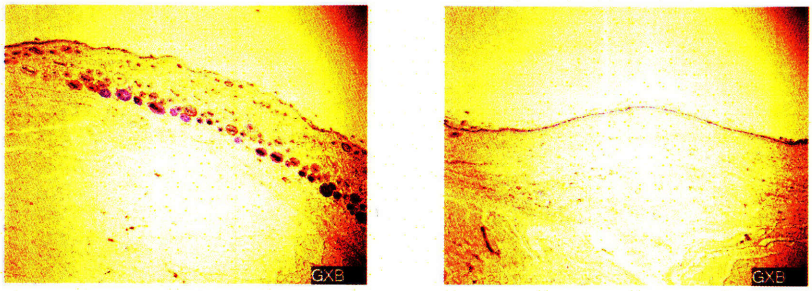


(a) 4X (b) 4X

Figure J-10: **Animal GXB (GCSF with scaffold)**

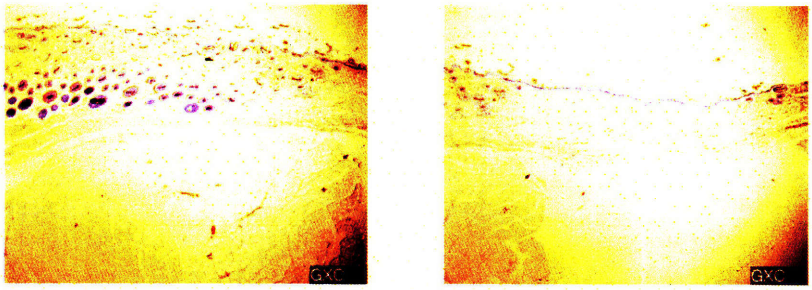


(a) 4X (b) 4X

Figure J-11: **Animal GXC (GCSF with scaffold)**

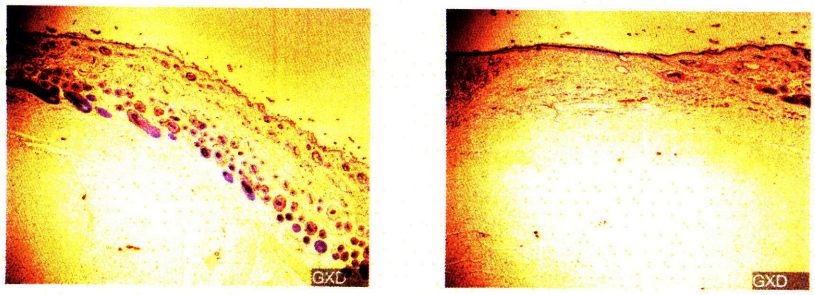


(a) 4X (b) 4X

Figure J-12: **Animal GXD (GCSF with scaffold)**

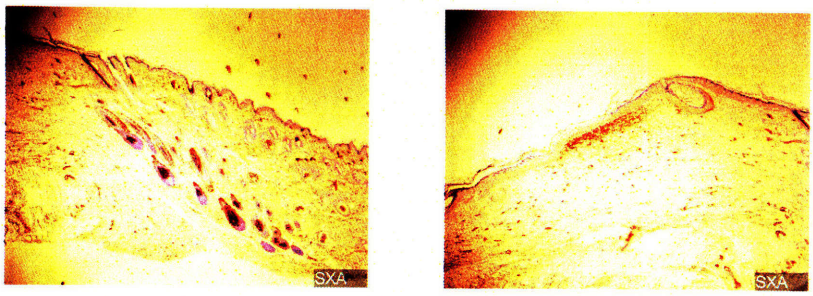


(a) 4X (b) 4X

Figure J-13: **Animal SXA (SDF-1 with scaffold)**

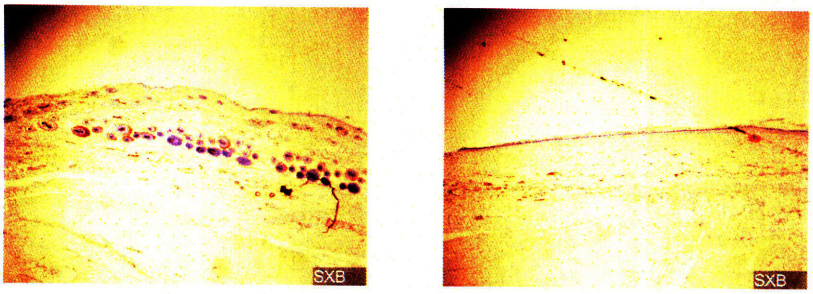


(a) 4X (b) 4X

Figure J-14: **Animal SXB (SDF-1 with scaffold)**

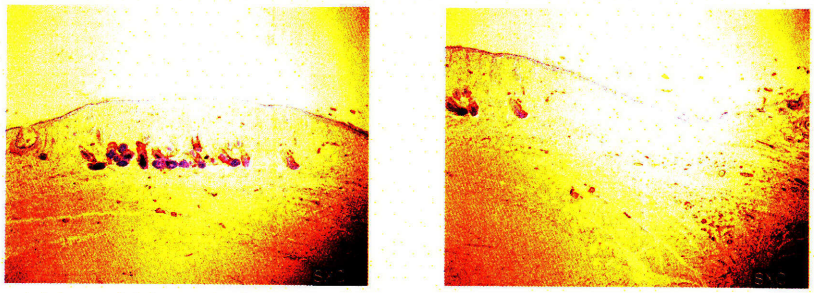

(a) 4X (b) 4X

Figure J-15: **Animal SXC (SDF-1 with scaffold)**

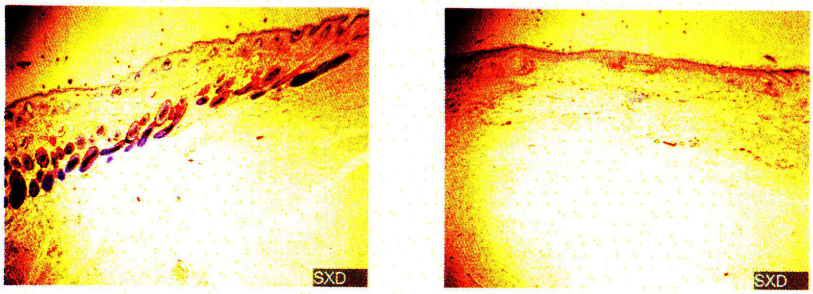


(a) 4X (b) 4X

Figure J-16: **Animal SXD (SDF-1 with scaffold)**

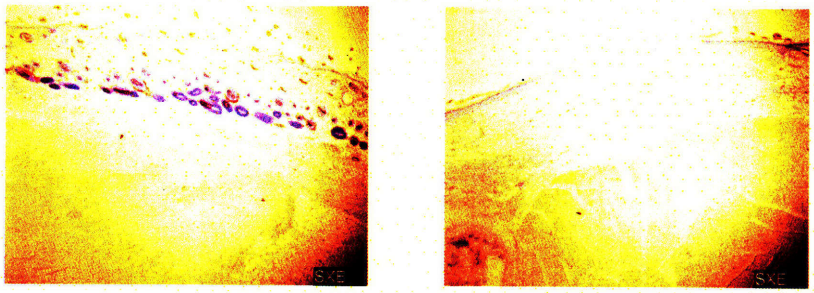


(a) 4X (b) 4X

Figure J-17: **Animal SXE (SDF-1 with scaffold)**

| Group Type | Closure Day | Animal Name | ASMA Center (Normal) Observation | ASMA Area Center (Wound Dermis) | ASMA Area 10um (Normal Dermis) Observation | Total Wound Dermis Area (Center) | ASMA Difference (%) | AVERAGE | STD. DEV |
|---|---|---|---|---|---|---|---|---|---|
| Control | | CXA | ASMA present around hair follicles | 6762 | | 659268 | 1.0257 | 12.4166 | 13.0251 |
| | | CXB | ASMA present around hair follicles | 171935 | ASMA present around hair follicles | 674493 | 25.4910 | | |
| | | CXC | ASMA present around hair follicles | 2651 | ASMA present around hair follicles | 188693 | 1.4049 | | |
| | | CXD | ASMA present around hair follicles | 147778 | | 679607 | 21.7446 | | |
| GCSF | 18 | GXA | Less ASMA present around hair follicles | 19356 | | 443108 | 4.3682 | 5.1591 | 1.1252 |
| | | GXB | Less ASMA present around hair follicles | 44692 | | 729672 | 6.1249 | | |
| | | GXC | Less ASMA present around hair follicles | 25270 | | 412491 | 6.1262 | | |
| | | GXD | Less ASMA present around hair follicles | 16556 | | 412161 | 4.0169 | | |
| GCSF+SDF-1 | 17 | GSXA | ASMA present around hair follicles | 9117 | | 260028 | 3.5062 | 13.1859 | 8.3804 |
| | | GSXB | Less ASMA present around hair follicles | 69999 | Less ASMA present around hair follicles | 604365 | 11.5822 | | |
| | | GSXC | ASMA present around hair follicles | 153392 | | 642727 | 23.8658 | | |
| | | GSXD | ASMA present around hair follicles | 84437 | Less ASMA present around hair follicles | 612340 | 13.7892 | | |
| SDF-1 | 16 | SXA | ASMA present around hair follicles | 183376 | | 1074749 | 17.0622 | 14.3477 | 5.5150 |
| | | SXB | Less ASMA present around hair follicles | 71634 | ASMA present around hair follicles | 351396 | 20.3854 | | |
| | | SXC | ASMA present around hair follicles | 60249 | | 713383 | 8.4455 | | |
| | | SXD | ASMA present around hair follicles | 85821 | | 495067 | 17.3352 | | |
| | | SXE | Less ASMA present around hair follicles | 47516 | | 556340 | 8.5102 | | |

| ASMA Area (%) | | | | |
|---|---|---|---|---|
| | Control | GCSF | GCSF+SDF-1 | SDF-1 |
| Average | 12.41655874 | 5.159062566 | 13.18586103 | 14.34771597 |
| Standard Deviation | 13.02512803 | 1.125206084 | 8.380404772 | 5.51495922 |

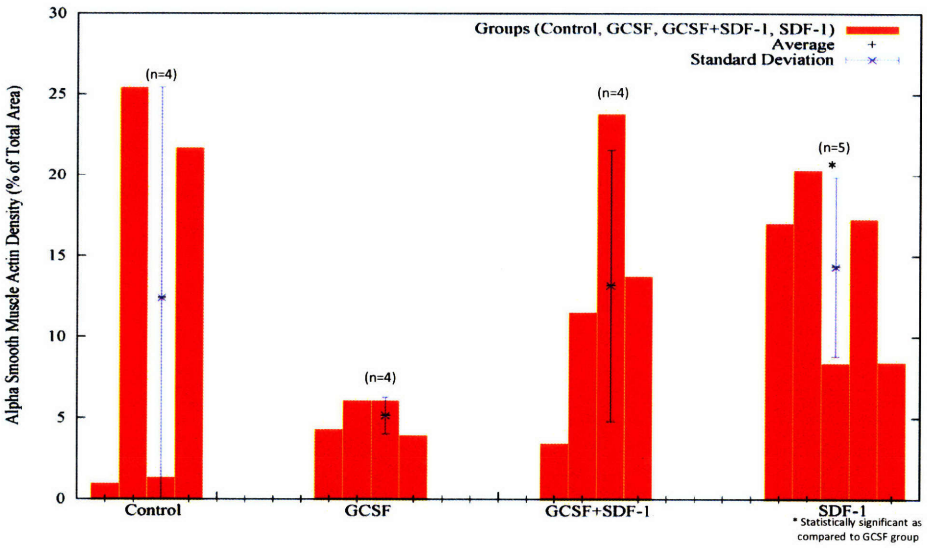


| ASMA RESULTS | | |
|---|---|---|
| p-value p<0.05 is significant | Group comparison types | ttest value |
| | Control versus SDF-1 | 0.8540131602 |
| | Control versus GCSF+SDF-1 | 0.9246405080 |
| | Control versus GCSF | 0.3468027363 |
| | GCSF versus GCSF+SDF-1 | 0.1506398540 |
| | GCSF versus SDF-1 | 0.0227311859 |
| | SDF-1 versus GCSF+SDF-1 | 0.8206428258 |

# Appendix K

# Gross Macroscopic pictures of Wound Tissue (Day 18 Post-Surgery)

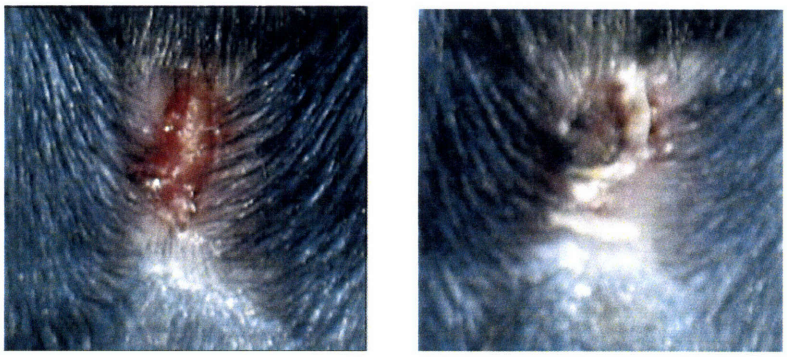

(a) Animal CXA (b) Animal CXB

Figure K-1: **Untreated Control Group with scaffold**

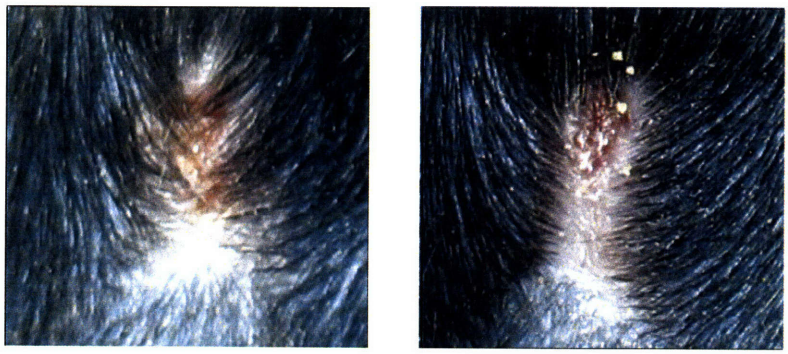

(a) Animal CXC

(b) Animal CXD

Figure K-2: **Untreated Control Group with scaffold**

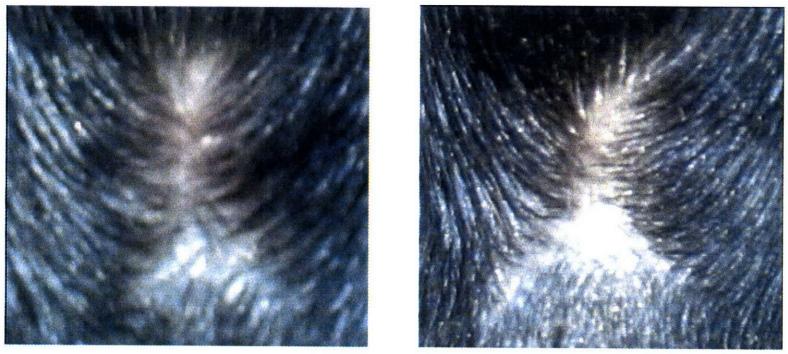

(a) Animal GSXA

(b) Animal GSXB

Figure K-3: **GCSF + SDF-1 Group with scaffold**

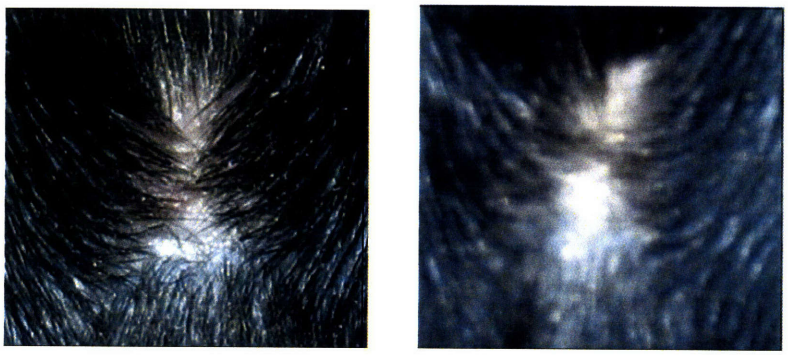

(a) Animal GSXC

(b) Animal GSXD

Figure K-4: **GCSF + SDF-1 Group with scaffold**

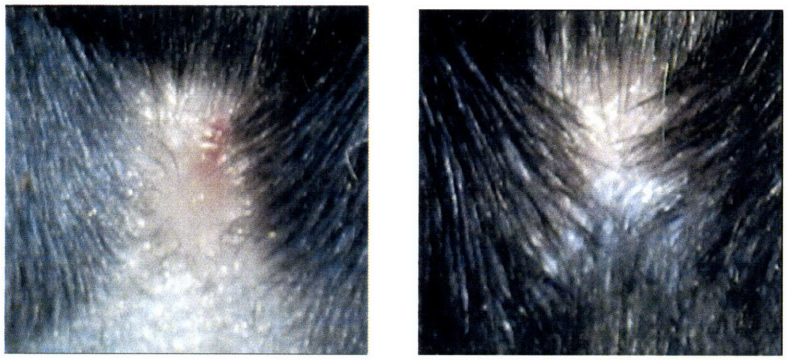

(a) Animal SXA (b) Animal SXB

Figure K-5: **SDF-1 Group with scaffold**

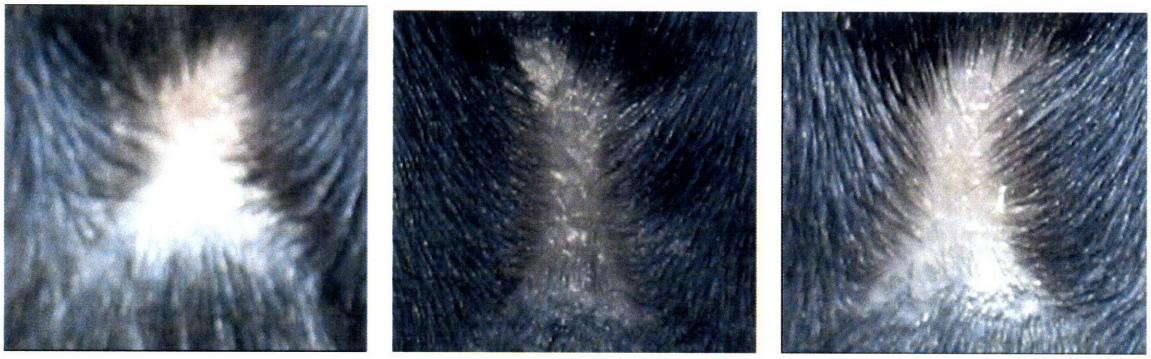

(a) Animal SXC (b) Animal SXD (c) Animal SXE

Figure K-6: **SDF-1 Group with scaffold**

| Surgery Date | Tissue Harvest Date | Group Type | Closure Day | Animal Name | Day 0 Area (Pixels) | Day 18 Area (Pixels) | Difference in Area (%) | AVERAGE | STD. DEV |
|---|---|---|---|---|---|---|---|---|---|
| November 14, 2007 | December 2, 2007 | Control | | CXA | 218592 | 14272 | 6.529058703 | 6.532880733 | 0.591052488 |
| | | | | CXB | 202216 | 14892 | 7.364402421 | | |
| | | | | CXC | 190879 | 11520 | 6.035236983 | | |
| | | | | CXD | 193428 | 11998 | 6.202824824 | | |
| | | | | | | | | | |
| | | GCSF | 18 | GXA | 208234 | 1518 | 0.728987581 | 0.989768186 | 0.277022149 |
| | | | | GXB | 180520 | 1592 | 0.881896743 | | |
| | | | | GXC | 174828 | 2408 | 1.377353742 | | |
| | | | | GXD | 198592 | 1928 | 0.970834676 | | |
| | | | | | | | | | |
| | | GCSF+SDF-1 | 17 | GSXA | 199468 | 7200 | 3.60960154 | 3.342615531 | 0.486878637 |
| | | | | GSXB | 210272 | 6084 | 2.893395221 | | |
| | | | | GSXC | 199086 | 7750 | 3.892790051 | | |
| | | | | GSXD | 215284 | 6404 | 2.974675313 | | |
| | | | | | | | | | |
| | | SDF-1 | 16 | SXA | 205410 | 19224 | 9.358843289 | 8.86207573 | 0.859038631 |
| | | | | SXB | 200094 | 16328 | 8.160164723 | | |
| | | | | SXC | 207436 | 20532 | 9.897992634 | | |
| | | | | SXD | 187048 | 16978 | 9.076814508 | | |
| | | | | SXE | 218408 | 17072 | 7.816563496 | | |

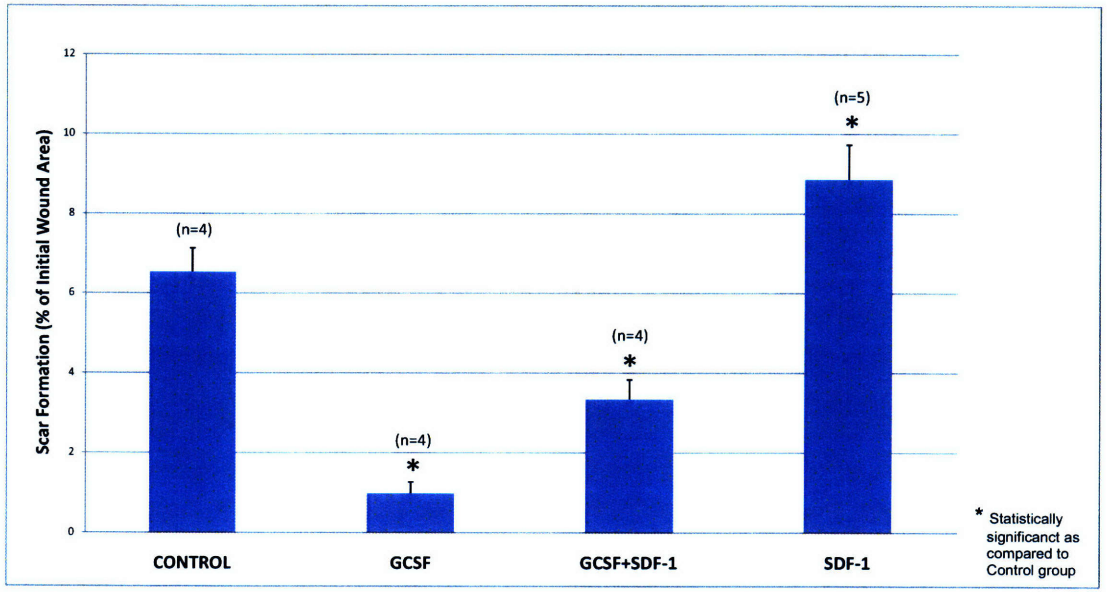


| Scar Area (%) | | | | |
|---|---|---|---|---|
| | Control | GCSF | GCSF+SDF-1 | SDF-1 |
| Average | 6.532880733 | 0.989768186 | 3.342615531 | 8.862076 |
| Standard Deviation | 0.591052488 | 0.277022149 | 0.486878637 | 0.859039 |

| RESULTS | | |
|---|---|---|
| p-value | Group comparison types | ttest value |
| p<0.05 is significant | Control versus SDF-1 | 0.0020259758 |
| | Control versus GCSF+SDF-1 | 0.0001957381 |
| | Control versus GCSF | 0.0000450024 |
| | GCSF versus GCSF+SDF-1 | 0.0004974679 |
| | GCSF versus SDF-1 | 0.0000069905 |
| | SDF-1 versus GCSF+SDF-1 | 1.08988E-05 |

# Bibliography


[1] M. Braddock, C. J. Campbell, and D. Zuder. Current therapies for wound healing: electrical stimulation, biological therapeutics, and the potential for gene therapy. *Int J Dermatol*, 38(11):808–17, 1999.

[2] Espicom Business Intelligence. The global market for advanced wound care products 2008. 2008.

[3] Centers for Disease Control and National Center for Health Statistics Prevention. Vital and health statistics, detailed diagnoses and procedures, national hospital discharge survey, 1994. *Hyattsville, Maryland: DHHS Publication*, 127:701–12, 1997. Journal Article.

[4] Taglich Brothers Inc. http://www.taglichbrothers.com/equityuniverse/companies /dermasci/dermasci-12262006.pdf. Report sourced on May 9, 2008.

[5] D. M. Nathan. Long-term complications of diabetes mellitus. *N Engl J Med*, 328(23):1676–85, 1993.

[6] G.E. Reiber, E.J Boyko, and D.G. Smith. Lower extremity foot ulcers and amputations in diabetes. *In: Diabetes in America. 2nd ed. Bethesda, MD: National Diabetes Data Group, National Institutes of Health, National Institute of Diabetes and Digestive and Kidney Diseases*, pages 409–428, 1995.

[7] C. Grunfeld. Diabetic foot ulcers: etiology, treatment, and prevention. *Adv Intern Med*, 37:103–32, 1992.

[8] M. Ehrenreich and Z. Ruszczak. Update on tissue-engineered biological dressings. *Tissue Eng*, 12(9):2407–24, 2006.

[9] S. Mendez-Eastman. Burn injuries. *Plast Surg Nurs*, 25(3):133–9, 2005.

[10] E. Andersson, A. Vahlquist, and I. Rosdahl. Beta-carotene uptake and bioconversion to retinol differ between human melanocytes and keratinocytes. *Nutr Cancer*, 39(2):300–6, 2001.

[11] L. L. Molinero, P. Zhou, Y. Wang, H. Harlin, B. Kee, C. Abraham, and M. L. Alegre. Epidermal langerhans cells promote skin allograft rejection in mice with nf-kappa b-impaired t cells. *Am J Transplant*, 8(1):21–31, 2008.

[12] C. Harvey. Wound healing. *Orthop Nurs*, 24(2):143–57; quiz 158–9, 2005.

[13] Yannas I.V. *Tissue and Organ Regeneration in Adults.* Springer, 1st edition, 2001.

[14] S.C. Smeltzer and B. Bare. *Brunner and Suddarth's textbook of medical-surgical nursing.* Philadelphia: Lippincott Williams & Wiikins, 10th edition, 2004.

[15] B. S. Atiyeh, J. Ioannovich, C. A. Al-Amm, and K. A. El-Musa. Management of acute and chronic open wounds: the importance of moist environment in optimal wound healing. *Curr Pharm Biotechnol*, 3(3):179–95, 2002.

[16] K.I. Cohen, R.F. Diegelmann, D.R. Yager, I.L. Wornum III, M.F. Graham, and M.C. Crossland. *Wound care and wound healing.* McGraw-Hill Book Company. New York, 7th edition, 1999.

[17] P. Morris and R. Shields. *Fundamentals of Surgical Practice.* Cambridge University Press, 1st edition, 2000.

[18] J.F. Hansbrough, W. Dominic, and M. Gadd. Burns: critical decisions. *Prob Crit Care*, pages 558–610, 1987.

[19] G. Pietramaggiori, A. Kaipainen, J. M. Czeczuga, C. T. Wagner, and D. P. Orgill. Freeze-dried platelet-rich plasma shows beneficial healing properties in chronic wounds. *Wound Repair Regen*, 14(5):573–80, 2006.

[20] J. M. Rhett, G. S. Ghatnekar, J. A. Palatinus, M. O'Quinn, M. J. Yost, and R. G. Gourdie. Novel therapies for scar reduction and regenerative healing of skin wounds. *Trends Biotechnol*, 26(4):173–80, 2008.

[21] J. J. Tomasek, G. Gabbiani, B. Hinz, C. Chaponnier, and R. A. Brown. Myofibroblasts and mechano-regulation of connective tissue remodelling. *Nat Rev Mol Cell Biol*, 3(5):349–63, 2002.

[22] G. Gabbiani. The myofibroblast in wound healing and fibrocontractive diseases. *J Pathol*, 200(4):500–3, 2003.

[23] A. Desmoulière, C. Chaponnier, and G. Gabbiani. Tissue repair, contraction, and the myofibroblast. *Wound Repair Regen*, 13(1):7–12, 2005.

[24] I. A. Darby and T. D. Hewitson. Fibroblast differentiation in wound healing and fibrosis. *Int Rev Cytol*, 257:143–79, 2007.

[25] N. Fausto, V. Kumar, and A.K. Abbas. *Robbins and Cotran Pathologic Basis of Disease.* Cambridge University Press, 7th edition, 2004.

[26] A. Ayello and S. Baranoski. *Wound Care Essentials: Practice Principles.* 1st edition, 2004.

[27] G. E. Mannor, R. G. Phelps, A. H. Friedman, and M. Meltzer. Eyelid healing after carbon dioxide laser skin resurfacing: histological analysis. *Arch Ophthalmol*, 117(7):913–6, 1999.

[28] K. Junge, R. Rosch, M. Anurov, S. Titkova, A. Ottinger, U. Klinge, and V. Schumpelick. Modification of collagen formation using supplemented mesh materials. *Hernia*, 10(6):492–7, 2006.

[29] R. K. Nath, W. Xiong, A. D. Humphries, and R. Beri. Treatment with antisense oligonucleotide reduces the expression of type i collagen in a human-skin organ-wound model: implications for antifibrotic gene therapy. *Ann Plast Surg*, 59(6):699–706, 2007.

[30] R.A.F Clark. Wound repair: overview and general considerations. In *The molecular and cellular biology of wound repair*, pages 3–50. Plenum Press, New York, 1996.

[31] Y. M. Bello, A. F. Falabella, and W. H. Eaglstein. Tissue-engineered skin. current status in wound healing. *Am J Clin Dermatol*, 2(5):305–13, 2001.

[32] M. H. Cottler-Fox, T. Lapidot, I. Petit, O. Kollet, J. F. DiPersio, D. Link, and S. Devine. Stem cell mobilization. *Hematology Am Soc Hematol Educ Program*, pages 419–37, 2003.

[33] S. Fu and J. Liesveld. Mobilization of hematopoietic stem cells. *Blood Rev*, 14(4):205–18, 2000.

[34] X. Fu, L. Fang, X. Li, B. Cheng, and Z. Sheng. Enhanced wound-healing quality with bone marrow mesenchymal stem cells autografting after skin injury. *Wound Repair Regen*, 14(3):325–35, 2006.

[35] H. Nakagawa, S. Akita, M. Fukui, T. Fujii, and K. Akino. Human mesenchymal stem cells successfully improve skin-substitute wound healing. *Br J Dermatol.*, 153(1):29–36., 2005.

[36] H. Satoh, K. Kishi, T. Tanaka, Y. Kubota, T. Nakajima, Y. Akasaka, and T. Ishii. Transplanted mesenchymal stem cells are effective for skin regeneration in acute cutaneous wounds. *Cell Transplant*, 13(4):405–12, 2004.

[37] O. Agbulut, S. Vandervelde, N. Al Attar, J. Larghero, S. Ghostine, B. Leobon, E. Robidel, P. Borsani, M. Le Lorc'h, A. Bissery, C. Chomienne, P. Bruneval, J. P. Marolleau, J. T. Vilquin, A. Hagege, J. L. Samuel, and P. Menasche. Comparison of human skeletal myoblasts and bone marrow-derived cd133+ progenitors for the repair of infarcted myocardium. *J Am Coll Cardiol.*, 44(2):458–63., 2004.

[38] C. Castagnoli, C. Trombotto, S. Ondei, M. Stella, M. Calcagni, G. Magliacani, and S. T. Alasia. Characterization of t-cell subsets infiltrating post-burn hypertrophic scar tissues. *Burns*, 23(7-8):565–72, 1997.

[39] R. Bucala, L. A. Spiegel, J. Chesney, M. Hogan, and A. Cerami. Circulating fibrocytes define a new leukocyte subpopulation that mediates tissue repair. *Mol Med*, 1(1):71–81, 1994.

[40] L. Yang, P. G. Scott, J. Giuffre, H. A. Shankowsky, A. Ghahary, and E. E. Tredget. Peripheral blood fibrocytes from burn patients: identification and quantification of fibrocytes in adherent cells cultured from peripheral blood mononuclear cells. *Lab Invest*, 82(9):1183–92, 2002.

[41] T. E. Quan, S. Cowper, S. P. Wu, L. K. Bockenstedt, and R. Bucala. Circulating fibrocytes: collagen-secreting cells of the peripheral blood. *Int J Biochem Cell Biol*, 36(4):598–606, 2004.

[42] S. Aiba and H. Tagami. Inverse correlation between cd34 expression and proline-4-hydroxylase immunoreactivity on spindle cells noted in hypertrophic scars and keloids. *J Cutan Pathol*, 24(2):65–9, 1997.

[43] A. L. Mescher and A. W. Neff. Regenerative capacity and the developing immune system. *Adv Biochem Eng Biotechnol*, 93:39–66, 2005.

[44] G. P. Yang, I. J. Lim, T. T. Phan, H. P. Lorenz, and M. T. Longaker. From scarless fetal wounds to keloids: molecular studies in wound healing. *Wound Repair Regen*, 11(6):411–8., 2003.

[45] I. Mensik, E. N. Lamme, J. Riesle, and P. Brychta. Effectiveness and safety of the pegt/pbt copolymer scaffold as dermal substitute in scar reconstruction wounds (feasibility trial). *Cell Tissue Bank*, 3(4):245–53, 2002.

[46] A. J. Singer and S. A. McClain. Persistent wound infection delays epidermal maturation and increases scarring in thermal burns. *Wound Repair Regen*, 10(6):372–7, 2002.

[47] D. Druecke, E. N. Lamme, S. Hermann, J. Pieper, P. S. May, H. U. Steinau, and L. Steinstraesser. Modulation of scar tissue formation using different dermal regeneration templates in the treatment of experimental full-thickness wounds. *Wound Repair Regen*, 12(5):518–27, 2004.

[48] M. P. Crump, J. H. Gong, P. Loetscher, K. Rajarathnam, A. Amara, F. Arenzana-Seisdedos, J. L. Virelizier, M. Baggiolini, B. D. Sykes, and I. Clark-Lewis. Solution structure and basis for functional activity of stromal cell-derived factor-1; dissociation of cxcr4 activation from binding and inhibition of hiv-1. *Embo J.*, 16(23):6996–7007, 1997.

[49] M. Kucia, J. Ratajczak, R. Reca, A. Janowska-Wieczorek, and M. Z. Ratajczak. Tissue-specific muscle, neural and liver stem/progenitor cells reside in the bone marrow, respond to an sdf-1 gradient and are mobilized into peripheral blood during stress and tissue injury. *Blood Cells Mol Dis.*, 32(1):52–7., 2004.

[50] J. Yamaguchi, K. F. Kusano, O. Masuo, A. Kawamoto, M. Silver, S. Murasawa, M. Bosch-Marce, H. Masuda, D. W. Losordo, J. M. Isner, and T. Asahara. Stromal cell-derived factor-1 effects on ex vivo expanded endothelial progenitor cell recruitment for ischemic neovascularization. *Circulation.*, 107(9):1322–8., 2003.

[51] E. R. Fedyk, D. Jones, H. O. Critchley, R. P. Phipps, T. M. Blieden, and T. A. Springer. Expression of stromal-derived factor-1 is decreased by il-1 and tnf and in dermal wound healing. *J Immunol*, 166(9):5749–54, 2001. 0022-1767 (Print) Journal Article.

[52] I. Petit, M. Szyper-Kravitz, A. Nagler, M. Lahav, A. Peled, L. Habler, T. Ponomaryov, R. S. Taichman, F. Arenzana-Seisdedos, N. Fujii, J. Sandbank, D. Zipori, and T. Lapidot. G-csf induces stem cell mobilization by decreasing bone marrow sdf-1 and up-regulating cxcr4. *Nat Immunol*, 3(7):687–94, 2002.

[53] A. T. Askari, S. Unzek, Z. B. Popovic, C. K. Goldman, F. Forudi, M. Kiedrowski, A. Rovner, S. G. Ellis, J. D. Thomas, P. E. DiCorleto, E. J. Topol, and M. S. Penn. Effect of stromal-cell-derived factor 1 on stem-cell homing and tissue regeneration in ischaemic cardiomyopathy. *Lancet*, 362(9385):697–703, 2003.

[54] A. Schober, S. Knarren, M. Lietz, E. A. Lin, and C. Weber. Crucial role of stromal cell-derived factor-1alpha in neointima formation after vascular injury in apolipoprotein e-deficient mice. *Circulation*, 108(20):2491–7, 2003.

[55] K. A. Gallagher, Z. J. Liu, M. Xiao, H. Chen, L. J. Goldstein, D. G. Buerk, A. Nedeau, S. R. Thom, and O. C. Velazquez. Diabetic impairments in no-mediated endothelial progenitor cell mobilization and homing are reversed by hyperoxia and sdf-1 alpha. *J Clin Invest*, 117(5):1249–59, 2007.

[56] S. Straino, A. Germani, A. Di Carlo, D. Porcelli, R. De Mori, A. Mangoni, M. Napolitano, F. Martelli, P. Biglioli, and M. C. Capogrossi. Enhanced arteriogenesis and wound repair in dystrophin-deficient mdx mice. *Circulation*, 110(21):3341–8, 2004.

[57] S. Avniel, Z. Arik, A. Maly, A. Sagie, H. B. Basst, M. D. Yahana, I. D. Weiss, B. Pal, O. Wald, D. Ad-El, N. Fujii, F. Arenzana-Seisdedos, S. Jung, E. Galun, E. Gur, and A. Peled. Involvement of the cxcl12/cxcr4 pathway in the recovery of skin following burns. *J Invest Dermatol*, 126(2):468–76, 2006.

[58] C. J. Eaves. Sdf-1 tells stem cells to mind their p's and z's. *J Clin Invest.*, 115(1):27–9., 2005.

[59] T. Papayannopoulou. Current mechanistic scenarios in hematopoietic stem/progenitor cell mobilization. *Blood.*, 103(5):1580–5. Epub 2003 Nov 6., 2004.

[60] A. Aiuti, I. J. Webb, C. Bleul, T. Springer, and J. C. Gutierrez-Ramos. The chemokine sdf-1 is a chemoattractant for human cd34+ hematopoietic progenitor cells and provides a new mechanism to explain the mobilization of cd34+ progenitors to peripheral blood. *J Exp Med.*, 185(1):111–20., 1997.

[61] C. H. Kim and H. E. Broxmeyer. In vitro behavior of hematopoietic progenitor cells under the influence of chemoattractants: stromal cell-derived factor-1, steel factor, and the bone marrow environment. *Blood*, 91(1):100–10, 1998.

[62] A. Toksoy, V. Muller, R. Gillitzer, and M. Goebeler. Biphasic expression of stromal cell-derived factor-1 during human wound healing. *Br J Dermatol*, 157(6):1148–54, 2007.

[63] P. Cipriani, A. Franca Milia, V. Liakouli, A. Pacini, M. Manetti, A. Marrelli, A. Toscano, E. Pingiotti, A. Fulminis, S. Guiducci, R. Perricone, B. Kahaleh, M. Matucci-Cerinic, L. Ibba-Manneschi, and R. Giacomelli. Differential expression of stromal cell-derived factor 1 and its receptor cxcr4 in the skin and endothelial cells of systemic sclerosis patients: Pathogenetic implications. *Arthritis Rheum*, 54(9):3022–33, 2006.

[64] S. K. Gupta, P. G. Lysko, K. Pillarisetti, E. Ohlstein, and J. M. Stadel. Chemokine receptors in human endothelial cells. functional expression of cxcr4 and its transcriptional regulation by inflammatory cytokines. *J Biol Chem.*, 273(7):4282–7., 1998.

[65] M. V. Volin, L. Joseph, M. S. Shockley, and P. F. Davies. Chemokine receptor cxcr4 expression in endothelium. *Biochem Biophys Res Commun.*, 242(1):46–53., 1998.

[66] C. Feil and H. G. Augustin. Endothelial cells differentially express functional cxc-chemokine receptor-4 (cxcr-4/fusin) under the control of autocrine activity and exogenous cytokines. *Biochem Biophys Res Commun.*, 247(1):38–45., 1998.

[67] R. Salcedo, K. Wasserman, H. A. Young, M. C. Grimm, O. M. Howard, M. R. Anver, H. K. Kleinman, W. J. Murphy, and J. J. Oppenheim. Vascular endothelial growth factor and basic fibroblast growth factor induce expression of cxcr4 on human endothelial cells: In vivo neovascularization induced by stromal-derived factor-1alpha. *Am J Pathol.*, 154(4):1125–35., 1999.

[68] S. Bhakta, P. Hong, and O. Koc. The surface adhesion molecule cxcr4 stimulates mesenchymal stem cell migration to stromal cell-derived factor-1 in vitro but does not decrease apoptosis under serum deprivation. *Cardiovasc Revasc Med.*, 7(1):19–24., 2006.

[69] B. R. Son, L. A. Marquez-Curtis, M. Kucia, M. Wysoczynski, A. R. Turner, J. Ratajczak, M. Z. Ratajczak, and A. Janowska-Wieczorek. Migration of bone marrow and cord blood mesenchymal stem cells in vitro is regulated by stromal-derived factor-1-cxcr4 and hepatocyte growth factor-c-met axes and involves matrix metalloproteinases. *Stem Cells*, 24(5):1254–64, 2006.

[70] F. Mirshahi, J. Pourtau, H. Li, M. Muraine, V. Trochon, E. Legrand, J. Vannier, J. Soria, M. Vasse, and C. Soria. Sdf-1 activity on microvascular endothelial cells: consequences on angiogenesis in in vitro and in vivo models. *Thromb Res*, 99(6):587–94, 2000.

[71] J. M. Butler, S. M. Guthrie, M. Koc, A. Afzal, S. Caballero, H. L. Brooks, R. N. Mames, M. S. Segal, M. B. Grant, and E. W. Scott. Sdf-1 is both necessary and sufficient to promote proliferative retinopathy. *J Clin Invest*, 115(1):86–93, 2005.

[72] D. M. Brainard, W. G. Tharp, E. Granado, N. Miller, A. K. Trocha, X. H. Ren, B. Conrad, E. F. Terwilliger, R. Wyatt, B. D. Walker, and M. C. Poznansky. Migration of antigen-specific t cells away from cxcr4-binding human immunodeficiency virus type 1 gp120. *J Virol*, 78(10):5184–93, 2004.

[73] M. C. Poznansky, I. T. Olszak, R. Foxall, R. H. Evans, A. D. Luster, and D. T. Scadden. Active movement of t cells away from a chemokine. *Nat Med*, 6(5):543–8, 2000.

[74] F. Vianello, I. T. Olszak, and M. C. Poznansky. Fugetaxis: active movement of leukocytes away from a chemokinetic agent. *J Mol Med*, 83(10):752–63, 2005.

[75] M. C. Poznansky, I. T. Olszak, R. H. Evans, Z. Wang, R. B. Foxall, D. P. Olson, K. Weibrecht, A. D. Luster, and D. T. Scadden. Thymocyte emigration is mediated by active movement away from stroma-derived factors. *J Clin Invest*, 109(8):1101–10, 2002.

[76] W. G. Tharp, R. Yadav, D. Irimia, A. Upadhyaya, A. Samadani, O. Hurtado, S. Y. Liu, S. Munisamy, D. M. Brainard, M. J. Mahon, S. Nourshargh, A. van Oudenaarden, M. G. Toner, and M. C. Poznansky. Neutrophil chemorepulsion in defined interleukin-8 gradients in vitro and in vivo. *J Leukoc Biol*, 79(3):539–54, 2006.

[77] N. Kohrgruber, M. Groger, P. Meraner, E. Kriehuber, P. Petzelbauer, S. Brandt, G. Stingl, A. Rot, and D. Maurer. Plasmacytoid dendritic cell recruitment by immobilized cxcr3 ligands. *J Immunol*, 173(11):6592–602, 2004.

[78] P. Ogilvie, S. Paoletti, I. Clark-Lewis, and M. Uguccioni. Eotaxin-3 is a natural antagonist for ccr2 and exerts a repulsive effect on human monocytes. *Blood*, 102(3):789–94, 2003.

[79] N. Papeta, T. Chen, F. Vianello, L. Gererty, A. Malik, Y. T. Mok, W. G. Tharp, J. Bagley, G. Zhao, L. Stevceva, V. Yoon, M. Sykes, D. Sachs, J. Iacomini, and M. C. Poznansky. Long-term survival of transplanted allogeneic cells engineered to express a t cell chemorepellent. *Transplantation*, 83(2):174–83, 2007.

[80] C. Rajnoch, S. Ferguson, A. D. Metcalfe, S. E. Herrick, H. S. Willis, and M. W. Ferguson. Regeneration of the ear after wounding in different mouse strains is dependent on the severity of wound trauma. *Dev Dyn*, 226(2):388–97, 2003.

[81] D. G. Greenhalgh. Models of wound healing. *J Burn Care Rehabil*, 26:293–305, 2005.

[82] I. V. Yannas. Studies on the biological activity of the dermal regeneration template. *Wound Repair Regen*, 6(6):518–23, 1998. Journal Article Review.

[83] F. W. Peter, D. A. Schuschke, J. H. Barker, B. Fleishcher-Peter, S. Pierangeli, P. M. Vogt, and H. U. Steinau. The effect of severe burn injury on proinflammatory cytokines and leukocyte behavior: its modulation with granulocyte colony-stimulating factor. *Burns*, 25(6):477–86, 1999.

[84] K. Minamino, Y. Adachi, M. Okigaki, H. Ito, Y. Togawa, K. Fujita, M. Tomita, Y. Suzuki, Y. Zhang, M. Iwasaki, K. Nakano, Y. Koike, H. Matsubara, T. Iwasaka, M. Matsumura, and S. Ikehara. Macrophage colony-stimulating factor (m-csf), as well as granulocyte colony-stimulating factor (g-csf), accelerates neovascularization. *Stem Cells*, 23(3):347–54, 2005. Journal Article.

[85] T. A. Davis, M. Amare, S. Naik, A. L. Kovalchuk, and D. Tadaki. Differential cutaneous wound healing in thermally injured mrl/mpj mice. *Wound Repair Regen*, 15(4):577–88, 2007.

[86] G. Pietramaggiori, S. S. Scherer, J. C. Mathews, M. Alperovich, H. J. Yang, J. Neuwalder, J. M. Czeczuga, R. K. Chan, C. T. Wagner, and D. P. Orgill. Healing modulation induced by freeze-dried platelet-rich plasma and micronized allogenic dermis in a diabetic wound model. *Wound Repair Regen*, 16(2):218–25, 2008.

[87] B. Kinner, D. M. Pacicca, L. C. Gerstenfeld, C. A. Lee, T. A. Einhorn, and M. Spector. Expression of smooth muscle actin in cells involved in distraction osteogenesis in a rat model. *J Orthop Res*, 21(1):20–7, 2003.

[88] D. M. Douglas, J. C. Forester, and R. R. Ogilvie. Physical characteristics of collagen in the later stages of wound healing. *Br J Surg*, 56(3):219–22, 1969.

[89] C. Fathke, L. Wilson, J. Hutter, V. Kapoor, A. Smith, A. Hocking, and F. Isik. Contribution of bone marrow-derived cells to skin: collagen deposition and wound repair. *Stem Cells*, 22(5):812–22, 2004.

[90] Y. Wu, L. Chen, P. G. Scott, and E. E. Tredget. Mesenchymal stem cells enhance wound healing through differentiation and angiogenesis. *Stem Cells*, 25(10):2648–59, 2007.

[91] The Freedonia Group. Cosmetic surgery products to 2010-demand and sales forecasts, market share, market size, market leaders. *Study no. 2099*, 2006.

[92] S. R. Sullivan, R. A. Underwood, N. S. Gibran, R. O. Sigle, M. L. Usui, W. G. Carter, and J. E. Olerud. Validation of a model for the study of multiple wounds in the diabetic mouse (db/db). *Plast Reconstr Surg*, 113(3):953–60, 2004.

[93] G. Erdag, D. A. Medalie, H. Rakhorst, G. G. Krueger, and J. R. Morgan. Fgf-7 expression enhances the performance of bioengineered skin. *Mol Ther*, 10(1):76–85, 2004. Journal Article.

[94] G. Erdag and J. R. Morgan. Allogeneic versus xenogeneic immune reaction to bioengineered skin grafts. *Cell Transplant*, 13(6):701–12, 2004. Journal Article.

[95] I. V. Yannas. Similarities and differences between induced organ regeneration in adults and early foetal regeneration. *J R Soc Interface*, 2(5):403–17, 2005.

[96] D. S. Kohane, J. Y. Tse, Y. Yeo, R. Padera, M. Shubina, and R. Langer. Biodegradable polymeric microspheres and nanospheres for drug delivery in the peritoneum. *J Biomed Mater Res A*, 77(2):351–61, 2006.

[97] Y. Yeo, T. Ito, E. Bellas, C. B. Highley, R. Marini, and D. S. Kohane. In situ cross-linkable hyaluronan hydrogels containing polymeric nanoparticles for preventing postsurgical adhesions. *Ann Surg*, 245(5):819–24, 2007.

[98] K. Aschheim. Profile: Anthony Atala. *Nat Biotechnol*, 24(11):1311, 2006.